# Field measurements and analyses of electrokinetic seismoelectric signals generated in sedimentary environments

by

J. Christian Dupuis

**M.Sc.E., University of New Brunswick, 2004**
**B.Sc.E., University of New Brunswick, 2001**

**A THESIS SUBMITTED IN PARTIAL FULFILLMENT OF THE REQUIREMENTS FOR THE DEGREE OF**

**Doctor of Philosophy**

In the Graduate Academic Unit of Geology

| | |
|---|---|
| Supervisors: | Karl E. Butler, Ph.D., Geology |
| | Brent R. Petersen, Ph.D., Electrical and Computer Engineering |
| Examining Board: | Kenneth B. S. Burke, Ph.D., Geology |
| | William Ward, Ph.D., Physics |
| | Dennis F. Lovely, Ph.D., Electrical and Computer Engineering |
| External Examiner: | Stéphane Garambois, Ph.D., Université Joseph Fourier |

This thesis is accepted

Dean of Graduate Studies

**THE UNIVERSITY OF NEW BRUNSWICK**

**December, 2008**

*To my family and friends.*

# Abstract

Significant advances in quantitative understanding of seismoelectric effects of electrokinetic origin have been made since they were first observed, but field data needed to validate theoretical models and associated numerical simulations have remained scarce.

The high quality field data presented in this work serve to verify conceptual and quantitative models. Clear seismoelectric signals with amplitudes on the order of 1 microvolt per metre provide a unique opportunity to study amplitude and phase characteristics of seismoelectric signals measured on surface and in boreholes. Complementary geological and geophysical data are used to determine the characteristics of sediments and interfaces that have made these aquifers and aquitards amenable to seismoelectric investigation.

The results of vertical profiling experiments in glaciogenic sediments at Fredericton, Canada, represent the first field measurements to confirm that the co-seismic fields predicted by a quasi-static model are consistent with field measurements. The amplitudes of the co-seismic field are influenced by the resistivity and porosity of the sediments where the measurements are made. Further experiments, in a sandy unconfined aquifer near Perth, Australia, demonstrated that it is possible to measure interfacial seismoelectric signals in boreholes. Measurements of signal amplitude versus depth, and polarity reversals, observed for the first time in a borehole, have

confirmed the strong bipolar character of the interfacial seismoelectric conversion in the near field. The conductivity of sediments around the interface was found to have a significant influence on the amplitude of the signal and the field distribution.

A surface-based seismoelectric imaging experiment over the same aquifer succesfully imaged both the base of the vadose zone and a shallower water retentive layer. The seismoelectric shot records presented in this work are the first example of such clear interfacial signals measured from hydrogeological interfaces deeper than 10 m. The amplitude distribution of the dominant interfacial signal was found to agree, to a first-order approximation, with that of a short electric dipole.

Results from these experiments suggest that hydrogeological targets exhibiting significant contrasts in water saturation, electrical conductivity and acoustic impedance, due to cementation, are amongst the best candidates to be imaged using seismoelectric conversions.

# Acknowledgements

During my doctoral studies I have been fortunate to be surrounded by people who have contributed in a positive way to my endeavors. The field successes and scientific advancements presented in this thesis have been made possible by their support, encouragement and through their willingness to share their knowledge with me.

At the forefront is my principal supervisor Dr. Karl E. Butler, who first introduced me to seismoelectric phenomena. His contagious enthusiasm for this research topic and his genuine interest of the subject has made it an exciting and rewarding area of research for me. Beyond his scientific insight into my research and his encouragement to publish my results, he has provided me with several opportunities that are seldom afforded to other graduate students and thus I am very grateful to him.

Dr. Brent R. Petersen, provided me with important advice and mentorship throughout all of my postgraduate studies. As a co-supervisor for my two postgraduate degrees, he has provided invaluable insight and has helped guide my progression as a researcher and academic.

The field work in Australia was an important turning point in my research. Dr. Anton W. Kepic and Dr. Brett D. Harris from Curtin University of Technology are acknowledged for their efforts in identifying possible field sites and organizing

# Table of Contents

# List of Tables

# List of Figures

# Nomenclature

| | |
|---|---|
| $\alpha_\infty$ | Tortuosity |
| $\Delta\psi$ | Electric potential difference (V) |
| $\ell$ | Length of capillary (m) |
| $\epsilon_0$ | Electric permittivity of free space ($8.8 \times 10^{-12}$ F/m) |
| $\epsilon_f$ | Dielectric constant of the electrolyte |
| $\eta$ | Fluid viscosity (Pa $\cdot$ s) |
| $\kappa^{-1}$ | Thickness of the double layer (Debye Length) (m) |
| $\phi$ | Porosity |
| $\psi$ | Electric potential (V) |
| $\psi_0$ | Electric potential at surface of solid grain (V) |
| $\psi_d$ | Electric potential at the Stern plane (V) |
| $\rho_B$ | Bulk density (kg/m$^3$) |
| $\rho_f$ | Fluid density (kg/m$^3$) |
| $\sigma(\omega)$ | Electrical conductivity of the material (S/m) |
| $\sigma_f$ | Electric conductivity of the fluid (S/m) |
| $\sigma_s$ | Surface conductance (S) |
| $\mathbf{w}$ | Relative grain/fluid displacement (m) |
| $\boldsymbol{\tau_B}$ | Bulk stress tensor (Pa) |
| $\boldsymbol{\tau_f}$ | Fluid tensor (Pa) |
| $\boldsymbol{\tau_s}$ | Solid tensor (Pa) |

| | |
|---|---|
| $\boldsymbol{B}$ | Magnetic flux density (T) |
| $\boldsymbol{D}$ | Electric flux density (C/m$^2$) |
| $\boldsymbol{E}$ | Electric field strength (V/m) |
| $\boldsymbol{H}$ | Magnetic field strength (A/m) |
| $\boldsymbol{I}$ | Identity matrix |
| $\boldsymbol{J}$ | Current density (A/m$^2$) |
| $\boldsymbol{u_s}$ | Particle displacement (m) |
| $\zeta$ | Electric potential at the slip plane of the electric double layer (V) |
| $c(+)$ | Concentration of positive ions (ions/m$^3$) |
| $c(-)$ | Concentration of negative ions (ions/m$^3$) |
| $c^0$ | Concentration of ions in a region where $\psi = 0$ |
| $c_i$ | Electrolyte concentration (ions/m$^3$) |
| $d$ | Distance that separates the charges (m) |
| $e$ | Elementary (protonic) charge ($1.602 \times 10^{-19}$ C) |
| $G_{fr}$ | Grain framework shear modulus (Pa) |
| $I_c$ | Conduction current (A) |
| $I_s$ | Streaming current (A) |
| $I_{cs}$ | Conduction current flowing along a solid surface (A) |
| $k$ | Boltzmann's constant ($1.38 \times 10^{-23}$ J/K) |
| $k(\omega)$ | Hydraulic permeability (m$^2$) |
| $k_0$ | DC hydraulic permeability |
| $K_f$ | Bulk modulus of the fluid (Pa) |
| $K_G$ | Undrained bulk modulus (Pa) |
| $K_s$ | Bulk modulus of the solid (Pa) |
| $K_{fr}$ | Bulk modulus of drained framework (Pa) |

$L(\omega)$    Electrokinetic coupling coefficient $((C \cdot m)/(N \cdot s))$

$p$       Pressure (Pa)

$q$       Charge density $(C/m^2)$

$q_1$     Charge associated with an ion at the surface of the solid (C)

$q_2$     Charge associated with a counterion in the electrolyte (C)

$R$      Radius of capillary (m)

$r$       Radial distance from center of capillary (m)

$T$      Temperature (K)

$v$       Fluid velocity (m/s)

$x$       Distance from solid surface (m)

$z_+$     Valence of the positive ion

$z_-$     Valence of the negative ion

$z_i$     Ionic valence for species $i$

# Chapter 1

# Introduction

Seismoelectric effects were first observed at the end of the 1930s and have remained a subject of scientific curiosity for researchers in industry and academia alike. The interest in these effects stems from their potential to provide information on porous material and pore fluid characteristics that are difficult and costly to obtain with more traditional geophysical techniques. In particular, the potential for seismoelectric methods to identify changes in porosity, permeability and pore fluid at the resolution of seismic methods have fueled the development of these techniques (e.g. *Thompson and Gist*, 1993; *Haartsen and Pride*, 1997; *Garambois and Dietrich*, 2002; *Berryman*, 2003; *Singer et al.*, 2005).

Development of fast, reliable and economic seismoelectric surveys could provide geoscientists with permeability contrast information which would help manage resources (e.g. groundwater) and protect them from possible sources of contamination. Geotechnical engineers would also benefit from this information as seepage, consolidation and stability of soils are all issues that relate to water content and flow. The electrokinetic properties of the soils obtained with seismoelectric experiments could assist engineers and scientists to develop eletro-osmosis remediation campaigns

to flush out contaminants from the soil or to dewater and stabilize terrains (*Mitchell*, 1993).

In the oil and gas industry, the ability to image properties of the pore fluid and permeability remotely would be a great asset for the commercial development of a production field. It could assist the engineers in developing an exploitation program that maximizes recovery and the life expectancy of the wells. Seismoelectric methods could also prove useful in assessing characteristics of depleted reservoirs to be used in carbon capture and sequestration schemes, as the change in permeability contrast and the pore fluid can be studied over time.

Despite the advances in our quantitative understanding of this effect in recent years (*Neev and Yeatts*, 1989; *Pride*, 1994), and our ability to generate numerical models (*Haartsen and Pride*, 1997; *Garambois and Dietrich*, 2002; *Haines and Pride*, 2006), there remains a need for convincing field measurements with which theoretical and numerical simulations can be validated and the viability of geophysical exploration can be demonstrated.

The dearth of convincing field measurements in the literature is a consequence of difficulties associated with making the measurements under field conditions, particularly when the sources and receivers are both on surface. To begin, the signals are often orders of magnitude weaker than the ambient electrical noise, and existing seismic or EM/electrical recording systems are not optimized for their measurement. Additionally, as will be explained later in this chapter, there exist two different types of seismoelectric signals: (1) co-seismic and (2) interfacial signals. Although there exists potential to develop borehole logging techniques with the co-seismic signal, the exploration potential of the seismoelectric method stems from the interfacial signals. Attempts to measure seismoelectric responses from interfaces at depth are compli-

cated by the earlier arrival of stronger co-seismic effects that constitute coherent noise similar to surface wave interference in seismic reflection surveys.

## 1.1 Thesis objectives

The objectives throughout this work have been to (1) advance the collective understanding of seismoelectric signals by contributing high-quality field datasets that can be used to confirm theoretical models and numerical simulations, (2) use the measured data to confirm simple conceptual and quantitative models, (3) to develop robust methodology and field procedures that can assist other researchers in making seismoelectric measurements, (4) to determine the characteristics of interfaces that generate interfacial signals, and (5) to demonstrate that interfacial signals can be used to image geological targets of hydrogeological importance.

## 1.2 Thesis contribution

Following this introductory chapter, Chapter 2 introduces important considerations when planning a seismoelectric survey and solutions to common acquisition problems. The contributions of the thesis are presented in the form of three journal articles that appear as Chapters 3, 4, 5 followed by conclusions in Chapter 6. The first two articles have already been published in international peer-reviewed journals and the third has been submitted to the Journal of Geophysical Research for review. These articles represent a significant contribution to our evolving understanding of how seismically induced electrokinetic effects can be measured, interpreted and perhaps ultimately applied in hydrodgeological and other (e.g. reservoir characterization) applications.

The first article (*Dupuis and Butler*, 2006), published in Geophysical Research Letters and reprinted in Chapter 3, involves the design of a carefully controlled field experiment and the acquisition and processing of weak, but remarkably clear, co-seismic seismoelectric data as a function of depth in a borehole. Measurements are compared to the predictions of a theoretical model, and the effects of sediment properties on the strength of the seismoelectric signal are investigated. This vertical seismoelectric profiling approach is recommended for making field measurements more reliably so that models and simulations can be validated by field observations.

The second article (*Dupuis et al.*, 2007), published in Geophysics and reprinted in Chapter 4, presents the most convincing evidence to date that seismoelectric methods can be used to map near-surface interfaces in sedimentary environments. Interfacial seismoelectric signals from depths exceeding 10 m have been measured and results demonstrate that the method could become a valuable tool, sensitive to the presence of pore water and complementary to current methods such as ground penetrating radar for the characterization of aquifers.

In the last article, emphasis is placed on results from vertical seismoelectric profiling experiments in which interfacial signals have been measured. The measurements were made in the same region as the seismoelectric imaging experiment published in Geophysics. The objective of this work was to better understand the interfacial signals, and observe the formation of the signal in-situ. Amplitude characteristics of the signal and the polarity reversal observed due to an expanding source zone of finite size is explained. These in-situ measurements corroborate the conceptual model that describe the source zone of the interfacial signal as the first Fresnel zone at the interface. The characteristics of the interfaces that generated the interfacial signals are further studied and evidence of thin partially cemented layers

that straddle the water table at two field sites is shown. The results of these experiments confirm that vertical seismoelectric profiles are appropriate to gain greater insight into the generation of seismoelectric signals and provide the best geometry to validate theoretical and numerical models.

I designed the experiments, processing flows and various instruments used in these experiments. In all, three downhole electrode arrays, a PVC striking rod, a normal resistivity probe, a borehole geophone, a hydrophone, a borehole hammer source, and a fiber optic trigger were designed and built. I performed the analyses on the data, drafted the text and figures, implemented editorial changes and submitted the papers for publication. Scientific and editorial guidance were offered by my co-authors.

## 1.3 Seismoelectric theory

*Ivanov* (1939) was the first to observe seismoelectric signals from an electrokinetic origin. In *Ivanov* (1940), it is hypothesized that the electrical double layer that forms between the solid and liquid phase proposed by Helmholtz could explain the signal observed in the field experiments. *Ivanov* uses the Helmholtz-Smoluchowski equation, derived to describe electrokinetic phenomena of electro-osmosis and streaming potential in a capillary, to explain how translocation of the pore fluid and the solid could generate an electric field.

The hypothesis that the electrical double layer and electrokinetic coupling lie at the root of most seismoelectric phenomena observed in porous media remains current today and has been supported by many theoretical and experimental investigations (although the possible existence of other unrecognized mechanisms cannot be ruled

out). The concept of the electric double layer and how it applies to seismoelectric signals is presented in this section.

### 1.3.1 Electric double layer

According to *Sparnaay* (1972) the concept of the electric double layer at the interface of a solid and fluid was first proposed by *Helmholtz* (1853). The model depicted in Figure 1.1 illustrates the electric double layer proposed by *Helmholtz* (1853) and refinements proposed by *Gouy* (1910) and *Chapman* (1913) with the addition of a diffuse zone which is found beyond the Stern plane proposed by *Stern* (1924) (*Shaw*, 1980).

The surface charge on the solid can be caused by at least six mechanisms according to *Everett* (1988):

**Ionization of surface groups** If acidic groups are dissociated from the surface it results in a negative surface charge, while dissociation of basic groups from a surface will lead it to be positive. The tendency for dissociation can be altered by altering the pH and thus the surface ionization can be reduced to zero.

**Differential solutions of ions from the surface of sparingly soluble crystals** To illustrate this example, *Everett* (1988) proposes an example for silver iodide $Ag^+ I^-$ crystals. He points out that $Ag^+$ ions dissolve preferentially and thus the surface of the crystal becomes negative.

**Isomorphous substitution** As an example, *Everett* (1988) proposes a clay that may exchange an intercalated, or structural ion with one of lower valency, which produces a negatively charged surface. He gives as an example aluminum, Al,

which has valence of three, replacing Si, which has a valence of four, in the tetrahedral layer of a clay.

**Charged crystal surface** This may occur when a crystal is broken, exposing surfaces with unstastified bonds.

**Specific ion adsorption** This may be the case when ions are specifically adsorbed. A cationic surfactant leads to a positive surface, while a anionic surfactant leads to a negative surface charge.

According to *Mitchell* (1993) the most likely charge development mechanisms encountered in soils are isomorphous substitution, charged crystal surfaces and specific ion adsorption. He also comments that the most common cations in residual and non-marine sedimentary soils are, in order of decreasing importance: calcium, magnesium, sodium and potassium, while in marine clays and saline soils, sodium is the dominant cation. As for sources of anions in soils, he suggests that sulfate, chloride, phosphate and nitrate are the most commonly encountered.

In Figure 1.1 the surface of the solid has a negative charge and cations of the electrolyte are attracted to the surface by electrostatic forces.

The arrangement of charges in Figure 1.1 is simplistic and does not occur in reality, since the electrostatic force is not the only one acting on the system. Thermal motion, which exists in every system at temperatures above $0^o$ K, will cause the counterions to be distributed following Boltzmann's distribution law, which relates the probability of particles being at a given point at a given energy, or free energy given a reference point (e.g. absolute zero) (*Everett*, 1988).

According to *Everett* (1988), the concentration of cations ($c(+)$) and anions ($c(-)$) ions in a region in an electrolyte solution at temperature $T$ near a point where
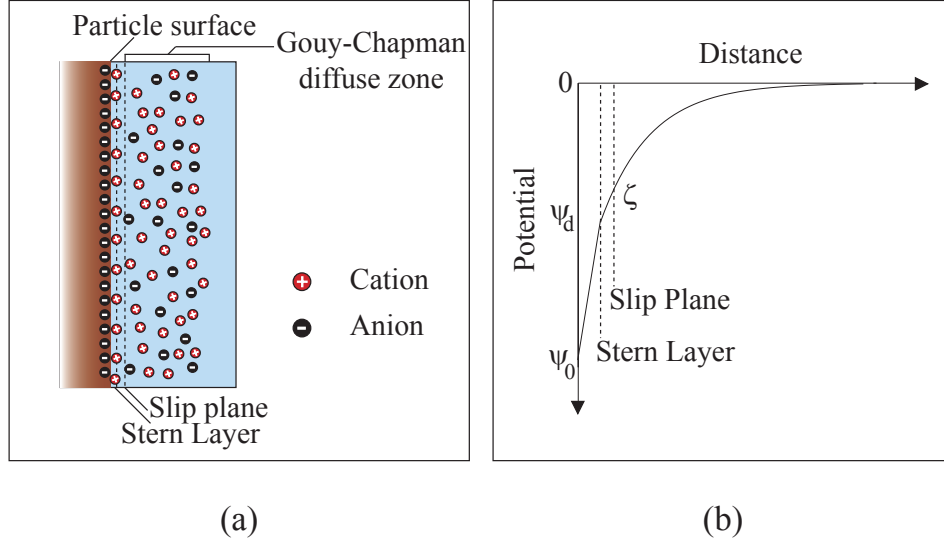
Figure 1.1: Stern-Gouy-Chapman electric double layer model

there is an electrical potential $\psi$ is given by:

$$c(+) = c^0 \exp\left\{\frac{-z_+ \, e \, \psi}{k \, T}\right\}, \tag{1.1}$$

and

$$c(-) = c^0 \exp\left\{\frac{+z_- \, e \, \psi}{k \, T}\right\}, \tag{1.2}$$

where $z_+$ is the valence of the positive ion, $z_-$ is the valence of the negative ion, $e$ is the elementary (protonic) charge, $k$ is Boltzmann's constant and $c^0$ is the concentration of ions in a region where $\psi = 0$.

If we take an example for monovalent ions (i.e. $z_+ = z_- = 1$), at a point where

$\psi \neq 0$, the difference in concentration of positive and negative ions can be written as

$$c(+) - c(-) = c^0 \left( \exp\left\{ \frac{-e\,\psi}{k\,T} \right\} - \exp\left\{ \frac{+e\,\psi}{k\,T} \right\} \right). \tag{1.3}$$

In our example, where the surface of the solid is negatively charged, $\psi$ will be negative and thus Equation 1.3 will be positive, meaning that there is an excess of cations surrounding the charged surface. The counterions amongst this charge cloud, will be subject to different forces depending on their position relative to the ions present in the Stern layer. The ones closest to the surface will be attracted more strongly to the surface due to the electrostatic and Van der Wall forces. These forces are sufficient for these counterions to overcome the thermal agitation and form an adsorbed layer on the surface of the solid which is called the Stern plane (*Shaw*, 1980). According to *Ishido and Mizutani* (1981) the Stern plane may be subdivided into two additional subplanes they call the inner Helmholtz and outer Helmholtz planes. The distinction between these two planes is the hydration of the counterions making contact with either bare solid or hydrated solid. Within the inner Helmholtz plane, the potential changes from the surface potential ($\psi_0$) to the potential of the Stern plane ($\psi_d$) as shown in Figure 1.1 b. *Shaw* (1980) points out that the value of $\psi_d$ depends on the nature of ions adsorbed and thus it is possible for $\psi_d$ to have a polarity which is opposite to $\psi_0$. Given a steady-state chemical environment, the ions that form the Stern plane will remain adsorbed on the surface. Thus to explain electrokinetic coupling between seismic fields and electric fields, we must consider another region of the electric double layer.

The Gouy-Chapman diffuse zone is found beyond the Stern layer and contains counterions that are subjected to weaker attractive forces than the counterions in the Stern layer. Within this diffuse zone, at a small distance from the Stern layer, lies

a slip plane beyond which counterions can be sheared off from the double layer by relative motion between the solid and the electrolyte. The potential in the Gouy-Chapman diffuse zone is given by *Everett* (1988)

$$\psi = \psi_d \exp\{-\kappa\, x\}, \tag{1.4}$$

where $\psi_d$ is the potential of the Stern layer, $\kappa^{-1}$ is sometimes called the thickness of the double layer or the Debye length and $x$ is the distance from the wall. The Debye length is given by *Everett* (1988)

$$\kappa^{-1} = \sqrt{\frac{\epsilon_f\, k\, T}{e^2 \Sigma\, c_i\, z_i^2}}, \tag{1.5}$$

where $k$ is Boltzmann's constant, $T$ is the temperature in degrees Kelvin, $e$ is the elementary (protonic) charge and $\Sigma c_i z_i^2$ is the summation of concentration of ions ($c_i$) (ions/m$^3$) and the ionic valence ($z_i$) for species $i$. For a given electrolyte, the thickness of the double layer will vary proportionally with the square root of the temperature and inversely to the square root of the electrolyte concentration.

The potential at the slip plane is called the $\zeta$ potential. This important parameter in determining the characteristics of electrokinetic coupled flows has been measured in various geological sediments and with various electrolytes by *Ishido and Mizutani* (1981) and *Morgan et al.* (1989) for pH ranging between 2 and 12. The reported values for the $\zeta$ potential range between -10 mV to -100 mV for most water-saturated geological sediments and empirical relationships have been derived for quartz and brine (NaCl and KCl), by *Pride and Morgan* (1991) and *Wurmstich and Morgan* (1994) for pH ranging between 5 and 7.

*Revil et al.* (1999) derive an analytical equation for the $\zeta$ potential based on

chemical reactions for silica-dominated porous sediments filled with a binary symmetric electrolyte (such as NaCl, KCl or $KNO_3$). The specifics of the formation of the electric double layer for silica are well explained by *Revil et al.* (1999). They explain that for silica there exists two different type of surface groups. The first group is called siloxal ($Si_2O$) and the second silanol (SiOH). The protonation of the siloxal group is extremely low and therefore it is generally accepted that these groups can be considered inert as suggested by *Hiemstra and Van Riemsdijk* (1990) (*Revil et al.*, 1999). For pH in the range of 6 to 8, the surface mineral reaction at the silanol surface in contact with a 1:1 electrolyte causes three different surface sites. The first two, SiOH and SiOMe (where $Me^+$ stands for a metal cation in the electrolyte solution i.e. $Na^+$ for NaCl) are electroneutral. The third, $SiO^-$ is the only charged surface group and is responsible for the surface charge of the mineral. The surface charge is obtained by summing the $SiO^-$ sites on the surface of the mineral. With this result and the expression derived for the charge density of the diffuse layer, *Revil et al.* (1999) derive an analytic expression for the Stern potential, which he equates to the $\zeta$ potential, to avoid the use of a free adjustable parameter. The model obtained agrees well to measurements found in the literature.

## 1.3.2   The streaming potential

The steady state equilibrium between the inner and outer part of the electric double layer can be altered by fluid flow through the pore space, which leads to what is known as streaming potentials.

To understand how the fluid flow generates streaming potentials, we can consider a simple experiment designed to measure the $\zeta$ potential described in *Evans and Wennerström* (1999). This also allows us to derive the Helmholtz-Smoluchowski
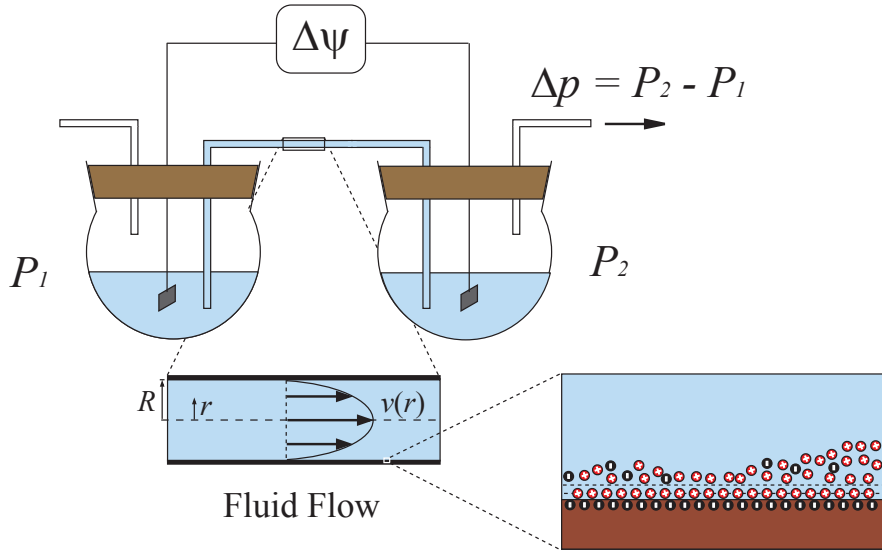
Figure 1.2: Apparatus for measuring streaming potential.

equation, that relates the fluid pressure drop ($\Delta p$) to the potential difference ($\Delta \psi$) along a capillary tube (Figure 1.2). The air pressure is increased in the left flask which causes fluid to flow in the capillary toward the right flask. We assume that the flow in the capillary is laminar (i.e. velocity is not high enough to create turbulence) and thus Poiseuille's law applies and the fluid velocity $v$ at radius $r$ in a capillary of radius $R$ and length $\ell$ caused by a pressure gradient of $\Delta p$ is written as (*Evans and Wennerström*, 1999)

$$v = \frac{\Delta p}{4 \, \eta \, \ell}(R^2 - r^2).\tag{1.6}$$

The electrical current $dI_s$ associated with the fluid flow can be computed by

considering the charge density $q$ being carried through the cross-section of the capillary $dA = 2\pi r dr$ with velocity $v$ and fluid viscosity $\eta$

$$dI_s = q\,v\,dA = \frac{q\,\Delta p}{4\,\eta\,\ell}(R^2 - r^2)2\,\pi\,r\,dr. \tag{1.7}$$

Assuming that the double layer is thin in comparison to the radius of the capillary and using Poisson's equation for $q$, the integral can be performed and yields (*Evans and Wennerström*, 1999)

$$I_s = \frac{\pi\,\epsilon_f\,\epsilon_0\,\Delta p\,R^2\,\zeta}{\eta\,\ell}, \tag{1.8}$$

where $\epsilon_f$ is the permittivity of the fluid, $\epsilon_0$ is the permittivitty of free space and $\zeta$ is the potential at the slip plane described earlier.

The streaming current gives rise to a potential difference between the two flasks and this potential difference creates a backflow current termed conduction current. Assuming that the walls of the capillary are non-conductive, this current must travel through the solution and thus is simply described by Ohm's law

$$I_c = \pi\,R^2\,\sigma_f\,\frac{\Delta\psi}{\ell} \tag{1.9}$$

where $\sigma_f$ is the conductivity of the fluid. By conservation of charge, the conduction current $I_c$ is equal to the streaming current $I_s$ but is flowing in the opposite direction (i.e. $I_s + I_c = 0$). We can combine Equations 1.8 and 1.9 to obtain the Helmholtz-Smoluchowski equation

$$\frac{\Delta\psi}{\Delta p} = \frac{\epsilon_f\,\zeta}{\eta\,\sigma_f}. \tag{1.10}$$

The importance of the $\zeta$ potential and the fluid conductivity $\sigma_f$, both functions of the concentration of electrolyte in solution, is evident in Equation 1.10. The assumption that only the solution contributes to the conduction current has removed the geometric terms and thus the radius and the length of the capillary do not influence the electrokinetic coupling.

Obviously, the assumption that only the solution is conductive may not always hold true, and in cases where the concentration of electrolyte is low, the surface conductivity of the capillary can play an important role. The conduction current flowing along the solid surface of a cylindrical capillary $I_{cs}$, assuming negligible thickness, is

$$I_{cs} = 2\,\pi\,R\,\sigma_s \frac{\Delta\psi}{\ell}, \tag{1.11}$$

where $\sigma_s$ is the surface conductance. Equation 1.10 can be modified by assuming that the streaming current flows in the opposite direction to the conduction currents (i.e. $I_s + I_{cs} + I_c = 0$) and becomes

$$\frac{\Delta\psi}{\Delta p} = \frac{\epsilon_f\,\zeta}{\eta\,(\sigma_f + \frac{2\,\sigma_s}{R})}. \tag{1.12}$$

In addition to streaming potentials that exist in fully saturated sediments, it is possible for streaming potentials to exist in sediments that are only partially saturated. Recently, *Revil et al.* (2007) extended the model proposed by *Revil and Linde* (2006) for streaming potentials to include unsaturated porous materials under two-phase flow conditions. In their derivation it was assumed that the pore space is filled with a wetting and a non wetting phase; both of which are assumed to be continuous at the scale of a representative elementary volume of the porous media. While the wetting phase in their model was assumed to be water, the non-wetting

phase was assumed to be electrically insulating and immiscible with the wetting phase (e.g. air or oil). *Revil et al.* (2007) derived the macroscopic governing equations by volume averaging Ampère's law, together with the Nerst-Plank and Stokes equations written at the pore scale.

The results from the numerical simulation based on this model presented by *Revil et al.* (2007) demonstrate that the relative streaming potential coupling coefficient, which is the streaming potential coupling coefficient at a given saturation divided by the streaming potential coupling coefficient at full saturation, depends on the water saturation, the material properties and the saturation history of the medium. *Revil et al.* (2007) also compared the predictions made with this model to laboratory experiments conducted on four dolomite samples and found very good matches between measurements and prediction.

### 1.3.3   Conceptual model for electrokinetic seismoelectric effects

The streaming currents described in the previous section explain how an electric potential is generated when a pressure gradient causes fluid to flow and disturb the electric double layer that forms at the solid/liquid interface in a capillary. This is a good starting point to understand how electrokinetic seismoelectric signals are generated in porous media, but a few distinctions must be made.

The streaming currents described earlier are those for a system at steady state, that is the potential difference generated by a steady fluid flow through a capillary. This is not the case for electrokinetic seismoelectric signals, since a transient pressure pulse is applied to the system. For this discussion, let us consider a compressional wave, also called a P-wave. As shown in Figure 1.3 (a), the seismic wavelet has regions

of maximum compression and maximum expansion separated by half the seismic wavelength. The solid and the fluid phases undergo different accelerations from the pressure gradient and therefore the two phases move relative to one another. If the fluid is accelerated at a different rate than the solid (i.e. $\ddot{u}_f \neq \ddot{u}_s$ in Figure 1.3 (b)), less fluid will be present in a defined reference volume and therefore less counterions to balance the surface charge of the solid which will dominate in that region. The inverse occurs in the region of expansion, which becomes richer in counterions and therefore dominated by the charge of the counterions.

Electric fields perpendicular to the wavefront and internal to the seismic wave arise from this charge separation which in turn gives rise to conduction currents. The conduction current in a homogeneous media exactly balances the streaming current and therefore no magnetic fields exist and the electric field is local to the seismic wave (*Haartsen and Pride*, 1997) as depicted in Figure 1.4. This can also be demonstrated by considering a pair of charged spherical caps for which the field is entirely confined between the caps (*Butler et al.*, 1996). At the instant in time just after the shot, depicted in Figure 1.4 (a), the seismic wave and the associated co-seismic electric field have not reached the receivers yet and therefore the measured potential difference is zero. At a later instant in time, depicted in Figure 1.4 (b), the seismic wave and the co-seismic field have reached the receivers and the field at those receivers is non-zero and of opposite polarity on either side of the shot. On the left hand side of the shot, the negative and positive portion of the co-seismic field coincide with the negative and positive electrodes of the receiver respectively, which leads to a positive voltage being measured. On the right hand side of the shot, the negative and positive portion of the co-seismic field coincide with electrodes of the opposite polarity such that the voltage being measured is negative.

(a)



(b)
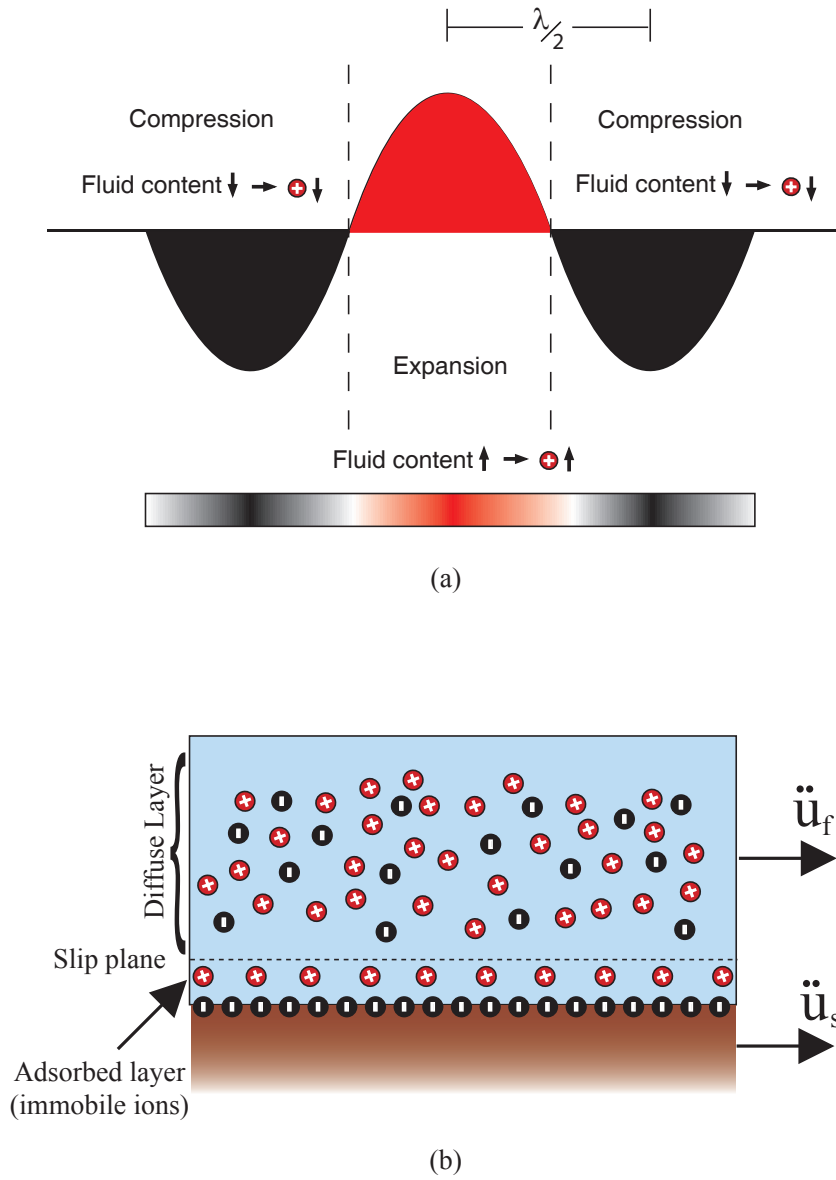
Figure 1.3: Compressional seismic wave (a) and associated regions of compression and expansion that cause, at pore scale (b), differential acceleration between the pore fluid ($\ddot{u}_f$) and the solid grain ($\ddot{u}_s$)
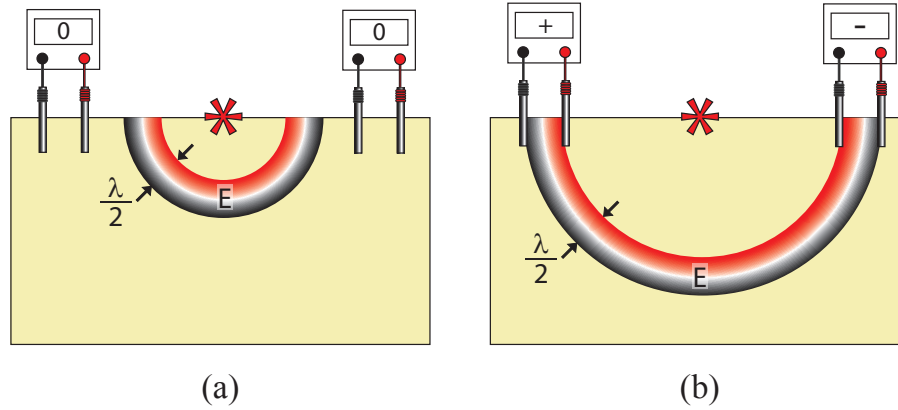
Figure 1.4: Conceptual illustration of the co-seismic signal proposed by *Butler et al.* (1996). The potential difference before the seismic wave reaches the receivers (a) is everywhere 0. Once it reaches the receivers (b), the potential difference will have opposite polarity on either side of the shot.

The balance between the conduction current and the streaming current that exists for the co-seismic wave can be broken by distorting the charge distribution associated with the wavefront. This break in symmetry is caused when the wavefront encounters a heterogeneity in either mechanical and/or electrical properties (e.g. acoustic impedance, permeability, conductivity, $\zeta$ potential or pore fluid type). To illustrate this concept, *Butler et al.* (1996) considered a perfect seismic reflector interface as depicted in Figure 1.5. The dynamic current imbalance at the interface results in a localized charge separation across the interface, which takes shape as the wavefront continues to impinge upon the interface. According to *Garambois and Dietrich* (2002), the source zone at the interface corresponds to the first Fresnel zone of the reflector. This lens shaped region depicted in Figure 1.5 constitutes a multi-polar response which has a strong dipole moment that often dominates the farfield

(a)                                                    (b)
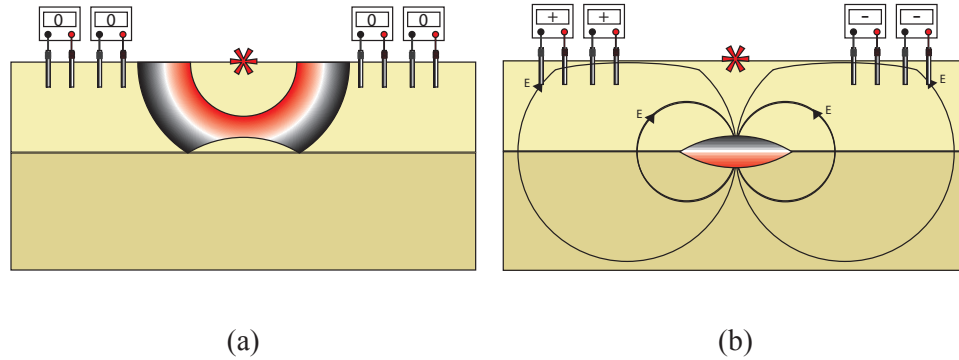
Figure 1.5: Conceptual illustration of the reflected charge distribution as a superposition of two signals as proposed by *Butler et al.* (1996). In (a), the co-seismic signal has not reached the receivers yet and therefore the potential difference measured from the co-seismic is 0. The contribution of the interfacial signal formed at the interface by the distortion of the co-seismic wavefield generates a signal that arrives simultaneously at all receiver positions and has reversed polarity on either side of the shot.

response (*Thompson and Gist*, 1993; *Butler*, 1996; *Butler et al.*, 1996; *Haartsen and Pride*, 1997).

Another distinguishing attribute of the interfacial signal is that it is not bound within a seismic wave and therefore it propagates at electromagnetic velocities. For all intents and purposes, the travel time for this signal is therefore insignificant in terms of the seismic time scale and it will reach all the receivers at the same time, at approximately the one way travel time to the interface, as shown in Figure 1.6.

The last attribute of the interfacial signal is the inversion of the polarity on either side of the shot, similar to the co-seismic signal discussed earlier. This polarity reversal arises because the electric field measured on either side are polarized in opposite direction.
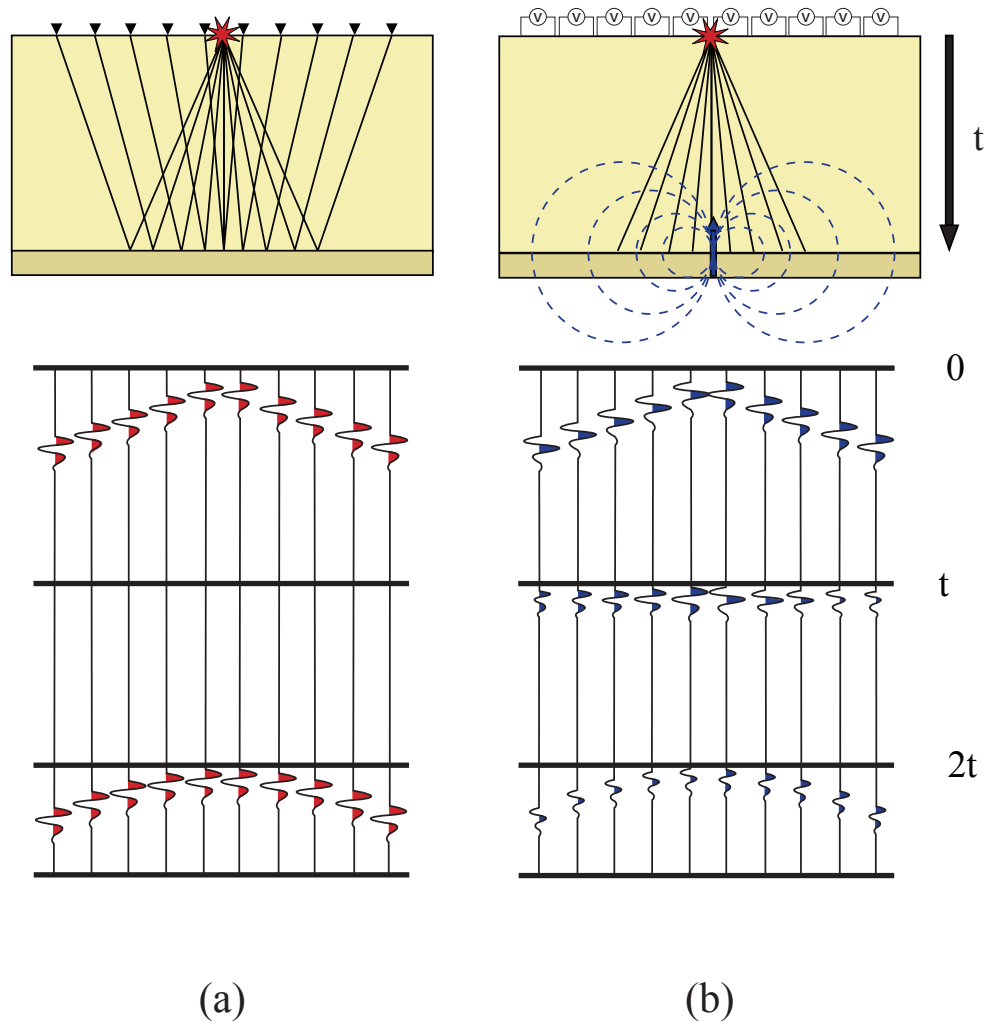
Figure 1.6: Illustration of expected shot records for surface seismic (a) and seismo-electric (b) experiments
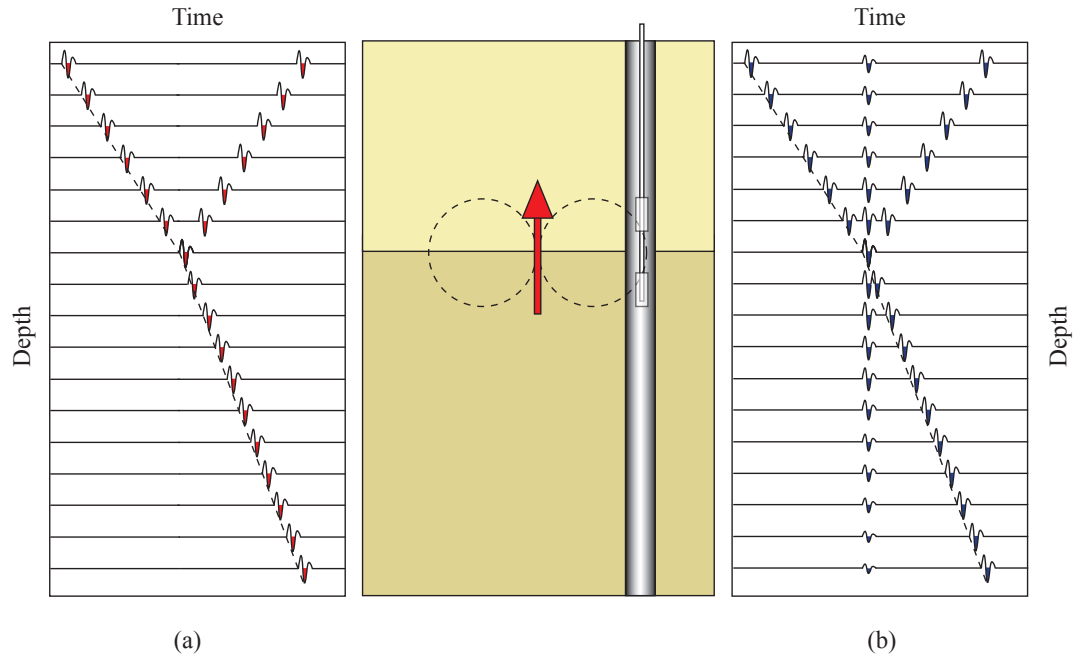
Figure 1.7: Illustration of expected vertical seismic (a) and seismoelectric (b) profiles

Seismoelectric records are thus made of two contributing parts, the co-seismic signal and the interfacial signal and therefore a composite signal can be obtained by adding both contributions. Figures 1.6 and 1.7 show comparisons between the idealized seismic and seismoelectric shot records that would be expected with receivers on surface and in a borehole respectively. Both exhibit co-seismic and interfacial signals.

### 1.3.4 Electrokinetic coupling in saturated porous media

The idea of *Ivanov* (1940) that electrokinetic coupling may be at the source of his field observations inspired *Frenkel* (1944) to devise a theory to explain the phenomenon. His first observation was that, according to the Helmholtz-Smoluchowski Equation (Equation 1.10), the fields measured by *Ivanov* (1940) should be larger than what was measured. He explained, however, that the Helmholtz-Smoluchowski equation was derived for steady flow through capillary tubes and thus could not adequately describe the conditions under which the seismoelectric signals are generated. While the capillary is rigid and represents an invariable pore, seismoelectric signals are generated by the propagation of seismic waves with periodical compression and expansion of both particles and pore space and the fluid present in the pore space. *Frenkel* (1944) further explained that the relaxation time of the system for these rapid vibrations must be taken into consideration. The only electrokinetic seismoelectric phenomenon to be observed at this point was the co-seismic effect and therefore the theory was only derived to explain that signal.

Before he could derive the transfer function for the co-seismic, *Frenkel* (1944) had to derive a theory for the propagation of elastic waves in saturated porous media since Biot's theory (*Biot*, 1956a) would only be published twelve years later. His derivation led him to postulate the existence of a fast and a slow compressional wave. This derivation by *Frenkel* (1944) is often overlooked in the literature and credit is attributed to *Biot* (1962) for deriving the equations that bear his name. According to *Pride and Garambois* (2005), the derivation of *Frenkel* (1944) would have allowed him to obtain nearly identical equations to those of *Biot* (1956a,b), if not for two mistakes in his derivation. The first mistake was the inclusion of an extraneous fluid-pressure gradient in his force balance equation. The second mistake was an

incorrect summation that prevented him from properly identifying the poroelastic compressibility moduli (*Pride and Garambois*, 2005).

*Neev and Yeatts* (1989) extended the theory of *Biot* (1956a) for elastic wave propagation in fluid saturated poroelastic media to include the electrokinetic effects of streaming potential and electro-osmosis in the low-frequency domain, assuming quasi-static conditions. This was done by adding terms to the equations of motion (*Biot*, 1956a, Equations (6) and (7)) to account for the electric forces acting upon the macroscopic charge densities of the solid and fluid phase. They derived a solution for the propagation of plane waves in homogeneous poroelastic media and showed that an electrical potential accompanies the fast and slow compressional waves. Their results show that no seismoelectric signals are associated with transverse waves (shear waves). *Neev and Yeatts* (1989) concluded that the mechanical motion is not affected by the electromechanical coupling because it is a second order effect and that the relative motion of the solid and the fluid is determined mostly by: viscosity of the fluid, the electrical conductivity and the electrokinetic coefficient ($\zeta$ potential). In subsequent work, *Butler* (1996) pointed out several typographical errors in the article by *Neev and Yeatts* that make the development of their theory difficult to follow. He presented a list of corrections but confirmed that the conclusions and figures presented in *Neev and Yeatts* (1989) are correct despite the typographical errors. In his work, *Butler* (1996) also derived a transfer function (Equation 3.1) based on the work of *Neev and Yeatts* (1989) that relates the electric field to the particle velocity.

*Pride* (1994) made an important contribution by deriving a theory for electrokinetic coupling in homogeneous saturated media, starting from first principles, by considering the underlying constituent properties of packed solid grains and the saturating electrolyte of porous media. In the motivation for this work, *Pride* explained

that the Helmholtz-Smoluchowski equation used by *Frenkel* (1944) assumed that the net electrical current is zero everywhere (i.e. $I = I_c + I_s = 0$). For time-varying flow, however, this is erroneous and the full set of Maxwell's equations should be used. According to *Pride* (1994), the results obtained by *Neev and Yeatts* (1989), which conclude that shear waves do not generate electromagnetic disturbances, is also erroneous, because shear waves generate a divergence-free streaming current, which acts as a source in Ampère's law and thus demonstrates further that models describing electrokinetic coupling must make use of the full set of Maxwell's equations.

*Pride* (1994) obtained his macroscopic-governing equations by volume averaging the microscopic equations that describe the electromagnetic and mechanical behavior at the pore and grain scale (i.e. Maxwell and conservation of linear momentum equations written at the pore and grain scale). The theory he derived is based on two postulates: (1) the surface charge density adsorbed on the solid grain is uniform and (2) the net charge in a volume of porous material is zero prior to the arrival of a disturbance.

A series of simplifying/limiting assumptions were made before deriving the model. The first was that the input to the model is linear so that superposition can be used. The second was that the fluid was limited to an ideal electrolyte. The third was that the solid grains and the constitutive laws were assumed to be isotropic and the fourth was that there was no wave scattering from individual grains. The later is true if the wavelength of the disturbance $\lambda$ is much greater than the grain size, which for solid particles as big as 1 mm, means that the frequency content of the disturbance must be less than 1 MHz. The fifth and final assumption was that the electrical double layer is thin in relation to the geometrical dimensions of the solid particle. *Pride* (1994) suggests that this assumption is justified because the

concentration of the most dilute electrolyte likely to be encountered in pores is $10^{-4}$ mol/L and thus using Equation 1.5, a monovalent electrolyte at room temperature will have a Debye length of $3 \times 10^{-8}$ m, which is four orders of magnitude smaller than typical sand grains (radii $\approx 10^{-4}$ m) and two orders of magnitude smaller than most clays (length $\approx 10^{-6}$ m). This enabled *Pride* (1994) to model the electric double layer between the solid and liquid phase as a plane surface, which simplified the boundary value problem.

The resulting macroscopic governing equations obtained by *Pride* (1994) are as follows:

$$\nabla \times \boldsymbol{E} = i\,\omega\,\boldsymbol{B}, \tag{1.13}$$

$$\nabla \times \boldsymbol{H} = -i\,\omega\,\boldsymbol{D} + \boldsymbol{J}, \tag{1.14}$$

$$\nabla \cdot \boldsymbol{\tau_B} = -\omega^2 \left[ \rho_B\,\boldsymbol{u_s} + \rho_f\,\mathbf{w} \right], \tag{1.15}$$

$$\boldsymbol{J} = \sigma(\omega)\,\boldsymbol{E} + L(\omega) \left[ -\nabla p + \omega^2\,\rho_f\,\boldsymbol{u_s} \right], \tag{1.16}$$

$$-i\,\omega\,\mathbf{w} = L(\omega)\,\boldsymbol{E} + \frac{k(\omega)}{\eta} \left[ -\nabla p + \omega^2\,\rho_f\,\boldsymbol{u_s} \right], \tag{1.17}$$

$$\boldsymbol{D} = \epsilon_0 \left[ \frac{\phi}{\alpha_\infty}(\epsilon_f - \epsilon_s) + \epsilon_s \right] \boldsymbol{E}, \tag{1.18}$$

$$\boldsymbol{B} = \mu_0\,\boldsymbol{H}, \tag{1.19}$$

$$\boldsymbol{\tau_B} = \left( K_G\,\nabla \cdot \boldsymbol{u_s} + C\,\nabla \cdot \mathbf{w} \right) \boldsymbol{I} + G_{fr} \left[ \nabla \boldsymbol{u_s} + \nabla \boldsymbol{u_s}^T - \frac{2}{3} \nabla \cdot \boldsymbol{u_s}\,\boldsymbol{I} \right], \tag{1.20}$$

$$-p = C\,\nabla \cdot \boldsymbol{u_s} + M\,\nabla \cdot \mathbf{w}, \tag{1.21}$$

where $\boldsymbol{E}$ is the electric field strength vector, $\boldsymbol{B}$ is the magnetic flux density vector, $\boldsymbol{H}$ is the magnetic field strength vector, $\boldsymbol{D}$ is the electric flux density vector, $\boldsymbol{J}$ is the current density vector, $\boldsymbol{\tau_B}$ is the bulk tensor vector (i.e. a combination of the

averaged fluid tensor vector $\boldsymbol{\tau_f}$ and averaged solid tensor vector $\boldsymbol{\tau_s}$), $\boldsymbol{u_s}$ is the particle displacement, $\mathbf{w}$ is the relative grain/fluid displacement, $\rho_B$ is the bulk density, $\rho_f$ is the fluid density, $\sigma(\omega)$ is the conductivity of the material, $L(\omega)$ is electrokinetic coupling coefficient, $p$ is the pore fluid pressure, $k(\omega)$ is the hydraulic permeability, $\eta$ is the fluid viscosity, $\epsilon_0$ is the electric permittivity of free space, $\phi$ is porosity, $\alpha_\infty$ is the tortuosity, $\epsilon_f$ is the electric permittivity of the fluid, $\epsilon_s$ is the electrical permittivity of the solid, $\mu_0$ is the permeability of free space, $G_{fr}$ is the grain framework shear modulus and $\boldsymbol{I}$ is the identity matrix. The undrained bulk modulus, $K_G$, and the other poroelastic coefficients $C$ and $M$ are written in terms of the bulk modulus of the drained framework $K_{fr}$ and the bulk modulus of the solid and fluid ($K_s$ and $K_f$ respectively):

$$K_G = \frac{K_{fr} + \phi\, K_f + (1 + \phi)\, K_s\, \Delta}{1 + \Delta}, \tag{1.22}$$

$$C = \frac{K_f + K_s\, \Delta}{1 + \Delta}, \tag{1.23}$$

$$M = \frac{1}{\phi}\, \frac{K_f}{1 + \Delta}, \tag{1.24}$$

where, $\tag{1.25}$

$$\Delta = \frac{K_f}{\phi\, K_s^2}\, \left[ (1 - \phi)\, K_s - K_{fr} \right]. \tag{1.26}$$

The two equations of most interest in explaining seismoelectric coupling are the transport Equations (Equation 1.16 and Equation 1.17), where the electrokinetic coupling coefficient $L(\omega)$ is present. By setting the electrokinetic coupling coefficient to zero, Equation 1.16 simply becomes a statement of Ohm's law that relates the electric current to the conductivity of the medium and the electric field applied. In a similar fashion, setting $L(\omega)$ to zero in Equation 1.17 reduces the equation to Darcy's

Law for fluid flow in a porous medium modified for the fact that the fluid and the solid components are both in motion. *Pride*'s theory was the first to recognize the frequency dependence of the electrokinetic coupling coefficient, the conductivity and the hydraulic permeability. A distinction was made between low frequency viscous flow and high frequency inertial flow with the transition frequency, $\omega_t$, being given by

$$\omega_t = \frac{\phi}{\alpha_\infty k_0} \frac{\eta}{\rho_f} \qquad (1.27)$$

where $\phi$ is the porosity, $\alpha_\infty$ is the tortuosity, $k_0$ is the DC permeability, $\eta$ is the fluid viscosity and $\rho_f$ is the fluid density. *Pride* suggested that an estimate of the transition frequency can also be written in terms of pore radius such that the transition frequency, $f_t$, is given by

$$f_t \approx \frac{\eta}{2\,\pi\,\rho_f\,R^2} \qquad (1.28)$$

where $\eta$ is the fluid viscosity, $\rho_f$ is the fluid density and $R$ is the pore radius. Assuming pore space filled with water and a typical pore radius $R$ of $10^{-5}$ m, $f_t \approx 2$ kHz which is greater than the achieved bandwidth in field measurements and therefore we can expect that the low frequency assumption should apply when trying to simulate field data.

A few years later *Pride and Haartsen* (1996) derived the governing equations and the boundary conditions that hold at interfaces for electrokinetic coupling in anisotropic and heterogeneous porous material. They obtained solutions for a plane-wave and a point-source excitation in an isotropic and homogeneous wholespace.

A new quasi-static electrokinetic coupling model for saturated microporous media has recently been proposed by *Revil and Linde* (2006). This model differs

from that of *Pride* (1994) in that the thickness of the double layer is assumed to be of the same scale as the pore space and thus the assumption of a thick double layer is made. *Revil and Linde* (2006) point out that this model applies for all materials with microporosity and especially for clay-rich materials. Although the solid is assumed to be non-conductive, as in *Pride* (1994)'s case, they considered the Stern layer to be part of the solid phase, and therefore the solid phase has an intrinsic conductivity that they call the surface conductivity. The linear governing equations derived by *Revil and Linde* make use of the excess electrical charge in the pore space to model electrokinetic processes instead of the $\zeta$ potential. *Revil and Linde* used similar volume averaging techniques as *Pride* (1994) to average the Nerst-Planck and Navier-Stoke equations written at the pore scale for the fluid phase in order to derive the macroscopic governing equations that describe the transport of ions and water. All of the material properties of the governing equations depend solely on the permeability and electrical formation factor, which are two fundamental textural parameters used to describe the topology of the fluid phase in the porous media.

## 1.4  Review of previous experimental studies

Since the 1930s, at least four distinct conversion mechanisms have been identified (*Russell et al.*, 1997) and fall under the umbrella term seismoelectric: (1) the modulation, by seismic stress, of resistivity in a volume of Earth through which steady currents flow, (2) seismically induced electrokinetic effects analogous to streaming potentials, (3) piezoelectric effects and (4) highly nonlinear processes that generate high audio and radio frequency impulsive responses in sulfides. The seismoelectric signals of interest in this work are of the second type (i.e. electrokinetic origin) and thus the

other conversion mechanisms are only briefly discussed to offer a historical context to the conversion mechanisms of interest. For readers interested in the other conversion mechanisms more information can be found in *Russell et al.* (1997), *Kepic et al.* (2001) and *Neishtadt et al.* (2006).

In the early literature, the term seismoelectric and electroseismic are often used interchangeably. This can be a source of confusion and thus it is important to explain the evolution of the techniques and keep this fact in mind when researching literature on seismoelectric methods. For clarity, this document will use the naming convention that seismoelectric signals are those that arise from the conversion of a seismic wave into EM fields. The term electroseismic will be reserved for the conversion of EM fields into seismic waves (e.g. *Thompson et al.*, 2007). This naming convention has slowly emerged in the more recent literature and there seems to be a growing consensus amongst researchers that this terminology helps to make the distinction between the two different methods of excitation.

## 1.4.1 Resistivity modulation

The first seismoelectric method to be proposed was the modulation of steady voltages in the Earth by seismic stress which is also known as the J-effect in the Russian literature (*Ivanov*, 1949). In a patent document, *Blau and Statham* (1936) describe an invention that samples a greater volume of earth than a seismograph and should therefore alleviate some of the problems caused by surface weathering. They also point out that the resistivity modulation that occurs at depth should be sensed on surface before the surface waves reach the sensors and hence allow separation of the surface waves and reflections.

*Thompson* (1936) is the first to report such seismoelectric measurements in the scientific literature. A battery connected to the primary winding of a transformer is used to inject a steady current to the ground via two grounded electrodes. The transformer is used to separate the modulated signal from the direct current applied to the electrodes. Since the modulated signal is time dependent it is sensed by the secondary winding of the transformer while the direct current of the battery does not induce a response (given that the core of the transformer is not driven to saturation). *Thompson* (1936) quickly discovered that noise sources limit the ability to make seismoelectric measurements. The two sources of noise he identifies are (1) contact impedance, which he solves partially by wetting the soil with a salt solution, and (2) possible telluric currents, which he shields with a three electrode arrangement. He also notes that the modulated signal is, in great part, generated at the location where the electric gradient is the greatest (i.e. at the electrodes) and thus does not integrate the seismic disturbance uniformly. Later, *Thompson* (1939) uses inductive loading in a test circuit to demonstrate that the signal is generated by resistivity modulation and not only by electrode surface effects.

It is interesting to note that although telluric currents are often discussed as a potential source for the production of seismoelectric signals due to resistivity modulation, in practice, the experiments reported in the literature always use a direct current source applied to the ground via grounded electrodes. The possibility to modulate strong telluric currents still exists, but has not been reported in the literature except for *Dupuis et al.* (2007), where it could explain the strong non-inverting simultaneous signal observed at early times in the shot-gathers. It is also interesting that no experiments have reported seismoelectric signals related to the modulation by seismic stress of the ground currents associated with the power grid, which constitute a

strong noise source in making electrical measurements. It is conceivable that these currents could be modulated and produce seismoelectric signals. The polarity of the simultaneous signal observed for individual shot records would be similar to what is expected for telluric currents (i.e. non-inverting on either side of the shot) but would depend on the phase of the powerline currents at the instant in time when they are modulated by the seismic stress. Since seismic sources are generally not synchronized to the power grid, the instant in time when the seismic stresses are applied should modulate different part of the alternating current that flows in the ground.

The last systematic investigation of resistivity modulation was reported by *Long and Rivers* (1975) who used a Wenner array to try to generate signals from deeper layers. They observed that the signals measured resembled most compressional and Rayleigh waves.

## 1.4.2   Electrokinetic coupling

### 1.4.2.1   Surface experiments

The seismoelectric mechanism of interest in this work was first reported by *Ivanov* (1939). He named the seismoelectric effect observed the E-effect in order to differentiate it from the earlier reported seismoelectric effect, which he called the J-effect. The E-effect is different from the J-effect in that it is not necessary to inject current in the ground to observe the signal. To confirm that the signal he observed is not modulation of telluric currents, he detonated explosives on opposite sides of the electrodes and observed that the polarity of the signal changed with shot position. This characteristic does not fit the model of the resistivity modulation, since compression of the ground by a seismic wave arriving beneath the electrodes should change resistivity the same way, regardless of the direction from which the

wave has travelled. He also demonstrated that the observed electric signal was not related to the vibration of the electrode by varying their mass and observing that the signal was independent of the mechanical vibration of the electrodes. As an additional confirmation, he observed that the E-effect often preceded the seismic wave and thus existed prior to any vibration of the electrodes. At the end of the article, *Ivanov* cautions the reader that these effects have only been observed in the Bashkir district in the former USSR, and that they were only observed above the background noise when large explosive charges were used, which limits their usefulness.

The following year, *Ivanov* published a second article (*Ivanov*, 1940) in which he presented further field results and explained some of the potential origin of the E-effect which he also called seismoelectric effect of the second kind. In his experiments, only one channel was recorded which made it very difficult to determine the origin of the signal since electric fields from spherics are often similar in character to the E-effect. Attempts at subtracting a remote reference signal and to use the three electrode method proposed by *Thompson* (1936) failed because of localized contact impedance mismatch. In the discussion of the results, *Ivanov* dismissed piezoelectricity to explain the signals measured and proposes instead that the signal may be of electrokinetic origin.

*Martner and Sparks* (1959) were the first to observe interfacial seismoelectric signals thought to be electrokinetic in origin. In their first experiment, shots were fired at varying depths and seismoelectric signals were measured by electrical receivers on surface. They observed what they called an "electroseismic pulse" (i.e. interfacial signal) that was generated in the subsurface and arrived at surface before the first seismic arrival. In a second experiment, explosives were detonated in deep shot holes, while the seismoelectric signals were measured by a single electrode placed in

a borehole and referenced to the surface. Based on their observations, *Martner and Sparks* (1959) concluded that the seismoelectric interfacial signal was generated at the base of the weathered layer. This led them to propose that the difference in arrival time between a critically refracted P-wave and the seismoelectric signal be used to determine the thickness of the weathered zone.

During the 1960s, seismoelectric methods were tested to determine if they were effective tools for detecting nuclear detonations. The experiments of *Zablocki and Keller* (1961) and *Broding et al.* (1963) concluded that geophones and seismometers are more sensitive and easier to use over wide ranging surficial conditions.

During the 1970s and 1980s, Russian scientists continued their efforts to develop seismoelectric methods as a tool for mineral exploration. The experiments and advancements made by the Russians to use piezoelectric and electrokinetic phenomena during this time are described by *Neishtadt et al.* (2006). In the west, seismoelectric methods seemed to fall out of favor until the 1990s.

The interest in seismoelectric effects was re-ignited in the western literature by *Thompson and Gist* (1993) who presented results from large scale seismoelectric experiments, where the seismoelectric interfacial signals were used to image interfaces between high permeability water-saturated sands and low permeability shales at depths up to 300 m. They give the first description of the interfacial signal characteristics which should arrive simultaneously at widely spaced receivers, and exhibit the symmetry and amplitude variation of a dipole source located at the interface. They conclude their article by proposing that more efforts be made to develop the seismoelectric and electroseismic methods for shallow exploration and environmental applications.

This field success by *Thompson and Gist* (1993) is soon followed by near-

surface experiments that record interfacial signals from shallow interfaces (*Butler et al.*, 1994, 1996; *Wolfe et al.*, 1996; *Mikhailov et al.*, 1997a). In every case, the interfacial signals appear early in the seismoelectric records. These early signals, however, make it difficult in some cases to distinguish from source related disturbances.

*Butler et al.* (1994, 1996) used seismoelectric on surface and in boreholes to generate a strong interfacial signal from the boundary between road fill and glacial till and used it to image the dipping interface up to 3 m deep. They measured the symmetry and amplitude vs offset characteristics of the signal and proposed a conceptual model for its formation. Interestingly, as was noted by *Martner and Sparks* (1959), they observed that the origin of the interfacial signal was independent of the height of the water table. In later experiments at the same site they used blasting cap sources in boreholes to achieve improved resolution and identified three seismoelectric effects (*Russell et al.*, 1997). They also demonstrated the linearity of the main interfacial effect by using a weight drop source to vary the input energy by a factor of 60 (*Butler et al.*, 1999). *Wolfe et al.* (1996) report an interfacial signal generated at a shallow water table (3 m) in an outwash plain near Yellow Springs Ohio and *Mikhailov et al.* (1997a) report interfacial signals from three interfaces at their test site: (1) top soil-glacial till, (2) water table and the (3) glacial till-bedrock interface. The interpretation of the first two interfacial signals as separate events may be a bit ambitious given the frequency content of the measured wavelet ($\approx$ 100 Hz) and the short separation between the interfaces ($\approx \lambda/3$). *Mikhailov et al.* (1997a) are however the first to compare their measured field data to a full waveform model developed by *Haartsen and Pride* (1997). The top soil-glacial till interface was chosen for simulation and *Mikhailov et al.* (1997a) found a good agreement between the synthetic and the measured signal amplitude (i.e. within an order of magnitude),

even if the amplitude versus offset characteristics of the synthetic and field data did not have the same character.

In their review of seismoelectric effects, *Beamish and Peart* (1998) present an alternative to multi-electrode experiments they call two-channel electrokinetic (EK) sounding. This technique is attributed to *Millar* (1995) and forms the basis of the only commercially available seismoelectric instrument for geophysical exploration. The claimed advantage of the two-channel EK sounding is that interfacial signals can be measured without contamination from surface waves, if the two electrode pairs are in close proximity to the shotpoint (*Beamish and Peart*, 1998; *Beamish*, 1999). Although *Beamish* (1999) acknowledges that the maximum strength of the interfacial signal should occur at a shot-receiver that corresponds to half the depth of the interface, he argues that strong co-seismic signals associated with various seismic wave arrivals (including direct P-waves, and surface waves) pass by the receivers much sooner when they are located close to the shot. There is some merit to this reasoning, but as multi-channel experiments demonstrate (e.g. *Dupuis et al.*, 2007) it is difficult to tell whether signals measured close to the shot are related to interfacial signals, or co-seismic effects, and it is impossible to know with only two channels. Additionally, the signals from electrodes in close proximity to the shot are often discarded, or simply omitted in multi-channel experiments, because they exhibit very strong low frequency signals that may be attributed to the plastic deformation of the ground at the shotpoint. For these reasons, the two-channel EK sounding method has not found wide acceptance in the scientific literature. Most recently, *Kulessa et al.* (2006) used this two-channel EK sounding technique to measure seismoelectric effects in a glacier and inferred that there may have been interfacial signals within the snow pack, and near the dry-wet ice and ice-bed interfaces, at depths of up to 98 m. It is worth

nothing however that they mistakenly conclude that co-seismic signals are in phase on opposite sides of the shot.

*Garambois and Dietrich* (2001) observed interfacial signals attributed to a shallow water table (1.5 m) at their field site but their analysis concentrated on the description of the co-seismic signal associated with a compressional seismic wave for which they derive a transfer function. They observe that the electric field measured by surface dipoles is approximately proportional to the particle acceleration measured with horizontal geophones. With respect to properties of the soil, they note that the transfer function is essentially independent of permeability, but depends strongly on salt concentration (through its effects on electrical conductivity and on the electrokinetic $\zeta$ potential described in Section 1.3) and on the dielectric constant of the fluid. *Garambois and Dietrich* (2001) also caution the reader that the transfer function based on *Pride*'s equations, was derived for saturated media and thus the signals may not match the model completely for the case of partial saturation.

*Strahser et al.* (2007) recently made measurements of seismoelectric signals using three orthogonal dipoles to study the polarization of the seismoelectric signals. They concluded that co-seismic and interfacial signals, as expected from conceptual models, have mostly radial and vertical components although they also may have a transverse component if a layer is dipping in the transverse direction. The argument is made that without recording the transverse component, a thin clay layer may have been overlooked as it did not generate a response in the vertical or radial components. They attribute the weakness of the signal to destructive interference from the top and the bottom of the layer, an idea borrowed from *Fourie* (2003, 2006). Interestingly this result, based purely on the opposing reflectivities of the top and bottom interfaces, contradicts results from full waveform numerical models that predict larger ampli-

tudes for thin layers than for a half-space (*Haartsen and Pride*, 1997; *Haines and Pride*, 2006). In fact, *Haartsen and Pride* (1997) predict that interfacial signals can exist free from any acoustic impedance variation. As an example, they show that a contrast in the conductivity alone can lead to a signal which is ten times larger than a contrast in seismic impedance.

Given the difficulty in measuring interfacial signals, *Haines et al.* (2007) conducted an interesting experiment which allowed them to create their own interfaces and measure interfacial signals using what they call the fan-geometry. Two trenches were dug, lined with a plastic membrane and filled with sand. Shot points and receivers were placed on either side of the trenches in order to provide separation between the arrival times of co-seismic and interfacial signals. During these experiments, *Haines et al.* (2007) also observed what they called the direct field predicted by *Pride and Haartsen* (1996). *Haines et al.* (2007) explain that the direct field is created at the shotpoint because of the asymmetry of the impact (i.e. with a impact source like a sledgehammer). They also comment on the Lorentz field of the hammer plate moving in the earth's magnetic field, and suggest that it can be a source of interference in records by obscuring any interfacial signals that occur at early times in the record. The explanation of this interference signal is not completely satisfactory since placing a simple piece of cardboard between the hammer and plate will generally eliminate the signal.

### 1.4.2.2   Laboratory experiments

The early laboratory experiments that relate to seismoelectric effects of electrokinetic origin are summarized in *Parkhomenko* (1971), although the bibliography has several typographical mistakes that make it difficult to find copies of the original

work cited.

According to *Parkhomenko* (1971), *Mauchly* (1918) was the first to observe the seismoelectric effect in the laboratory, while he was attempting to understand the pressure and temperature effects in earth current measurements. Sandy soil was packed in a glass tube and (amalgamated zinc) electrodes were placed at the top and bottom of the test tube. *Mauchly* observed a potential difference between the electrodes and a reversal of the polarity when the test tube was flipped upside down. He commented that this effect was observed when the material was neither completely dry nor fully saturated. Experiments by *Antsyferov* (1958, 1962) using an active ultrasonic source found that the amplitude of the seismoelectric signal was dependent on the water saturation of a slate sample.

Further experiments by *Parkhomenko and Chien-San* (1964) and *Parkhomenko and Gaskarov* (1971) corroborate the amplitude dependence of seismoelectric signals on water content, and demonstrate that there are no seismoelectric signals generated when the samples are completely dry. The seismoelectric field increases rapidly with the initial introduction of moisture in the sample, but further moisture increments yield more modest increases. The observed abrupt increase in seismoelectric effect at low water saturation is intuitively satisfying because the electrical double layer can only be formed if counterions of the pore fluid are present. More recent Russian literature (*Fedotov et al.*, 2004) explains this moisture dependence in soils by the presence of an organomineral gel layer made of colloid particles that coats the solid grains. In soils that are formed through weathering and contain organic compounds, the gelling is reported to be especially pronounced. *Fedotov et al.* (2004) explain that the organomineral gel forms a network that can affect properties of the soil such as mechanical properties, salt diffusion rates, and electrokinetic/seismoelec-

tric response. This organomineral gel network can be destroyed by drying the soil samples completely and can be restored by adding distilled water until the water content reaches its natural level. Once enough moisture is present for the electrical double layer to form, increases in water content may actually lead to a decrease in seismoelectric amplitude as observed by *Parkhomenko and Gaskarov* (1971) in one of their limestone samples when the water saturation was increased beyond 60%.

Following the derivation of the governing equations for seismoelectric effects in saturated porous media by *Pride* (1994) and *Pride and Haartsen* (1996), several scientists conducted laboratory experiments to verify the model.

*Zhu et al.* (1999) made measurements at ultrasonic frequencies in water saturated borehole models constructed from natural rocks (sandstone and slate) and artificial materials (lucite and glued sand). The receivers and the source were placed in the borehole model and both seismoelectric and electroseismic experiments were made. *Zhu et al.* (1999) concluded that the amplitude and frequency of the seismoelectric signals were related not only to the seismic wave, but also to the material properties, permeability and conductivity. They also found that electric sources placed either in the borehole, or on the borehole wall, induced Stonely waves that could be received by monopolar acoustic transducers and that the interface between lucite and glued sand produced an interfacial seismoelectric signal.

In a review of literature, (*Santamarina and Fratta*, 2003) noticed that amplitudes reported in field measurements for co-seismic seismoelectric signals were larger than would be expected using a theoretical model derived by *Debye* (1933). *Santamarina and Fratta* (2003) are aware of *Pride* (1994) and *Neev and Yeatts* (1989), but they elect to use *Debye*'s model instead. This choice may raise questions, however, since the model proposed by *Debye* (1933) was derived to explain the periodically changing

charge densities which may accompany sound waves in solution alone. In this model, the electric field was generated because of the differences in mass of the cations and anions which caused them to move at different rates in the solvent. *Santamarina and Fratta* (2003) noted that the high frequency laboratory experiments support *Debye*'s model and hypothesize that the differences at low frequencies were due to some weakness of the model to predict the EK coupling at these frequencies. *Santamarina and Fratta* devised a "low frequency" laboratory experiment where either a sodium chloride solution or a kaolinite specimen were enclosed in a thin cylindrical volume constructed of a plexiglass ring and capped by disc foil electrodes. The experimental setup was placed inside a chamber where the pressurization of the chamber caused the plate electrodes to seal the cylindrical volume and confine the sample. The sample and the test apparatus were deformed by a mechanical actuator driven by sinusoidal frequency sweep from a signal generator. The frequency was swept from 100 Hz to 10 kHz. The frequency dependence observed by *Santamarina and Fratta* seems to agree with the transfer function derived by *Butler* (1996) which is based on the work of *Neev and Yeatts* (1989), but *Santamarina and Fratta* did not seem to be aware of these previous results.

*Chen and Mu* (2005) designed an experiment in a sandbox made of plexiglass. An ultrasonic piezoelectric transducer was used as a source and platinum electrodes were used in combination with a data acquisition system to measure the seismoelectric signals. The sandbox was filled with quartz sand and sodium chloride solutions with varying concentrations were used in the experiments. The authors found that the amplitude of the co-seismic signal had a strong dependence on electrolyte concentration. At a concentration of 0.3%, the maximum amplitude was observed, while for electrolyte concentrations below and above this point, the amplitudes were smaller.

In a second set of experiments, an oil layer was introduced in the system. Interfacial signals were measured but their data showed a strong DC-bias component that obscured much of the character of the signal. *Chen and Mu* (2005) concluded that seismoelectric methods are sensitive to oil/brine interfaces and therefore should be of interest to the oil industry.

The dependence of the amplitude of the seismoelectric signal on the electrolyte concentration, and therefore the conductivity, was revisited in experiments by *Block and Harris* (2006). Their experimental setup consisted of a cylindrical PVC tube in which medium-grained sand or glass microspheres were saturated with NaCl solutions of varying concentration. Nine Ag/AgCl electrodes were distributed vertically in the column and used to measure the seismoelectric signals. The source was a 100 kHz acoustic transducer driven with 50 kHz sine wave bursts. This source was positioned at the top of the column and was separated from the porous material by $\approx 1$ m of the saline solution. *Block and Harris* observed interfacial signals at a fluid/sediment interface and measured a monotonical decrease of the amplitude of the co-seismic signal with increased electrolyte concentration. This result for microspheres differs from that obtained by *Chen and Mu* (2005) using quartz sand. The numerical model presented by *Block and Harris* (2006), which predicts the amplitude of the co-seismic signal, offered an explanation for the behaviour observed by *Chen and Mu* (2005), and for their own data. The increase in the amplitude of the co-seismic signal with increased electrolyte concentration occurs because the sands have non-negligible surface conductivities. The peak in amplitude occurs when the contributions from surface and pore conduction are approximately equal. *Block and Harris* (2006) concluded that their numerical simulations, based on governing equations derived by *Pride* (1994), show good agreement for a large range of pore fluid conductivities, but that it is

important to have a robust model of the bulk conductivity when the porous media is saturated by weak electrolytes.

In addition to seismoelectric signals associated with P-waves, *Pride* (1994); *Pride and Haartsen* (1996) predicted that seismomagnetic signals should be associated with shear waves. These magnetic fields are weaker than the seismoelectric signals and more difficult to measure because the magnetometers must be completely decoupled from any possible vibration sources that would induce a response from the movement of the magnetometer in the earths magnetic field.

The first experiment that claims the measurement of seismomagnetic signals was performed by *Zhu and Toksöz* (2005), but several instrumental and experimental choices can raise questions about the validity of the results. The experiments were performed in the earth's magnetic field using Hall effect sensors designed for the automotive industry. This device had relatively poor sensitivity (5 mV/Gauss) when considering the measurements attempted and the bandwidth of sensor only extends to 30 kHz, while the measurements were made at 120 kHz. There was no discussion of mechanical decoupling or magnetic shielding from the instruments and a piezo-electric transducer was used as the source. The peak magnetic signal recorded by *Zhu and Toksöz* (2005) converts to magnetic flux densities of approximately 800 nT. This value is much larger than the maximum magnetic field predicted by the numerical model of *Cui et al.* (2007), based on governing equations from *Pride* (1994), that reports expected amplitudes on the order of 12 pT. This means that the large magnetic signal measured by *Zhu and Toksöz* cannot be explained by using equations presented by *Pride* (1994).

*Bordes et al.* (2006) performed their seismomagnetic experiment in a low-noise underground laboratory, where the ambient magnetic noise density was less than

2 fT/$\sqrt{\text{Hz}}$ above 10 Hz. *Bordes et al.* took extra precautions to ensure the mechanical decoupling between the sand column, the pneumatic seismic source and the magnetometers used for the experiment to avoid spurious vibration of the magnetometer. Unfortunately, the results presented by *Bordes et al.* (2006) do not provide information on the magnetic field strength of the seismomagnetic signal observed. The amplitude of the signal is provided in terms of millivolts, but it is impossible to convert these amplitudes to magnetic field strength without more information on the induction magnetometer used in the experiment. The velocity of the signals measured by *Bordes et al.* (2006) confirm that seismoelectric and seismomagnetic signals are generated by compressional and shear waves respectively as predicted by *Pride* (1994) and *Pride and Haartsen* (1996).

### 1.4.2.3   Borehole experiments

While all the early field experiments reported up to this point were made in unconsolidated sedimentary environments, there has also been interest in determining the potential utility of seismoelectric phenomena in fractured rock. Boreholes have been the environment of choice for these investigations.

*Mikhailov et al.* (1997b, 2000) reported measurements of seismoelectric signals generated by Stonely waves in fractured rock boreholes and presented results from corresponding numerical simulations that treat the rock as an equivalent porous medium. *Mikhailov et al.* (2000) concluded that the normalized amplitude of the electrical field induced by the Stonely wave was proportional to the porosity, while the amplitude versus frequency behavior of the electric field was dependent on the permeability of the formation around the borehole. The same year, *Hunt and Worthington* (2000) performed borehole experiments in fracture-dominated rock, where both the

seismic source and electrodes were in the borehole. They observed that the electric field was at its maximum when the electrodes were placed opposite to the fractures and the source was placed a few meters above, suggesting that the signal was not simply related to squirt flow induced in the fractures. The results of *Mikhailov et al.* (2000) and *Hunt and Worthington* (2000) inspired the development of a prototype borehole seismoelectric logging tool that makes use of Stonely waves to determine the permeability of the formation around the borehole (*Singer et al.*, 2005).

## 1.5 Numerical modelling

The important contributions of *Pride* (1994) and *Pride and Haartsen* (1996) made it possible to develop full waveform numerical simulations of seismically-induced electrokinetic effects. Three different approaches (*Haartsen and Pride*, 1997; *Garambois and Dietrich*, 2002; *Haines and Pride*, 2006) have been employed to simulate seismoelectric effects expected from point sources of compressional and shear waves in layered/heterogeneous poroelastic media.

The first full waveform numerical model was proposed by *Haartsen and Pride* (1997). They began by recognizing that the macroscopic equations controlling the coupled electromagnetic and poroelastic wavefields could be decoupled into vertical and horizontal polarized wavefields and then they used a global matrix method to solve simultaneously for all the macroscopic electromagnetic and poroelastic wavefields excited by an explosive point-source in stratified porous media. They simulated three different types of targets and assumed in every case that the displacement currents are negligible relative to conduction currents (i.e. electromagnetic fields are assumed to be diffusive). The first target was a 100 m thick sand layer sandwiched

between two identical half-spaces, that were less porous than the sand layer, but otherwise had the same fluid chemistry and permeability. The results from the numerical simulation showed that the top of the sand layer generates an interfacial signal that is stronger than that generated at the base, which would be too weak to observe at the display gains used. The second target simulated by *Haartsen and Pride* (1997) was the interface between fresh water and brine pore fluids in homogeneous sands. The results from this simulation showed a strong interfacial signal that was 10 times larger than the one observed for the contrast in porosity of the first example. In the final example, *Haartsen and Pride* (1997) proposed to simulate the seismoelectric fields in a vertical seismoelectric profile configuration for a sand reservoir similar to the first example, but where in addition to the porosity being higher than the confining layers, the permeability is 100 times greater and the electrolyte concentration is 1000 times greater. The results of this simulation showed that both the top and bottom of the sand layer generated interfacial signals, but that the very high conductivity of the fluid in the sand layer would make it impossible to observe any seismoelectric signals within it. *Haartsen and Pride* (1997) compared the amplitude characteristics of the interfacial signals obtained from the simulation with a vertical electric dipole situated at the interface as proposed by *Thompson and Gist* (1993). They found that the amplitude of the field generated by the multipolar charge separation generated across the interface in the numerical model had a strong dipole component and as such the amplitude versus offset behaviour predicted by the vertical electric dipole agreed with the results of the full waveform simulation. *Haartsen and Pride* (1997) remarked that the frequency content of the interfacial signal was identical to that of the incident seismic pulse, and thus was higher than the frequency content of the reflection, because the seismoelectric interfacial signal did not suffer from high frequency

attenuation experienced by seismic waves returning to surface through near-surface sediments. Finally, although the results are not shown in their article, *Haartsen and Pride* (1997) discussed another simulation similar to the first target, a sand layer with higher porosity sandwiched between lower porosity layers, but where the thickness of the sand layer was reduced to 1 m. Their simulation showed a reduced response for the seismic reflection, but an enhanced response for the seismoelectric interfacial signal that was twice the amplitude observed for the 100 m thick sand layer. It follows that the higher frequency content of the interfacial signals, combined with the higher amplitudes for thin layers, could make seismoelectric imaging an important tool to resolve thin layers that cannot be suitably resolved by seismic reflection.

A few years later, *Garambois and Dietrich* (2002) adapted a generalized reflection and transmission matrix method designed for elastic wave propagation in layered media to handle coupled seismic and electromagnetic wave propagation in fluid saturated stratified porous media. This approach allows them to compute partial solutions or the complete response. Interfering co-seismic signals can therefore be omitted from the solution to allow one to focus on characteristics of the interfacial signals. The principle of the Fresnel zone for seismic converted waves of *Eaton et al.* (1991) was extended by *Garambois and Dietrich* (2002) to show that the conversion responsible for the interfacial signal occurs at the interface directly under the shot-point and over a zone equivalent to the first Fresnel zone for the P to EM converted wave. For coincident source and receiver they found that the radius of the first Fresnel zone for the P to EM converted wave was approximately 38% greater than for a seismic P-wave primary reflection. As was found by *Haartsen and Pride* (1997), *Garambois and Dietrich* found good agreement between the amplitude characteristics of the interfacial signal of the numerical simulation and that of the far field of a ver-

tical electric dipole positioned at the interface directly below the shotpoint. Signals were found to decay slightly faster with offset for the numerical solution in comparison to the vertical dipole, but the authors attributed this difference to the multipolar response at the interface and the shallow depth of the interface in comparison to the size of the Fresnel zone[1]. The sensitivity analysis performed by *Garambois and Dietrich* (2002) suggests that interfacial signals are particularly sensitive to contrasts in porosity, hydraulic permeability, fluid salinity and fluid viscosity while, being less influenced by contrasts in shear and bulk frame moduli, density, fluid and solid dielectric permittivity, temperature and tortuosity. They concluded that their results show a particular sensitivity to strong permeability and salinity contrasts.

The advent of these numerical simulations has allowed the refinement of our understanding of the mechanism at the interface responsible for the generation of the interfacial signal. In *Thompson and Gist* (1993), the interfacial signal was attributed to the conversion of a portion of the incident seismic wave into a Biot slow wave that distorts the charge distribution of the double layer on the surface grains at the interface. This interpretation however was challenged by the simulation results of *Pride and Garambois* (2002), where the Biot slow wave was actually presented as an important potential source of attenuation of interfacial signals and not as its source. *Pride and Garambois* (2002) compared results of simulations where the Biot slow wave was included, and where it was omitted, and concluded that its omission may lead to overestimating the amplitude of the interfacial signal by as much as an order of magnitude in cases where there was a contrast in elastic properties. In the case of a shear wave, very little energy was converted into the Biot slow wave and thus

---

[1]It is interesting to note that, in contrast, field measurements of a clear shallow interfacial response reported in Chapter 4 of this thesis (*Dupuis et al.*, 2007) decay more slowly with offset compared to the predictions of a vertical dipole model.

the results that omit the Biot slow wave only overestimated the amplitude by 10%. In the case of a salinity contrast, no seismic energy was converted to the Biot slow wave and thus the results with and without the Biot slow wave agreed. These are important results since they may help to explain the stronger response observed by *Haartsen and Pride* (1997) and *Garambois and Dietrich* (2002) for salinity contrast and may indicate that seismoelectric methods are more sensitive to targets that do not have significant energy conversions to Biot slow waves. Interfacial signals are therefore the result of the distortion of the co-seismic seismoelectric signal, rather than the conversion of the incident seismic signal into another elastic wave mode that causes streaming potentials.

The latest numerical model has been proposed by *Haines and Pride* (2006) and makes use of a finite difference algorithm to simulate seismoelectric phenomena in arbitrary heterogeneous porous media — an advance over previous approaches that were limited to the study of horizontally layered (1 D) models. In this approach, the seismic wavefields were computed using the finite difference code and the electrical potential distribution was computed at every time step. The finite difference code provides the opportunity to study arbitrary shaped targets and to better determine the resolving capacity of seismoelectric methods. This approach however seemed to lack the ability of the generalized reflection and transmission matrix method proposed by *Garambois and Dietrich* (2002) to only simulate partial response and thus interfering co-seismic signal are an important source of coherent noise. To alleviate this problem, *Haines and Pride* (2006) proposed to adopt the fan geometry, where receivers were deployed horizontally below the interface. This geometry allowed the interfacial signal, generated at the interface above, to reach the receivers before the direct wave and thus offered good signal separation. In their first example, *Haines and Pride*

(2006) demonstrated that layers that were as thin as $\lambda/20$ have greater amplitude interfacial signals than single interfaces. In their second example, they showed that the response of a laterally restricted layer gave a lower amplitude response in comparison to a layer with infinite lateral extent, but the amplitude distribution remained symmetric about the shotpoint, if the shotpoint was placed directly above the layer. If the shotpoint was offset, however, the peak amplitudes on either side of the shot exhibited asymmetry similar to what is expected from a dipping interface and the ambiguity can only be resolved by using multiple shotpoints. In their last example, *Haines and Pride* (2006) simulated a time lapse survey using vertical seismoelectric profiling experiments. The salinity of the fluid present in a sand channel surrounded by clay was increased over time and the simulated interfacial signal amplitudes were shown to decrease as the salinity in the channel increased. *Haines and Pride* (2006) noted that this sand channel would be difficult to image using conventional geophysical methods. Ground penetrating radar would yield poor results because of the depth of the target and the conductivity of the clays, seismic methods cannot distinguish changes in salinity and the target may be too small to be resolved with borehole tomography.

Although these numerical models have provided us with greater insight in the potential causes for the seismoelectric signals, they all share a common limitation in explaining field results for surface experiments because, they are derived for fully saturated porous media. Most of the experimental datasets in the literature, however, have co-seismic and interfacial signals that are generated, at least in part, in the unsaturated regions above the water table. Future numerical models may incorporate the model proposed by *Revil et al.* (2007) to account for changes in electrokinetic coupling with varying levels of saturation, but will also need to incorporate modifi-

cations to the poroelastic equations to account for the changes in relative fluid flow caused by partial saturation. These developments would prove very helpful to further the development of seismoelectric methods as a hydrogeological tool.

# References

Antsyferov, M. S. (1958), Laboratory reproduction of the seismo-electric effect of the 2nd kind, *Doklady Akademii Nauk SSSR*, *121*(5), 827–829, in Russian.

Antsyferov, M. S. (1962), Electro-seismic effect, *Doklady Akademii Nauk SSSR*, *144*(6), 1295, English translation published in 1964.

Beamish, D. (1999), Characteristics of near-surface electrokinetic coupling, *Geophysical Journal International*, *137*(1), 231–242.

Beamish, D., and R. J. Peart (1998), Electrokinetic geophysics - a review, *Terra Nova*, *10*(1), 48–55, doi:10.1046/j.1365-3121.1998.00160.x.

Berryman, J. G. (2003), Electrokinetic effects and fluid permeability, *Physica B*, *1-4*(338), 270–273, doi:10.1016/j.physb.2003.08.006.

Biot, M. A. (1956a), Theory of propagation of elastic waves in a fluid-saturated porous solid. I. low frequency range, *Journal of the Acoustical Society of America*, *28*(2), 168–178, doi:10.1121/1.1908239.

Biot, M. A. (1956b), Theory of propagation of elastic waves in fluid-saturated porous solid. II. higher frequency range, *Journal of the Acoustical Society of America*, *28*(2), 179–191, doi:10.1121/1.1908241.

Biot, M. A. (1962), Mechanics of deformation and acoustic propagation in porous media, *Journal of Applied Physics*, *33*(4), 1482–1498, doi:10.1063/1.1728759.

Blau, L. W., and L. Statham (1936), Method and apparatus for seismic-electric prospecting, U.S. Patent No. 2,054,067, September 15, 1936.

Block, I. B., and J. G. Harris (2006), Conductivity dependence of seismoelectric wave phenomena in fluid-saturated sediments, *Journal of Geophysical Research*, *111*(B1), doi:10.1029/2005JB003798.

Bordes, C., L. Jouniaux, M. Dietrich, J. P. Pozzi, and S. Garambois (2006), First laboratory measurements of seismo-magnetic conversions in fluid-filled Fontainebleau sand, *Geophysical Research Letters*, *33*(1), doi:10.1029/2005GL024582.

Broding, R. A., S. D. Buchanan, and D. P. Hearn (1963), Field experiments on the electroseismic effects, *IEEE Transactions on Geoscience Electronics*, *1*(1), 23–31, doi:10.1109/TGE.1963.271176.

Butler, K. E. (1996), Seismoelectric effects of electrokinetic origin, Ph.D. thesis, University of British Columbia, Vancouver, BC.

Butler, K. E., R. D. Russell, A. W. Kepic, and M. Maxwell (1994), Mapping of a stratigraphic boundary by its seismoelectric response, in *7th Symposium on the Application of Geophysics to Engineering and Environmental Problems*, pp. 689–699, Environmental and Engineering Geophysical Society.

Butler, K. E., R. D. Russell, A. W. Kepic, and M. Maxwell (1996), Measurement of the seismoelectric response from a shallow boundary, *Geophysics*, *61*(6), 1769–1778, doi:10.1190/1.1444093.

Butler, K. E., S. W. Fleming, and R. D. Russell (1999), Field test for linearity of seismoelectric conversions, *Canadian Journal of Exploration Geophysics*, *35*(1-2), 20–23.

Chapman, D. L. (1913), A contribution to the theory of electrocapillarity, *Philosophical Magazine*, *25*, 475–481.

Chen, B., and Y. Mu (2005), Experimental studies of seismoelectric effects in fluid-saturated porous media, *Journal of Geophysics and Engineering*, *2*(3), doi:10.1088/1742-2132/2/3/006.

Cui, Z. W., K. X. Wang, J. G. Sun, Z. Y. Zhu, G. J. Yao, and H. S. Hu (2007), Numerical simulation of shear-horizontal-wave-induced electromagnetic field in borehole surrounded by porous formation, *Chinese Physics Letters*, *24*(12), doi:10.1088/0256-307X/24/12/045.

Debye, P. (1933), A method for the determination of the mass of electrolytic ions, *Journal of Chemical Physics*, *1*(1), doi:10.1063/1.1749213.

Dupuis, J. C., and K. E. Butler (2006), Vertical seismoelectric profiling in a borehole penetrating glaciofluvial sediments, *Geophysical Research Letters*, *33*(16), doi:10.1029/2006GL026385.

Dupuis, J. C., K. E. Butler, and A. W. Kepic (2007), Seismoelectric imaging of the vadose zone of a sand aquifer, *Geophysics*, *72*(6), A81–A85, doi:10.1190/1.2773780.

Eaton, D. W. S., R. R. Stewart, and M. P. Harrison (1991), The Fresnel zone for P0SV waves, *Geophysics*, *56*(3), 360–364, doi:10.1190/1.1443050.

Evans, D. F., and H. Wennerström (1999), *The colloidal domain: where physics, chemistry, biology, and technology meet*, Wiley-VHC.

Everett, D. H. (1988), *Basic principles of colloid science*, Royal Society of Chemistry.

Fedotov, G. N., Y. D. Tretýakov, A. I. Pozdnyakov, D. V. Zhukov, and E. I. Pakhomov (2004), Effect of the colloidal structure of the organomineral gel on the properties of soils, *Doklady Chemistry*, *394*(1), 13–15.

Fourie, F. (2006), Aspects of the lateral and vertical resolution of surface electroseismic data with implications for groundwater exploration in fractured Karoo rocks, *South African Journal of Geology*, *109*(4), 571–584, doi:10.2113/gssajg.109.4.571.

Fourie, F. D. (2003), Application of electroseismic techniques to geohydrological investigation in Karoo rocks, Ph.D. thesis, University of Free State, Bloemfontein, South Africa.

Frenkel, J. (1944), On the theory of seismic and seismoelectric phenomena in moist soil, *Journal of Physics*, *3*(4), 230–241.

Garambois, S., and M. Dietrich (2001), Seismoelectric wave conversions in porous media: Field measurements and transfer function analysis, *Geophysics*, *66*(5), 1417–1430, doi:10.1190/1.1487087.

Garambois, S., and M. Dietrich (2002), Full waveform numerical simulations of seismoelectromagnetic wave conversions in fluid-saturated stratified porous media, *Journal of Geophysical Research*, *107*(B7), doi:10.1029/2001JB000316.

Gouy, G. (1910), Sur la constitution de la charge électrique à la surface d'un électrolyte, *Journal de Physique*, *4*(9), 457–468.

Haartsen, M. W., and S. Pride (1997), Electroseismic waves from point sources in layered media, *Journal of Geophysical Research*, *102*(B11), 24,745–24,769.

Haines, S. S., and S. R. Pride (2006), Seismoelectric numerical modeling on a grid, *Geophysics*, *71*(6), N57–N65, doi:10.1190/1.2357789.

Haines, S. S., S. L. Klemperer, and B. Biondi (2007), Seismoelectric imaging of shallow targets, *Geophysics*, *72*(2), G9–G20, doi:10.1190/1.2428267.

Helmholtz, H. (1853), Über einige gesetze der vertheilung elektrischer ströme in körperlichen leitern, mit anhwendung auf die thierisch-elektrischen versuche, *Poggendorffs Annalen der Physik und Chemie*, *89*, 211–233.

Hiemstra, T., and W. H. Van Riemsdijk (1990), Multiple activated complex dissolution of metal (hydr)oxyde:A thermodynamic approach applied to quartz., *Journal of Colloid and Interface Science*, *136*(1), 132–150, doi:10.1016/0021-9797(90)90084-2.

Hunt, C. W., and M. H. Worthington (2000), Borehole electrokinetic responses in fracture dominated hydraulically conductive zones., *Geophysical Research Letters*, *27*(9), 1315–1318.

Ishido, T., and H. Mizutani (1981), Experimental and theoretical basis for electrokinetic phenomena in rock-water systems and its application to geophysics., *Journal of Geophysical Research*, *86*(B3), 1763–1775, doi:10.1029/JB086iB03p01763.

Ivanov, A. G. (1939), Effect of electrization of earth layers by elastic waves passing through them., *Comptes Rendus (Doklady) de l'Academie des Sciences de l'URSS*, *24*(1), 42–45, english translation.

Ivanov, A. G. (1940), The seismoelectric effect of the second kind, *Izevestiya Akademii Nauk SSSR, seriya geograficheskaya i geofizicheskaya*, *4*, 699–727, English translation, US Library of Congress.

Ivanov, A. G. (1949), On the seismo-electric effect of the first kind (J) in the region near the electrode., *Doklady Akademii Nauk USSR*, *68*, 53–56.

Kepic, A., R. D. Russell, M. Maxwell, and K. E. Butler (2001), Underground tests of the radio pulsed effect seismoelectric method at the Lynx Mine, Canada, *Exploration Geophysics*, *32*(2), doi:10.1071/EG01107.

Kulessa, B., T. Murray, and D. Rippin (2006), Active seismoelectric exploration of glaciers, *Geophysical Research Letters*, *33*(7), doi:10.1029/2006GL025758.

Long, L. T., and W. K. Rivers (1975), Field measurements of the electroseismic response, *Geophysics*, *40*(2), 233–245, doi:10.1190/1.1440521.

Martner, S. T., and N. R. Sparks (1959), The electroseismic effect, *Geophysics*, *24*(2), 297–308, doi:10.1190/1.1438585.

Mauchly, S. J. (1918), A study of pressure and temperature effects in earth-current measurements, *Terrestrial magnetism and atmospheric electricity*, *23*(2), 73–91, doi:10.1029/TE023i002p00073.

Mikhailov, O. V., W. M. Haartsen, and M. N. Toksöz (1997a), Electroseismic investigation of the shallow subsurface: Field measurements and numerical modeling, *Geophysics*, *62*(1), 97–105, doi:10.1190/1.1444150.

Mikhailov, O. V., J. Queen, and M. N. Toksöz (1997b), Using borehole electroseismic measurements to detect and characterize fractured (permeable) zones, in *67th Annual International Meeting*, pp. 1981–1983, Society of Exploration Geophysicists, doi:10.1190/1.1885835.

Mikhailov, O. V., J. Queen, and M. N. Toksöz (2000), Using borehole electroseismic measurements to detect and characterize fractured (permeable) zones, *Geophysics*, *65*(4), 1098–1112, doi:10.1190/1.1444803.

Millar, J. (1995), A source of life made commercial, *Physics World*, *8*, 22–23.

Mitchell, J. K. (1993), *Fundamentals of soil behaviour*, second ed., John Willey & Sons, Inc.

Morgan, F. D., E. R. Williams, and T. R. Madden (1989), Streaming potential properties of westerly granite with applications., *Journal of Geophysical Research*, *94*(B9), 12,449–12,461.

Neev, J., and F. R. Yeatts (1989), Electrokinetic effects in fluid-saturated poroelastic media, *Physical Review B*, *40*(13), 9135–9141, doi:10.1103/PhysRevB.40.9135.

Neishtadt, N. M., L. V. Eppelbaum, and A. G. Livitski (2006), Application of piezoelectric and seismoelectrokinetic phenomena in exploration geophysics: Review of Russian and Israeli experience, *Geophysics*, *71*(2), B41–B53, doi:10.1190/1.2187714.

Parkhomenko, E. I. (1971), *Electrification phenomena in rocks*, Plenum Press, english translation by G.V. Keller.

Parkhomenko, E. I., and C. Chien-San (1964), A study of the influence of moisture on the magnitude of the seismoelectric effect in sedimentary rocks by laboratory method, *Izvestiya (Bulletin) Academy Sciences USSR, Geophysics series*, *2*, 115–118, English translation by American Geophysical Union.

Parkhomenko, E. I., and I. V. Gaskarov (1971), Borehole and laboratory studies of the seismoelectric effect of the second kind in rocks, *Izvestiya Academy Sciences USSR, Physics of the Solid Earth*, *7*, 663–666, English translation by American Geophysical Union.

Pride, S. (1994), Governing equations for the coupled electromagnetics and acoustics of porous media, *Physical Review B*, *50*(21), 15,678–15,696, doi:10.1103/PhysRevB.50.15678.

Pride, S., and M. W. Haartsen (1996), Electroseismic wave properties, *Journal of the Acoustical Society of America*, *100*(3), 1301–1315, doi:10.1121/1.416018.

Pride, S. R., and S. Garambois (2002), The role of Biot slow waves in electroseismic wave phenomena, *Journal of the Acoustical Society of America*, *111*(2), 697–706, doi:10.1121/1.1436066.

Pride, S. R., and S. Garambois (2005), Electroseismic wave theory of Frenkel and more recent developments, *Journal of Engineering Mechanics*, *131*(9), 898–907, doi:10.1061/(ASCE)0733-9399(2005)131:9(898).

Pride, S. R., and F. D. Morgan (1991), Electrokinetic dissipation induced by seismic waves, *Geophysics*, *56*(7), 914–925, doi:10.1190/1.1443125.

Revil, A., and N. Linde (2006), Chemico-electromechanical coupling in microporous media, *Journal of Colloid and Interface Science*, *302*(2), 682–694, doi:10.1016/j. jcis.2006.06.051.

Revil, A., P. A. Pezard, and P. W. J. Glover (1999), Streaming potential in porous media:1. theory of the zeta potential, *Journal of Geophysical Research*, *104*(B9), 20,021–20,031, doi:10.1029/1999JB900089.

Revil, A., N. Linde, A. Cerepi, D. Jougnot, S. Matthäi, and S. Finsterle (2007), Electrokinetic coupling in unsaturated porous media, *Journal of Colloid and Interface Science*, *313*(1), 315–327, doi:10.1016/j.jcis.2007.03.037.

Russell, R. D., K. E. Butler, A. W. Kepic, and M. Maxwell (1997), Seismoelectric exploration, *The Leading Edge*, *16*(11), 1611–1615, doi:10.1190/1.1437536.

Santamarina, J. C., and D. O. Fratta (2003), Dynamic electrical-mechanical energy coupling in electrolyte-mineral systems, *Transport in Porous Media*, *50*(1-2), 153–178, doi:10.1023/A:1020648204185.

Shaw, D. J. (1980), *Introduction to colloid and surface chemistry*, Butterworth & Co Ltd.

Singer, J., J. Saunders, L. Holloway, J. B. Stoll, C. Pain, W. Stuart-Bruges, and G. Mason (2005), Electrokinetic logging has the potential to measure permeability, in *46th Annual Logging Symposium*, pp. 1–16, Society of Petrophysicists and Well Log Analysts.

Sparnaay, M. J. (1972), *The electrical double layer*, Pergamon Press.

Stern, O. (1924), Zur theorie der electrolytischen doppelschist,, *Zeitschrift für Elektrochemie*, *30*(9), 508–516.

Strahser, M. H. P., W. Rabbel, and F. Schildknecht (2007), Polarisation and slowness of seismoelectric signals, a case study, *Near Surface Geophysics*, *5*, 97–114.

Thompson, A. H., and G. A. Gist (1993), Geophysical applications of electrokinetic conversion, *The Leading Edge*, *12*(12), 1169–1173, doi:10.1190/1.1436931.

Thompson, A. H., et al. (2007), Field tests of electroseismic hydrocarbon detection, *Geophysics*, *72*(1), N1–N9, doi:10.1190/1.2399458.

Thompson, R. R. (1936), The seismic-electric effect, *Geophysics*, *1*(3), 327–335, doi: 10.1190/1.1437119.

Thompson, R. R. (1939), A note on the seismic-electric effect, *Geophysics*, *4*(2), 102–105, doi:10.1190/1.1440485.

Wolfe, P. J., J. Yu, and N. Gershenzon (1996), Seismoelectric studies in an outwash plain, in *9th Symposium on the Application of Geophysics to Engineering and Environmental Problems*, pp. 21–30, Environmental and Engineering Geophysical Society.

Wurmstich, B., and F. D. Morgan (1994), Modelling of streaming potential responses caused by oil well pumping, *Geophysics*, *59*(1), 46–56, doi:10.1190/1.1443533.

Zablocki, C. J., and G. V. Keller (1961), Some observations of the seismic-electric effect, *Professional Paper 424-D*, United States Geological Survey.

Zhu, Z., and M. N. Toksöz (2005), Seismoelectric and seismomagnetic measurements in fractured borehole models, *Geophysics*, *70*(4), F45–F51, doi:10.1190/1.1996907.

Zhu, Z., M. W. Haartsen, and M. N. Toksöz (1999), Experimental studies of electrokinetic conversions in fluid-saturated borehole models, *Geophysics*, *64*(5), 1349–1356, doi:10.1190/1.1444639.

# Chapter 2

# Field procedures and signal processing

The weak amplitudes of seismoelectric signals have been a great source of difficulty in making meaningful measurements in the field. The pervasive natural and cultural electromagnetic noise is often two to three orders of magnitude greater than the seismoelectric signals sought and traditional seismic or electromagnetic/electrical recording systems are not optimized for their measurement. The basic principles for acquisition of field data and signal processing techniques used to separate the seismoelectric signals from the various noise sources are discussed in this section.

At the time when *Ivanov* (1939) made the first seismoelectric measurements, most of the electromagnetic noise originated from natural noise sources (i.e. telluric currents and spherics). Large explosive sources were used to improve the signal-to-noise ratio. Fortunately, powerline harmonic noise was not a problem encountered in rural Russia in the 1940s, because it would have made it almost impossible for *Ivanov* to discover this phenomenon with the equipment available at that period in

time. *Ivanov* used only one pair of electrodes which made it difficult to characterise the seismoelectric signal further.

The use of multi-channel acquisition systems improved the ability to characterise the signal and identify the two different types of seismoelectric signals (e.g. *Martner and Sparks*, 1959; *Thompson and Gist*, 1993; *Butler et al.*, 1996). Although some stand-alone multi-channel seismoelectric acquisition systems were designed and built by research groups (e.g. University of British Columbia), these systems require considerable development time and expense and thus researchers turned to multi-channel seismographs. These are, by far, the most common type of data acquisition system used to acquire seismoelectric signals at this time. The advent of digital seismographs with large dynamic range (24-bit) also have made it possible to develop post-acquisition data processing to combat the powerline harmonic noise, which is the strongest noise source observed in experiments at many sites around North America.

## 2.1 Signal buffering

Seismographs on their own however are not suitable for systematic acquisition of high quality seismoelectric data. They are designed to interface to geophones that are low impedance sources ($\approx 300\ \Omega$) and as such the input impedance of a seismograph is typically approximately 20 k$\Omega$ - suitable for interfacing with geophones, but not electrodes. The contact impedance of electrodes in soils is highly variable and depends on several factors such as water and clay content and pore water salinity. For individual surveys, clay and water content can vary spatially within the survey area leading to significant changes in contact impedance. Additionally, while the clay content at a site will remain constant over several years, the water content can vary
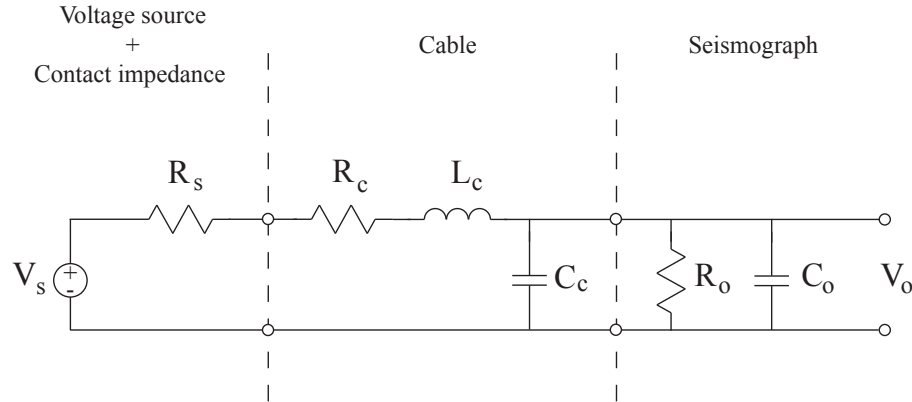
Figure 2.1: Equivalent circuit for dipole connected directly to a seismograph.

seasonally. If the grounded dipole antennas are not properly buffered, the variations of the contact impedance will affect the amplitude and the frequency content of the measured signal, and it will be difficult to determine if the changes in the seismoelectric signals at a given site are due to changes in surface conditions or hydrological properties.

### 2.1.1 Direct connection to seismograph

To better understand the influence that contact impedance exerts on the characteristics of the measured signal, consider the simple equivalent circuit presented in Figure 2.1 for one-half of a differential input grounded dipole, connected to a seismograph via a given length of seismic cable, where $L_c$, $C_c$ and $R_c$ are respectively the distributed inductance, capacitance and resistance of the cable, while $R_o$ and $C_o$ represent the input impedance of the seismograph.

It is possible to write a gain function that relates the voltage between the

electrodes ($V_s$) to the voltage measured at the seismograph ($V_o$). In order to simplify the algebra, the complex frequency $j\,\omega$ is replaced by $s$. The gain function $G(s) = V_o/V_s$ for the circuit in Figure 2.1 is given by

$$G(s) \quad = \quad \frac{a_0}{b_2 s^2 + b_1 s^1 + b_0},\tag{2.1}$$

where

$$
\begin{aligned}
a_0 &= R_o, \\
b_2 &= L_c\,R_o\,(C_o + C_c), \\
b_1 &= L_c + R_s\,R_o\,(C_c + C_o) + R_c\,R_o\,(C_c + C_o), \\
b_0 &= R_o + R_s + R_c.
\end{aligned}
$$

It is instructive to consider the DC response of the above gain function by setting $s = 0$ which leads to

$$G(s) = \frac{R_o}{R_o + R_s + R_c}.\tag{2.2}$$

The resulting DC gain function in Equation 2.2 is of the form of a simple voltage divider and thus the voltage measured at the seismograph is given by the ratio of the input resistance of the seismograph divided by the sum of all the resistance in the circuit. Clearly, from Equation 2.2, the largest voltages are measured at the seismograph when $R_s$ and $R_c$ are small.

Recognizing that $R_c$ and $L_c$ will generally be much smaller than the other parameters, it is possible to simplify Equation 2.1 by assuming that the products

involving $R_c$ and $L_c$ are insignificant in comparison to the other products of the gain function. Using this simplification, we can re-write Equation 2.1 as

$$G(s) = \frac{R_o}{s\,R_s\,R_o(C_o + C_c) + R_o + R_s} \tag{2.3}$$

The gain function of Equation 2.3 is that of a low-pass filter created by the combination of the electrode, cable capacitance and seismograph impedance. The corner frequency for this low-pass filter is given by

$$f_{\text{LP}} = \frac{R_o + R_s}{2\,\pi R_s\,R_o\,(C_c + C_o)} \tag{2.4}$$

From Equation 2.4 we can see that the bandwidth of this acquisition system is susceptible to change when the value of the components change. The values of $R_o$ and $C_o$ are fixed by the choice of seismograph and $C_c$ by the length and type of cable used to connect the electrode to the seismograph. By choosing an appropriate cable with low distributed capacitance, short lengths of cable should have minimal impact on the bandwith of the system. The variable that will have the most impact, and is the greatest unknown is $R_s$. Increases in $R_s$ will force the corner frequency at lower frequencies reducing the available bandwidth of the system.

To illustrate these findings, consider one-half of a differential input grounded dipole and a seismograph (such as the Geometrics Geode with input resistance and capacitance of 20 k$\Omega$ and 20 nF respectively), separated by 100 m cable having a distributed capacitance of 100 pF/m, assumed to be typical of twisted pair cables used in seismic instrumentation. The value of $R_s$ is varied from 1 k$\Omega$ to 50 k$\Omega$. The attenuation and the decrease in bandwidth associated with increases in $R_s$ are shown in Figure 2.2.
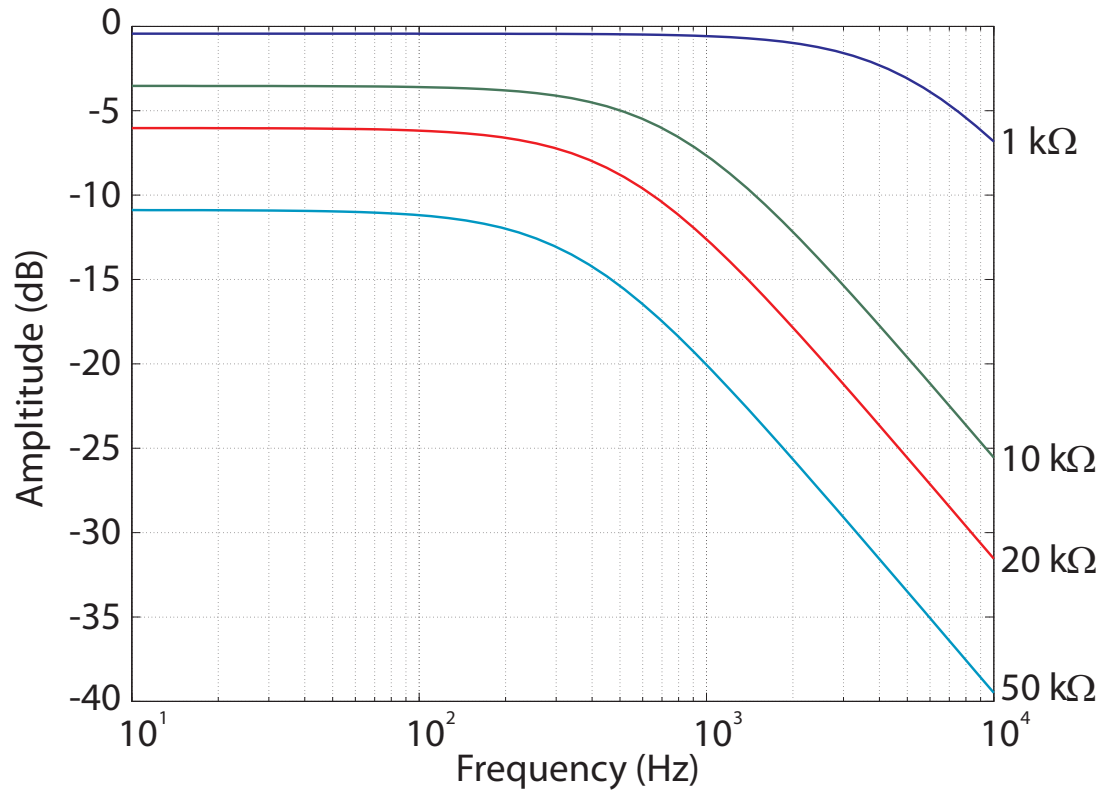
Figure 2.2: Frequency response for varying source impedance connected to a seismograph via 100 m of seismic cable. ($C_c$= 100 pF/m, $C_o$=20 nF, $R_o$=20 kΩ, $R_c$ = 150 mΩ/m, $L_c$=0.5 $\mu$H/m)

As expected from Equation 2.2, an increase in $R_s$ both attenuates the signal and limits the bandwidth of the system. Figure 2.2 clearly indicates that the best results are obtained when $R_s$ is less than 1/20 of the seismograph impedance.

## 2.1.2   Influence of the seismic cable

The connection points on the seismic cable, called "takeouts", are distributed at regular intervals, such that every dipole is separated from the seismograph by a different length of cable (commonly a multiple of 3 to 30 m depending on the desired depth of exploration). It was argued earlier that given a choice of low capacitance cable, the varying lengths of cable should not have a significant impact on the frequency response of the system if the cable length remains short enough. Figure 2.3 illustrates the effect of varying the length of the cable on the bandwidth of the system for $R_s = 1$ k$\Omega$. Since most seismoelectric measurements will usually be concerned with bandwidths below 1 kHz and cable lengths less than 100 m, the assumption that the different lengths of cable introduce minimal error is justified.

## 2.1.3   Step-up transformer

To provide voltage gain and to isolate channels from one another it is possible to use step-up transformers as proposed by *Haines et al.* (2007b). The idea of a step-up transformer is an interesting one since it is simple to deploy, relatively low-cost, no electronics are required and ground loops are avoided. A simplified schematic of transformer coupling (ignoring parasitic capacitance in the windings and the effects of cables for the sake of simplicity) is shown in Figure 2.4

The increase in voltage at the secondary of the transformer is obtained by increasing the number of turns by $N$ on the secondary winding. For example, if a
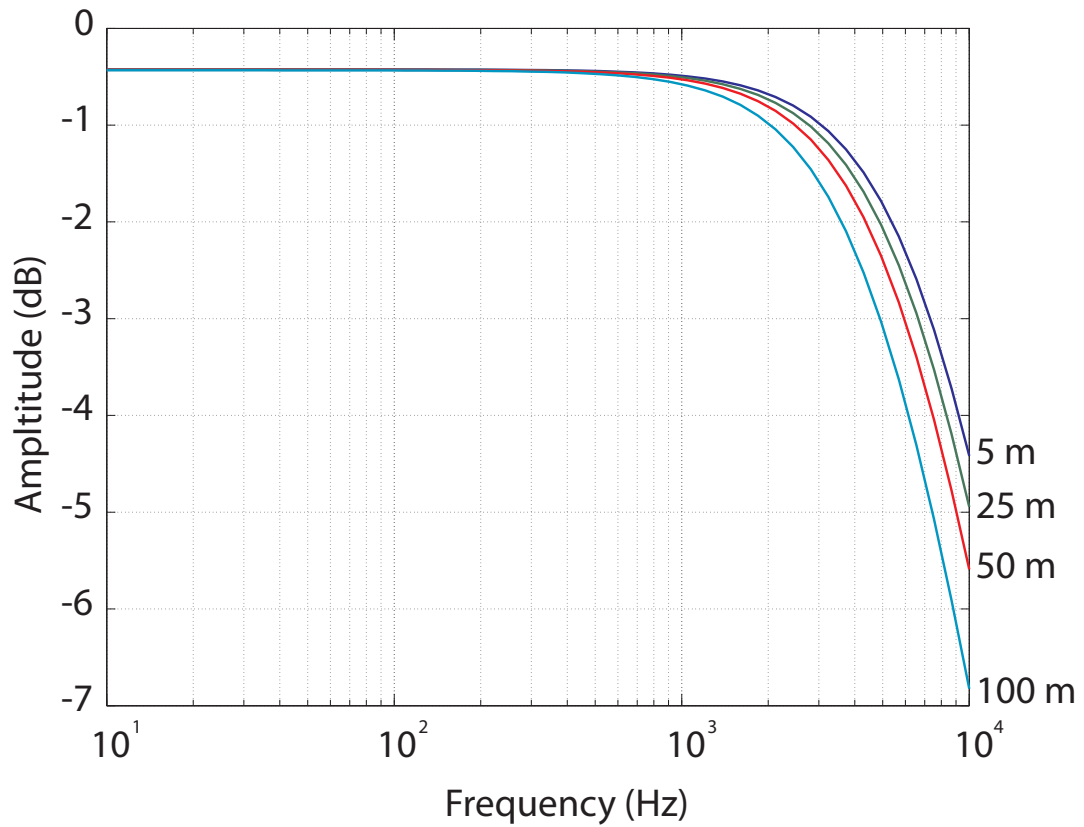
Figure 2.3: Frequency response for varying cable length with a source resistance of $R_s = 1$ k$\Omega$. ($C_c = 100$ pF/m, $C_o = 20$ nF, $R_o = 20$ k$\Omega$, $R_c = 150$ m$\Omega$/m, $L_c = 0.5$ $\mu$H/m)
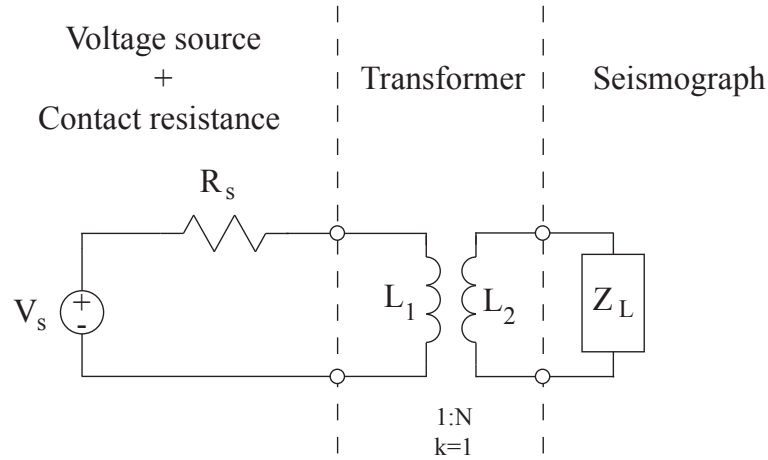
Figure 2.4: Simplified schematic of a step-up transformer for voltage gain.

primary has 100 turns and a 1:5 transformer is sought, there will be 500 turns on the secondary winding. The inductance of the secondary, however, will increase by the square of the number of turns $(N^2)$ and thus five times the number of turns on the secondary means an inductance that is 25 times that of the primary.

It is possible, as was done in the earlier example, to derive a gain function for this idealized transformer-coupled case:

$$G_{\text{transformer}}(s) = \frac{s\,M\,Z_L}{s^2\,(L_1\,L_2 - M^2)\, +\, s\,(L_2\,R_s\, +\, Z_L\,L_1)\, +\, Z_L\,R_s\,.} \tag{2.5}$$

The variable $M$ in Equation 2.5 is the mutual inductance between the primary $L_1$ and the secondary $L_2$. It is calculated using the coupling coefficient $k$ using the following Equation:

$$M = k\,\sqrt{L_1\,L_2}. \tag{2.6}$$

The value of $k$ varies between 0 and 1, with ideal transformers having a $k$ of 1. It is evident from Equation 2.5 that the DC gain of this circuit ($s = 0$) is 0 which is satisfying because the transformer operates on the principle of magnetic induction which requires a time varying signal. It is possible to simplify Equation 2.5 if it is assumed that $k \approx 1$, in which case the term $s^2 (L_1 L_2 - M^2)$ in the denominator goes to zero and we can write

$$G_{\text{transformer}}(s) \approx \frac{s\, M\, Z_L}{s\, (L_2\, R_s\, +\, Z_L\, L_1)\, +\, Z_L\, R_s}. \tag{2.7}$$

The gain function of Equation 2.7 is that of a high-pass filter. At low frequencies, the term $Z_L\, R_s$ in the denominator dominates but as the frequency increases and $s \to \infty$ only the terms that are multiplied by $s$ will be significant such that

$$G_{\text{passband}} \approx \frac{M\, Z_L}{L_2\, R_s\, +\, Z_L\, L_1}. \tag{2.8}$$

The 3dB corner frequency for the transformer occurs when the frequency becomes sufficiently high so that $s(L_2\, R_s\, +\, Z_L\, L_1) = (Z_L\, R_s)$. This transition frequency is given by

$$f_{\text{HP}} = \frac{Z_L\, R_s}{2\pi\, (L_2\, R_s\, +\, Z_L\, L_1)}. \tag{2.9}$$

Equations 2.8 and 2.9 allow us to see some of the limitations of using a step-up transformer. First, from Equation 2.8 we note that for any voltage gain to be acheived (i.e. $G > 1$)

$$R_s < \frac{Z_L\, (M - L_1)}{L_2}. \tag{2.10}$$

Since $L_2 = N^2 L_1$, the greater the step-up ratio, the smaller $R_s$ will have to be for any voltage gain to be acheived.

The response of the step-up transformer is thus strongly influenced by $R_s$ and it is impossible to make repeatable measurements if $R_s$ varies over a wide range of values. In fact, the use of a step-up transformer may actually attenuate the signal being measured and be worse than connecting the electrode directly to the seismograph. In order to illustrate how a step-up transformer may degrade the signal, let us consider a simple numerical example.

Let us assume that the lowest frequency of interest is 20 Hz, $R_o = R_s = 20$ k$\Omega$ and that we are using a 1:5 step-up transformer. It is possible to re-write Equation 2.9 using $L_2 = N^2 L_1$ to determine the required inductance of the primary needed to obtain a given corner frequency

$$L_1 = \frac{R_o R_s}{2\pi f_{HP}(N^2 R_s + R_o)}.$$

(2.11)

Using the values above and $L_1 = 6.12$ H and $L_2 = 153.03$ H (Transformers with these inductances are available from Lundahl transformers ). Setting the seismograph input impedance $Z_L$ equal to $R_o$ and computing $M$ using Equation 2.6, we can use Equation 2.8 to determine the gain (attenuation in this case) in the passband which is -14.3 dB or 8.3 dB less than would have been obtained by connecting the electrode directly to the seismograph (-6.0 dB). This example is illustrated in Figure 2.5.

It is possible to extend the example by re-introducing the impedance of the cable and the seismograph. This can be done by deriving a transfer function for the impedance $Z_L$ seen at the input of the cable as shown in Figure 2.6
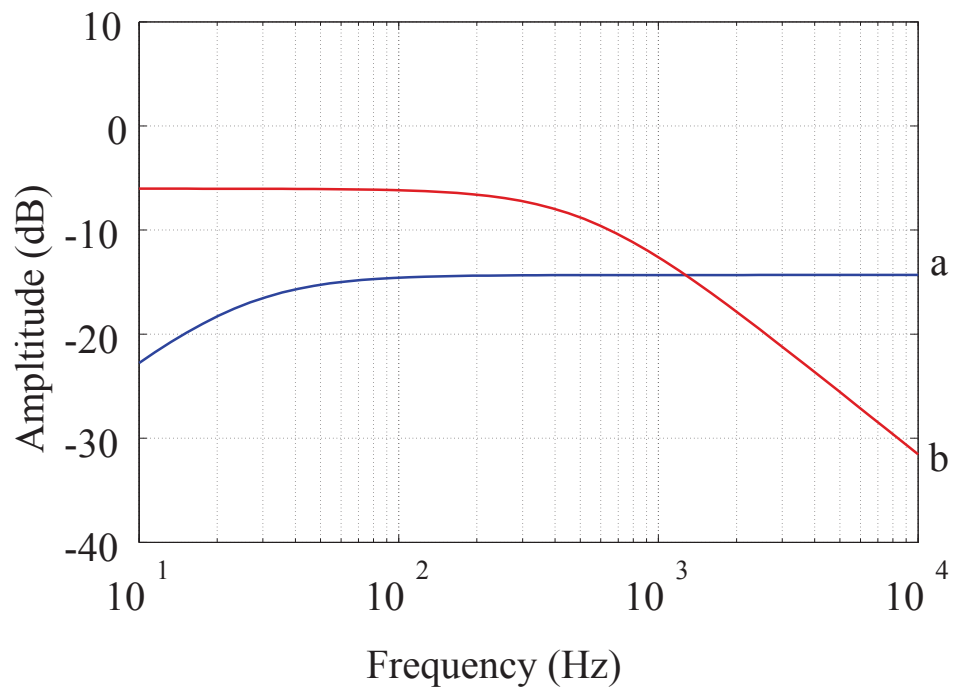
Figure 2.5: Comparison of the frequency response between one-half of a differential input grounded dipole ($R_s = 20$ k$\Omega$) connected to a 1:5 step-up transformer (a) and the same one-half of a differential input grounded dipole connected to a seismograph by a 100 m of seismic cable (b).
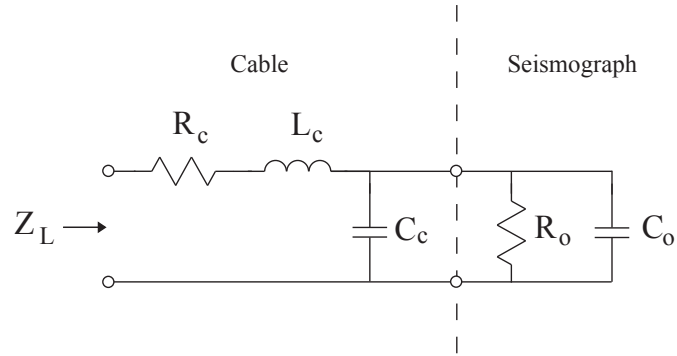
Figure 2.6: Equivalent circuit for the load impedance presented by the cable and seismograph.

$$Z_L = \frac{s^2 \, L_c \, R_o (C_o + C_c) \; + \; s \, (R_c \, R_o \, (C_o + C_c) \; + \; L_c) \; + \; (R_o + R_c)}{s \, (R_o \, C_o + R_o \, C_c) \; + \; 1 \, .} \qquad (2.12)$$

Combining Equations 2.5 and 2.12 it is possible to obtain the following gain function

for the combination of electrode, transformer, cable and seismograph:

$$G(s) \;=\; \frac{a_3 s^3 + a_2 s^2 + a_1 s^1 + a_0}{b_3 s^3 + b_2 s^2 + b_1 s^1 + b_0} \,, \tag{2.13}$$

where

$$a_3 \;=\; M\, L_c\, R_o\, (C_o \,+\, C_c)\,,$$

$$a_2 \;=\; M\, (R_c\, R_o\, (C_o \,+\, C_c) \,+\, L_c)\,,$$

$$a_1 \;=\; M\, (R_o + R_c)\,,$$

$$a_0 \;=\; 0\,,$$

$$b_3 \;=\; R_o\, (C_o \,+\, C_c)\, (L_c\, L_1 + L_1\, L_2 - M^2)\,,$$

$$b_2 \;=\; R_o\, (C_o \,+\, C_c)\, (L_2\, R_s + L_1\, R_c + L_c\, R_s) + L_1\, L_c + L_1\, L_2 - M^2\,,$$

$$b_1 \;=\; R_s\, (L_2 \,+\, L_c) + L_1 (R_o \,+\, R_c) + R_s\, R_c\, R_o\, (C_o \,+\, C_c)\,,$$

$$b_0 \;=\; R_s\, (R_o \,+\, R_c)\,.$$

The impedance of the cable and the seismograph transform the high-pass filter characteristics of the ideal transformer into a band-pass filter. The gain function in Equation 2.13 is more complex than the others, but the factors that dominated the response of the transformer and the cable/seismograph remain the same. The frequency response of the complete seismoelectric recording system using a step-up transformer, and where $R_s$ varies between 1 k$\Omega$ and 20 k$\Omega$, is shown in Figure 2.7.

Replacing $Z_L$ by $R_o$ in Equation 2.8 it is possible to obtain a good estimate of the attenuation in the passband of this circuit. It is also possible to obtain an estimate of the corner frequencies by using Equations 2.4 and 2.9.
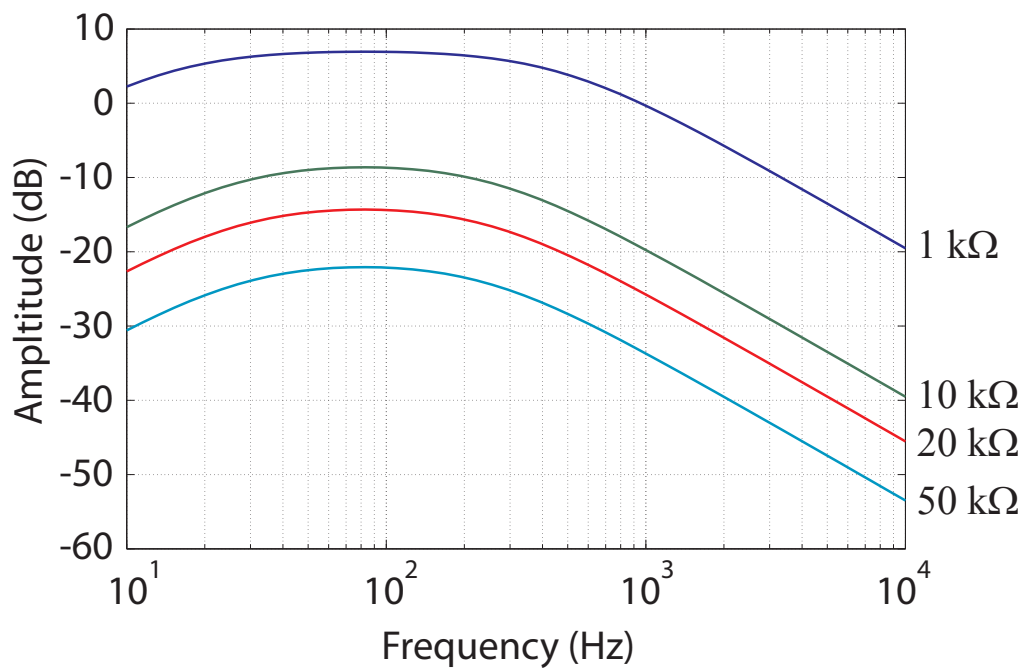
Figure 2.7: Impact of increases in source resistance $R_s$ on the attenuation and bandwidth of a transformer-coupled seismoelectric acquisition system including cable ($L_1 = 6.12$ H, $L_2 = 153.03$ H, $C_c= 100$ pF/m, $C_o$=20 nF, $R_o$=20 kΩ, $R_c = 150$ mΩ/m, $L_c$=0.5 $\mu$H/m)

### 2.1.4 Preamplifiers

In order to avoid these signal buffering problems, it is important to use a preamplifier that has a high input impedance and will not load the source. The design of this preamplifier is not trivial because of instrument limitations and noise considerations (*Kepic and Butler*, 2002). The first is that the preamplifiers must work over a wide range of source impedance and thus the choice of components can be difficult (i.e. must have low voltage and current noise). The second is brought upon by the digitizer of the seismograph, which has an input voltage capability usually of around $\pm$ 1.2 V and its own built-in preamplification (24 to 36 dB). This means that the preamplifier must be of relatively low gain in order for the powerline harmonic noise to be recorded without distortion for post-acquisition removal. This gain limitation also has implications for overall noise of the system. Finally, the design is also complicated by the presence of radio frequency interference in the form of amplitude modulated broadcasts (especially commercial AM radio transmissions) coupled to the near surface of the earth. In some surface conditions, the electrodes and cables readily pick up the signal and small non-linearities in the preamplifier will cause the broadcast to be demodulated into the audio-frequency band of the seismoelectric signal.

The preamplifiers used in this work were designed by Dr. Anton Kepic. They include a passive filter stage to reduce the AM demodulation, an intial J-FET buffering stage, followed by a differential amplifier stage, an intermediate unity buffer stage and a dual op-amp output stage that drives a differential signal. The differential output stage was chosen to increase the immunity of the signal to contamination from outside sources. This design provides good low noise characteristics at voltage gains of either 10 or 30 (adjusted via a jumper). For this design to succeed, good matching

of the components is of the utmost importance, especially for the first two stages. Failure to do so decreases the common-mode rejection ratio and makes the pream- plifiers more susceptible to demodulation of amplitude modulated radio frequency interference.

## 2.2  Spatial filtering effects of a dipole

In addition to buffering considerations, one should be aware of the spatial filter- ing that can occur when separation between the electrodes of the measurement dipole are comparable in size or larger than the dominant seismic wavelength. Figure 2.8 illustrates how spatial filtering occurs.

In Figure 2.8 we have a co-seismic wavefield of amplitude $E_0$ (peak to peak) moving in the positive direction $x$. The measurement of the signal is made at position $p_1$ and $p_2$. The resulting potential difference is given by Equation 2.14,

$$E_d = \frac{E_0}{2} \cos\left(\omega\, t - k_0\, p_1\right) - \frac{E_0}{2} \cos\left(\omega\, t - k_0\, p_2\right), \tag{2.14}$$

where $\omega$ is angular frequency, $t$ is time, $k_0 = \omega/V_p$, where $V_p$ is the P-wave velocity. We can write Equation 2.14 in terms of phasors such that

$$\frac{E_d}{E_0} = \frac{1}{2}\left(e^{-i\,k_0\,p_1} - e^{-i\,k_0\,p_2}\right) e^{i\,\omega\, t}. \tag{2.15}$$

Following Euler's formula the exponential terms can be re-writen as follows

$$\frac{E_d}{E_0} = \frac{1}{2}[(\cos(k_0 p_1) + j \sin(k_0 p_1)) - (\cos(k_0 p_2) + j \sin(k_0 p_2))], \tag{2.16}$$

where harmonic time dependence is assumed. Rearranging Equation 2.16 to group
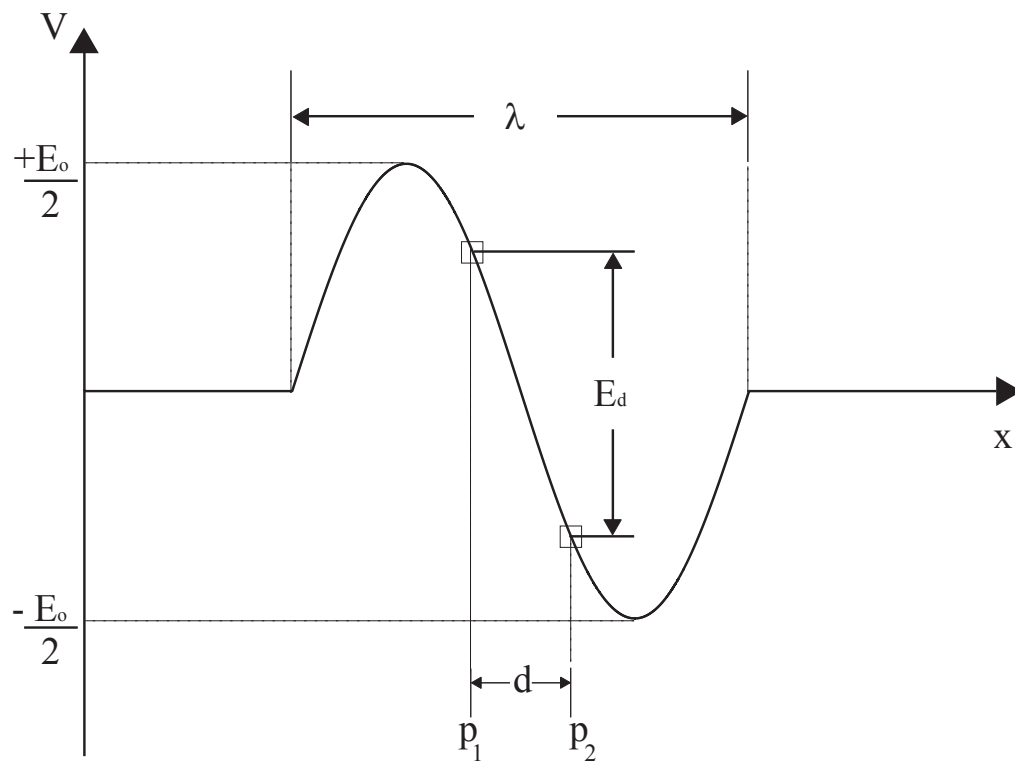
Figure 2.8: Influence of dipole length on magnitude of potential difference measured during the passage of a co-seismic seismoelectric signal of wavelength $\lambda$.

real and imaginary terms leads to

$$\frac{E_d}{E_0} = \frac{1}{2} \left[ \cos\left(k_0\,p_1\right) - \cos\left(k_0\,p_2\right) + j\,\left(\sin\left(k_0\,p_1\right) - \sin\left(k_0\,p_2\right)\right) \right], \tag{2.17}$$

If we designate $p_1 = 0$ as a reference position , we can simplify Equation 2.17 as follows

$$\frac{E_d}{E_0} = \frac{1}{2} \left[ 1 - \cos\left(k_0\,p_2\right) - j\,\sin\left(k_0\,p_2\right) \right]. \tag{2.18}$$

Calculating the magnitude of this complex expression yields

$$\left|\frac{E_d}{E_0}\right| = \frac{1}{2} \sqrt{[1 - \cos\left(k_0\,p_2\right)]^2 + [\sin\left(k_0\,p_2\right)]^2}. \tag{2.19}$$

If we now replace $p_2$ with the separation $d$ as measured from the reference point ($p_1$) and make the observation that $k_o$ can be written as $2\,\pi/\lambda$ we can write

$$\frac{E_d}{E_0} = \frac{1}{2} \sqrt{\left[ 1 - \cos\left(\frac{2\,\pi\,d}{\lambda}\right) \right]^2 + \left[ \sin\left(\frac{2\,\pi\,d}{\lambda}\right) \right]^2} \tag{2.20}$$

The optimal length for the dipole, can be established by evaluating Equation 2.20 in term of electrode separation ($d$) written in terms of fractions of a wavelength. The results presented in Figure 2.9 confirm that the best length for the measurement dipole, for the purpose of maximizing the co-seismic seismoelectric signal, is $d = \lambda/2$ since longer or shorter separation results in attenuation of the signal.

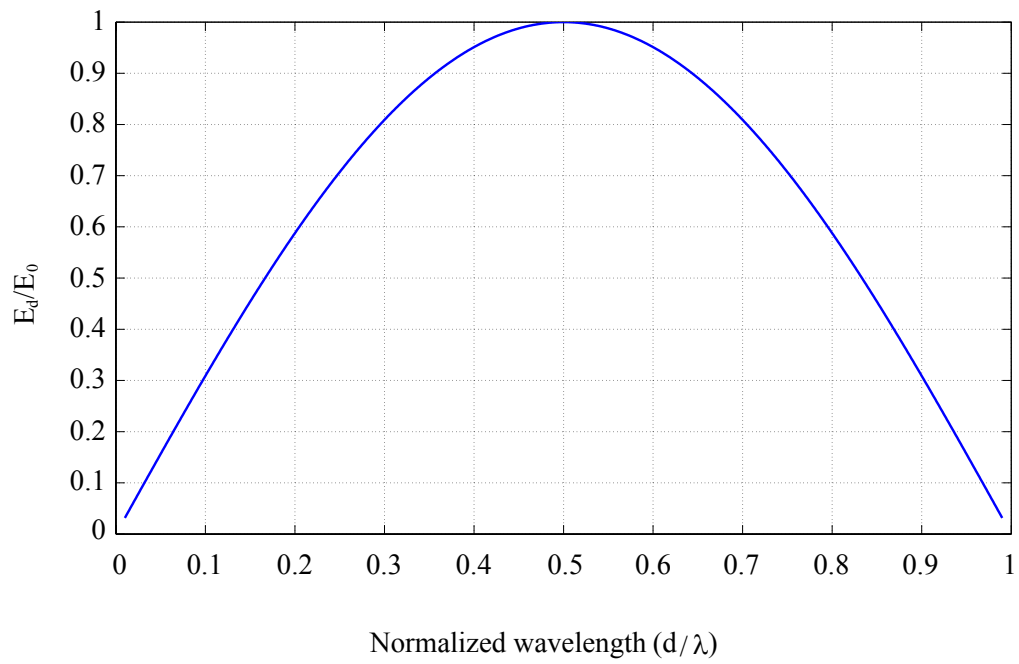It is also possible to substitute $k_o = \omega/V_p$ in Equation 2.19 to obtain the following Equation

Figure 2.9: Effects of the dipole length on the spectrum of the seismoelectric signal.

$$\left| \frac{E_d}{E_0} \right| = \frac{1}{2} \sqrt{\left[ 1 - \cos\left( \frac{\omega\, d}{V_p} \right) \right]^2 + \left[ \sin\left( \frac{\omega\, d}{V_p} \right) \right]^2}. \tag{2.21}$$

As the frequency increases in Equation 2.21 it is possible for the term $\omega\, d/V_p$ to become a multiple of $2\,\pi$ at which point $E_d/E_o$ becomes zero. These notches in the frequency spectrum of the signal caused by the length of the dipole will occur at the frequencies given by

$$f_{\text{notch}} = \frac{n\, V_p}{d}, \tag{2.22}$$

where $n$ is any positive integer.

To illustrate this phenomenon with a numerical example, consider recording dipoles with electrode spacing of 5 m and a p-wave velocity of 1500 m/s. The spectrum of the signal measured by the recording dipoles is shown in Figure 2.10 where the frequency notches occur at 300 Hz increments as predicted by Equation 2.22.

This spatial filtering effect is likely to be the most relevant when co-seismic seismoelectric signals are measured in boreholes where the frequency content of the signal can be especially broad. It could also find some application in helping to filter out the co-seismic signals from surface data. Evidence of notching of the seismoelectric signal spectrum at approximately 650 Hz was observed in co-seismic signals measured in a borehole at Fredericton (*Dupuis and Butler*, 2006a,b)
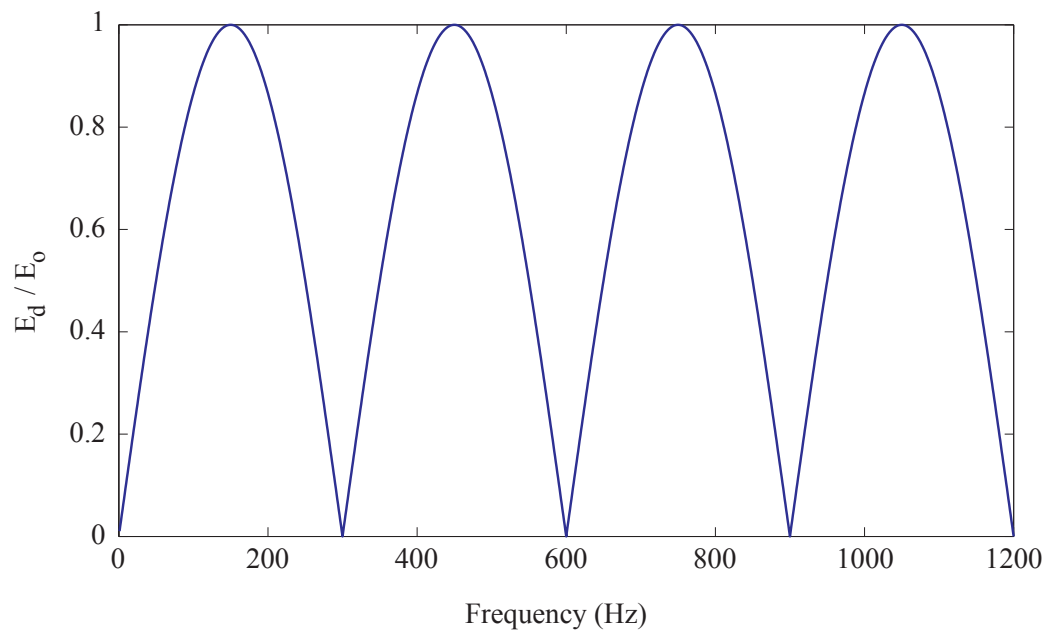
Figure 2.10: Notch filtering caused by length of the measurement dipole.

## 2.3  Post-acquisition processing

### 2.3.1  Powerline harmonic noise removal

At most sites in North America, powerline harmonic noise dominates the seismoelectric records. The main cause for this interference signal is ground currents that are introduced by connecting the neutral of a power system to ground. In principle, the power utility will attempt to balance the load across the three phases as best it can so that no current flows through the neutral. The distribution network however is a dynamic system and electric motors and appliances may require different current levels depending on their usage and load levels. These single and dual phase devices that switch on intermitently introduce an imbalance between the phases and therefore imbalance currents flow in the neutral. This problem has been quantified at dairy farms in Wisconsin in the United States (*Dorr et al.*, 2007). Their regulations require that stray voltages be below 1 V (RMS) across a 500 $\Omega$ resistor connected between any two points that are separated by at most six feet to avoid nuisance shocking of the cows and a decrease in the milk production. Fortunately, we do not have to conduct seismoelectric surveys at these farms as the maximum allowed stray voltage in dairy farms is two to three orders of magnitude larger than what we encounter at most remote field sites. Usually the powerline harmonic noise will be on the order of a few mV/m while the co-seismic signals will be on the order of tens of $\mu$V/m. Powerline harmonic noise issues are less problematic in some countries, like Australia, where a ground wire is included in the power transmission system.

To resolve this issue, *Butler and Russell* (1993) proposed to subtract an estimate of the harmonic noise formed on a pre-trigger portion of the record where no seismoelectric signal exists. *Butler and Russell* (2003) subsequently improved their
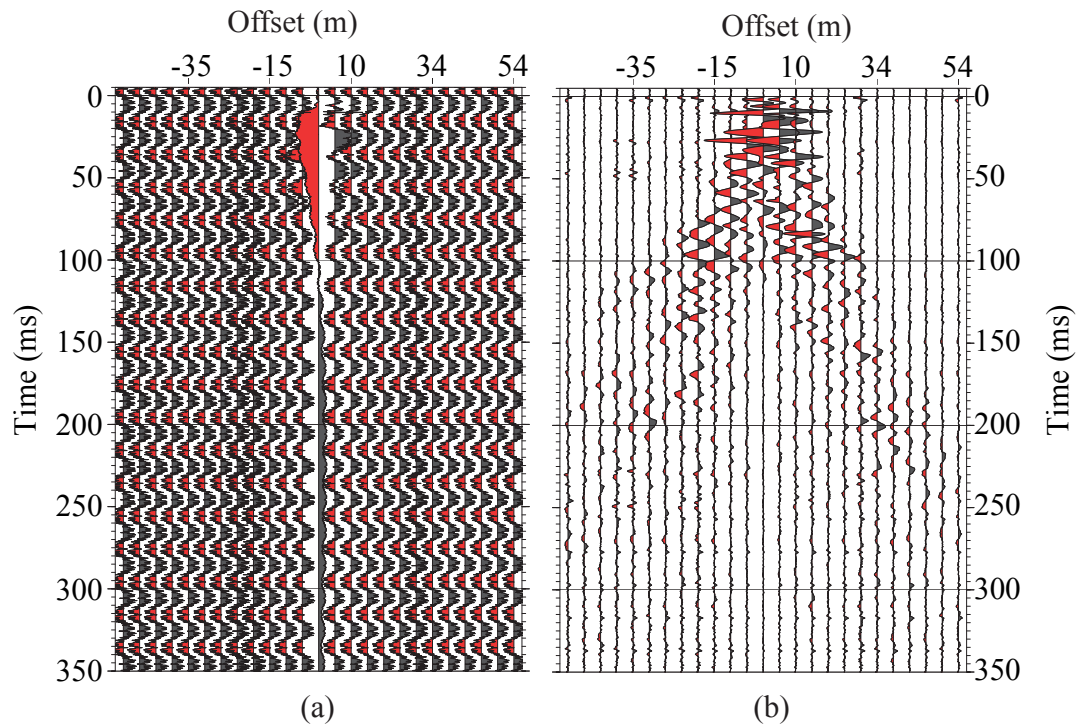
Figure 2.11: Seismoelectric shot record before (a) and after (b) harmonic subtraction.

algorithm to include the ability to refine the estimate of the fundamental frequency and to allow for removal of harmonics from two different fundamental frequencies. This later algorithm was used to process all the seismoelectric datasets presented in this work and an example of its effectiveness is shown in Figure 2.11.

## 2.3.2  Virtual shot gathers and velocity filters

The construction of preamplifiers is expensive and time consuming, and as such, the number of channels available was limited to 26. This modest channel count introduces difficulties in identifying the interfacial signal on so few traces. As an example, consider the seismoelectric shot record of Figure 2.12 (a). This shot gather

provides a hint of an interfacial signal but the co-seismic wavefields are spatially aliased making it difficult to distinguish different seismoelectric arrivals. *Kepic and Rosid* (2004) proposed to solve the trace density problem by introducing the virtual shot gather, or "supergather" approach; the results of which are depicted in Figure 2.12 (b). Instead of increasing the number of receivers on the ground, traces from multiple closely spaced shots with unique source-receiver offsets are combined. By appropriate selection of the shot positions, with respect to a stationary array of receivers, a wide range of offsets may be finely and evenly sampled. For example, shooting at 4 adjacent locations near the centre of an array of 24 receivers yields 96 traces. For this method to work optimally, the shot-to-shot repeatability is important, as are the near surface conditions for the adjacent shots. With the increase in trace density it becomes possible to identify various co-seismic fields and the interfacial signal becomes much easier to identify. Additionally, virtual shot gathers make it possible to obtain a higher trace density shot record more efficiently than with a higher receiver count, because deploying 96 antennas at such small spacing would require a considerable amount of time; it is much faster to make multiple closely spaced shots if a suitable source is available.

The greater trace density provided by the supergathers also makes it more feasible to use velocity filters to remove the interference from the co-seismic fields. This is possible because of the large difference in the velocities of interfacial and co-seismic signals (e.g. *Thompson and Gist*, 1993; *Kepic and Rosid*, 2004; *Strahser et al.*, 2007; *Haines et al.*, 2007a).

The f-k filter, used by *Kepic and Rosid* (2004) and *Strahser et al.* (2007), transforms the shot gather from the time-space (t-x) domain to the frequency-wavenumber (f-k) domain using a two dimensional Fourier transform. This velocity filter must be
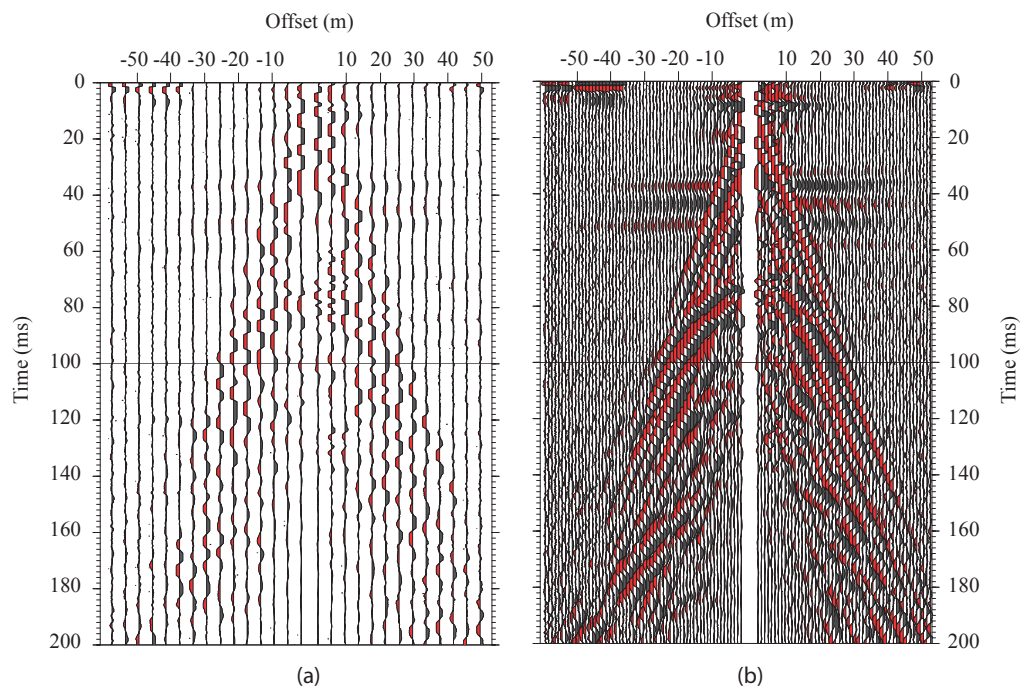
Figure 2.12: Single shot gather with receivers at 4 m spacing (a) versus virtual shot gather (b) with virtual receivers at 1 m spacing.

used with care however, because the trace density must be sufficient to avoid spatial aliasing of low velocity (high wavenumber) arrivals. Furthermore, the amplitude versus offset characteristics of the interfacial signal makes it plot in a larger part of the f-k space, making it difficult to separate from the other wave modes which may generate what appears to be high velocity events but are in fact processing artifacts (*Strahser et al.*, 2007). While *Kepic and Rosid* (2004) and *Strahser et al.* (2007) used f-k filters on field data, *Haines et al.* (2007a) attempted to prove the effectiveness of this velocity filter on synthetic data. They found that the f-k filter could not remove all of the co-seismic and that it disrupted the signal amplitude pattern of the interfacial signal.

In addition to the f-k filter, *Haines et al.* (2007a) also tested radon and prediction-error filters on their synthetic dataset. The principle of the radon filter, also called a $\tau$-p filter, is the conversion from the time-space (t-x) domain to the intercept time-slowness domain. The prediction-error filter seeks to model the co-seismic noise as a filtered version of a seismic record, recorded along with the seismoelectric data. *Haines et al.* (2007a) found that the prediction-error filter is the most suitable for separation of signal and noise, and to preserve the amplitude information, but that adequate patterns for the signal and noise must be available. On the basis of their test on a synthetic dataset, *Haines et al.* (2007a) conclude that radon filters are a better choice than the f-k filter for separation of interfacial signals from the co-seismic signals.

Fortunately, the interfacial signals measured in the experiments presented in this work did not require the use of velocity filters. As discussed in Chapters 4 and 5, the characteristics of the unsaturated (vadose) zone sediments on the Gnangara Mound provided natural separation between the interfacial and co-seismic arrivals

for measurements made on surface, while the source receiver geometry ensured the required separation for the signals measured in boreholes.

# References

Butler, K. E., and R. D. Russell (1993), Subtraction of powerline harmonics from geophysical records, *Geophysics*, *58*(6), 898–903, doi:10.1190/1.1443474.

Butler, K. E., and R. D. Russell (2003), Cancellation of multiple harmonic noise series in geophysical records, *Geophysics*, *68*(3), 1083–1090, doi:10.1190/1.1581080.

Butler, K. E., R. D. Russell, A. W. Kepic, and M. Maxwell (1996), Measurement of the seismoelectric response from a shallow boundary, *Geophysics*, *61*(6), 1769–1778, doi:10.1190/1.1444093.

Dorr, D., W. Howe, P. Lim, and C. Bray (2007), Understanding nuisance shocking from an electric power utility persepective, in *Power Engineering Conference, IPEC 2007, International, Singapore*, Institute of Electrical and Electronics Engineers.

Dupuis, J. C., and K. E. Butler (2006a), Vertical seismoelectric profiling in a borehole penetrating glaciofluvial sediments, *Geophysical Research Letters*, *33*(16), doi:10.1029/2006GL026385.

Dupuis, J. C., and K. E. Butler (2006b), Measurements and modelling of seismoelectric effects in a borehole penetrating glaciofluvial sediments, in *Australian Earth Sciences Convention, Melbourne, Australia*, Australian Society of Exploration Geophysicists.

Haines, S. S., A. Guitton, and B. Biondi (2007a), Seismoelectric data processing for surface surveys of shallow targets, *Geophysics*, *72*(2), G1–G8, doi:10.1190/1.2424542.

Haines, S. S., S. L. Klemperer, and B. Biondi (2007b), Seismoelectric imaging of shallow targets, *Geophysics*, *72*(2), G9–G20, doi:10.1190/1.2428267.

Ivanov, A. G. (1939), Effect of electrization of earth layers by elastic waves passing through them., *Comptes Rendus (Doklady) de l'Academie des Sciences de l'URSS*, *24*(1), 42–45, english translation.

Ivanov, A. G. (1940), The seismoelectric effect of the second kind, *Izevestiya Akademii Nauk SSSR, seriya geograficheskaya i geofizicheskaya*, *4*, 699–727, English translation, US Library of Congress.

Kepic, A., and K. Butler (2002), The art of measuring very low amplitude seismo-electric signals, in *64th Meeting*, p. 193, European Association of Geoscientists & Engineers.

Kepic, A., and M. Rosid (2004), Enhancing the seismoelectric method via a virtual shot gather, in *74th Annual International Meeting*, pp. 1337–1340, Society of Exploration Geophysicists, doi:10.1190/1.1851111.

Martner, S. T., and N. R. Sparks (1959), The electroseismic effect, *Geophysics*, *24*(2), 297–308, doi:10.1190/1.1438585.

Strahser, M. H. P., W. Rabbel, and F. Schildknecht (2007), Polarisation and slowness of seismoelectric signals, a case study, *Near Surface Geophysics*, *5*, 97–114.

Thompson, A. H., and G. A. Gist (1993), Geophysical applications of electrokinetic conversion, *The Leading Edge*, *12*(12), 1169–1173, doi:10.1190/1.1436931.

# Chapter 3

# Vertical seismoelectric profiling in a borehole penetrating glaciofluvial sediments

.

## 3.1 Abstract

Seismoelectric signals have been measured as a function of depth in a borehole penetrating glaciofluvial sands, silts, and glacial till using a broadband surface seismic source, and a downhole electrode array. Transient electric field pulses, with amplitudes between 1 and 4 $\mu$V/m, accompanied the arrival of seismic P-waves at the electrodes. The electrical field increased significantly in the porous sand layer relative to its amplitude in the clay/silt aquitard. The seismoelectric log was normalized

by particle velocity and electrical conductivity to investigate its dependence on sediment type. The measured co-seismic seismoelectric signal amplitudes in the aquifer compare favorably to values predicted by a theoretical model. The results of this experiment suggest that co-seismic effects show potential as a porosity/permeability logging tool in the borehole environment.

## 3.2 Introduction

Seismoelectric signals are produced when charge in the electrical double layer at solid-liquid interfaces in porous or fractured media is disturbed by seismically induced fluid flow. They are of interest in both hydrogeology and hydrocarbon reservoir exploration/characterization for the information they may be able to provide regarding pore fluid type, porosity and fluid flow permeability. Challenges remain however in the measurement of these signals and in determining how they may be interpreted quantitatively.

Previous borehole seismoelectric measurements were accomplished by *Hunt and Worthington* (2000) and *Mikhailov et al.* (2000). They demonstrated that fractured zones in open rock boreholes yielded stronger seismoelectric signals than unfractured zones. Our experiment investigates the use of a near surface P-wave seismic source for making seismoelectric measurements in porous (non-fractured) unconsolidated sediments.

The data for this experiment were acquired during the summer and fall of 2005. The monitoring borehole, UNB1-03, had been drilled and logged as part of a hydrogeophysical study (*Nadeau*, 2005). Slotted PVC casing was used below a bentonite seal placed at 12 m depth in order to allow for galvanic contact with the

formation. The 40 m meter borehole penetrated through fluvial sands, a thick clay/silt aquitard, silty sand and gravel from the flanks of the esker-like Fredericton aquifer, and glacial till interbedded with outwash sand and gravel as shown in Figure 3.1. The bottom five meters of the borehole were not accessible because of sediment infiltration.

## 3.3   Description of the experiment

### 3.3.1   Seismoelectric measurements

In order to eliminate the chances of cross-talk, the downhole seismic and seismoelectric data were acquired separately. The water level in the borehole remained at 9.2 m depth during the period of the experiment.

The electrodes, were constructed using 10 AWG stranded copper wire wrapped around segments of PVC pipe that were 10 cm long and 2.5 cm in diameter. The electrodes were connected to a multi-paired cable and the connections waterproofed with marine epoxy. The resulting array included four electrodes centred 2.2 m apart on the end of a 40 m cable. The measurements reported in this paper were made by pairing the electrodes so as to give three dipoles each 2.2 m in length as shown in Figure 3.1. The signals from the dipoles were buffered using our custom-built differential preamplifiers which provided a gain of 30. They were then digitized by a Geometrics Geode seismograph using a sample interval of 0.125 ms.

We initially experimented with a 12 gauge shotgun seismic source placed in a one meter hole. Unfortunately, the unsaturated sands at surface absorbed much of the high frequency content yielding poor vertical resolution. In order to bypass the surficial sands and deliver seismic energy directly to the water saturated aquitard we drilled a second borehole, 1.5 m away from UNB1-03, to a depth of 9.2 m. The
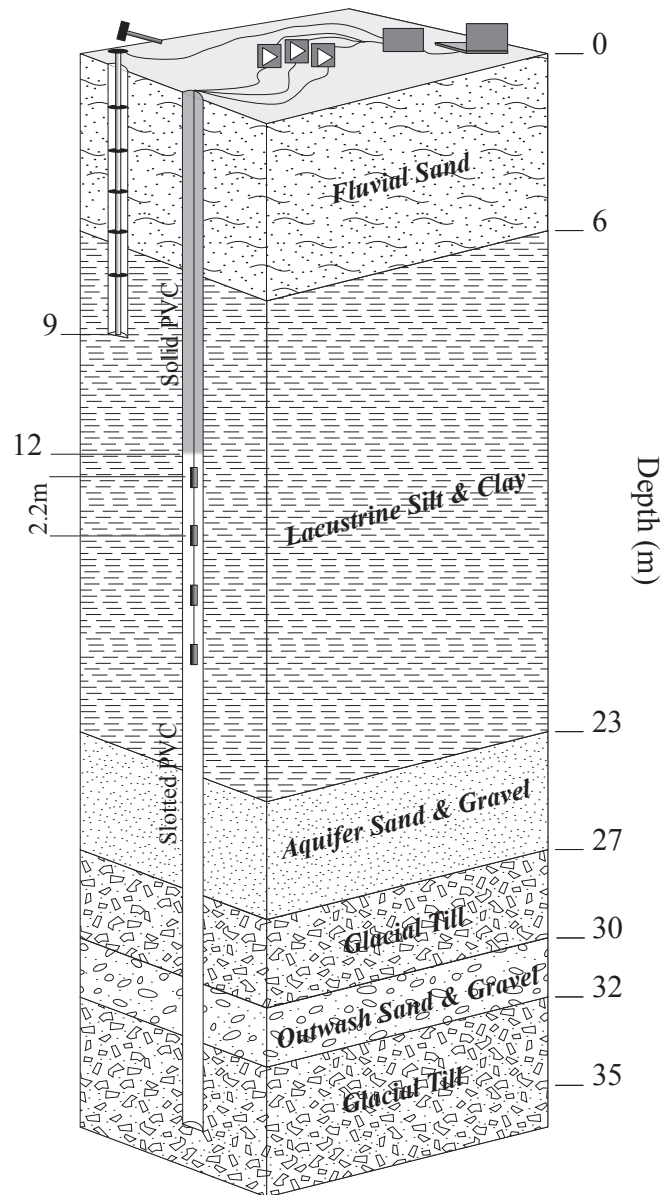
Figure 3.1: Geological log and experimental setup for vertical seismoelectric profiling at borehole UNB1-03

hole was lined with PVC casing and a rigid pole, constructed from multiple 1.5 m sections of 2.54 cm PVC conduit, was inserted until it reached the end cap. The pole was centered in the borehole by rubber spacers (constructed from hockey pucks). A small sledgehammer was used to lightly strike a protective wooden end cap on the top of the pole, and an accelerometer mounted on the cap was used to trigger the seismograph.

The seismoelectric data acquisition was done at night because records collected during the day time exhibited powerline harmonic noise with sudden variations that compromised the effectiveness of the noise removal process described below. The amplitude of the harmonic noise at night was also lower, about half of that measured during the afternoon, ranging from $\approx 500$ $\mu$V/m in the most resistive sediments near the bottom of the hole to $\approx 100$ $\mu$V/m in the more conductive clay/silt unit.

The electrode array was lowered to the bottom of the borehole and raised in increments of 55 cm - a spacing chosen to facilitate stacking of the signal from dipoles at common depths. Twenty shots were acquired at every depth, thereby providing sufficient data for a fold of 60 traces per depth taking into account the redundancy offered by the three dipoles. The traces were not stacked in the field to allow for quality assurance of the data to be stacked.

After acquiring a full set of seismoelectric data at 55 cm spacing, the experiment was repeated, but this time the intermediate points between the first set of depths were chosen. The resulting data set sampled our slotted PVC section in 27.5 cm increments.

### 3.3.2 Other borehole logs

A borehole resistivity log was acquired using a 'normal' resistivity probe connected to a resistivity meter (ABEM SAS 300) at surface. The probe was constructed using 5.08 cm ABS pipe and tinned copper wire. The short and long separation used between the current electrode and potential electrodes on the probe were 20 cm and 1 m respectively. Measurements were taken every 10 cm. The resulting log is found in Figure 3.3.

A borehole geophone was also constructed and used to measure the amplitude of the seismic P-wave arrival (i.e. its particle velocity) as a function of depth. The two geophone elements used in the borehole geophone were oriented vertically and had natural frequencies of 14 Hz and 28 Hz. Measurements were made at 50 cm intervals and five shots were recorded at every depth (Figure 3.3). We also had access to gamma ray, P-wave velocity and S-wave velocity logs and water content measurements from *Nadeau* (2005).

## 3.4 Processing of the data

### 3.4.1 Seismoelectric

Given the weakness of the seismoelectric signals relative to the ambient electrical noise, the raw field records did not show any signs of seismoelectric signal. The raw data were first filtered with a 100-500 Hz Butterworth bandpass filter and then processed with the harmonic noise subtraction algorithm of *Butler and Russell* (2003). This algorithm removed powerline noise at 60 Hz and its harmonics by creating an estimate of the fundamental and its harmonics and subtracting it from the record. The estimate was based on a 150 ms pre-trigger data window recorded with each shot

record. The processed shot records were inspected and those exhibiting high residual noise were killed in order to avoid noise contamination of the stacks.

Upon inspection of the shot records, it became apparent that our records showed trigger jitter which degraded the quality of our original common depth stacks. Statics corrections were applied prior to stacking in order to compensate for this problem. The signal to noise improvement by harmonic subtraction and by stacking was between 40 and 60 dB.

### 3.4.2 Seismic

The raw seismic data were filtered with the same Butterworth bandpass filter as the seismoelectric data. Noisy traces were removed and the remaining traces were stacked according to depth. The voltages measured from the geophone were converted into particle velocity using the transduction constant for the appropriate geophone element.

## 3.5 Results

Figure 3.2 illustrates the results obtained for the seismic and seismoelectric surveys. The traces in both records are plotted with true relative amplitudes. The co-seismic seismoelectric signal is easily followed along the entire depth of the borehole. Amplitude variations are apparent as we progress down the borehole and cross into different types of sediments. The signal to noise ratio degrades at depth, victim of weaker seismic signals and greater noise levels caused by the higher resistivity of the glacial till and the outwash sand and gravel. It is also evident that the dominant frequency of the seismoelectric data is higher than that of the seismic. The dominant

frequency estimated from the first arrival pulse width is ≈380 Hz for the seismoelectric and ≈290 Hz for the seismic. This increase is consistent with the linear frequency dependence in Equation 3.1 presented below. Also, since a potential difference is measured instead of a true electric field measurement, the electrode spacing can become significant in terms of the seismic wavelength and therefore will contribute to the shape of the spectrum. The effect of spatial filtering will be investigated in future work.

## 3.6  Validation of theoretical model

Plane wave solutions for electrokinetically-coupled seismic and electromagnetic waves in homogeneous, poroelastic media have been derived by *Pride and Haartsen* (1996). *Garambois and Dietrich* (2001) reported that co-seismic seismoelectric signal strengths measured at surface were consistent with predictions based on a low frequency form of that theory. In this case, we compare our borehole measurements to an alternative model, developed by *Neev and Yeatts* (1989) which has received less attention in the literature. The model is simpler and less general than that of *Pride and Haartsen* (1996) in that it ignores electromagnetic effects and any frequency dependence of physical properties. Plane wave solutions for seismolectric effects expected to accompany seismic P-waves were instead derived by treating the problem as quasi-static and modifying Biot's poroelastic equations of motion to account for electric forces that would arise due to electrokinetic coupling. We anticipate that this approximation may be adequate at seismic frequencies.

The transfer function, given by *Neev and Yeatts* (1989) in non-dimensional form, relating co-seismic seismoelectric effects to P-wave particle motions in the low
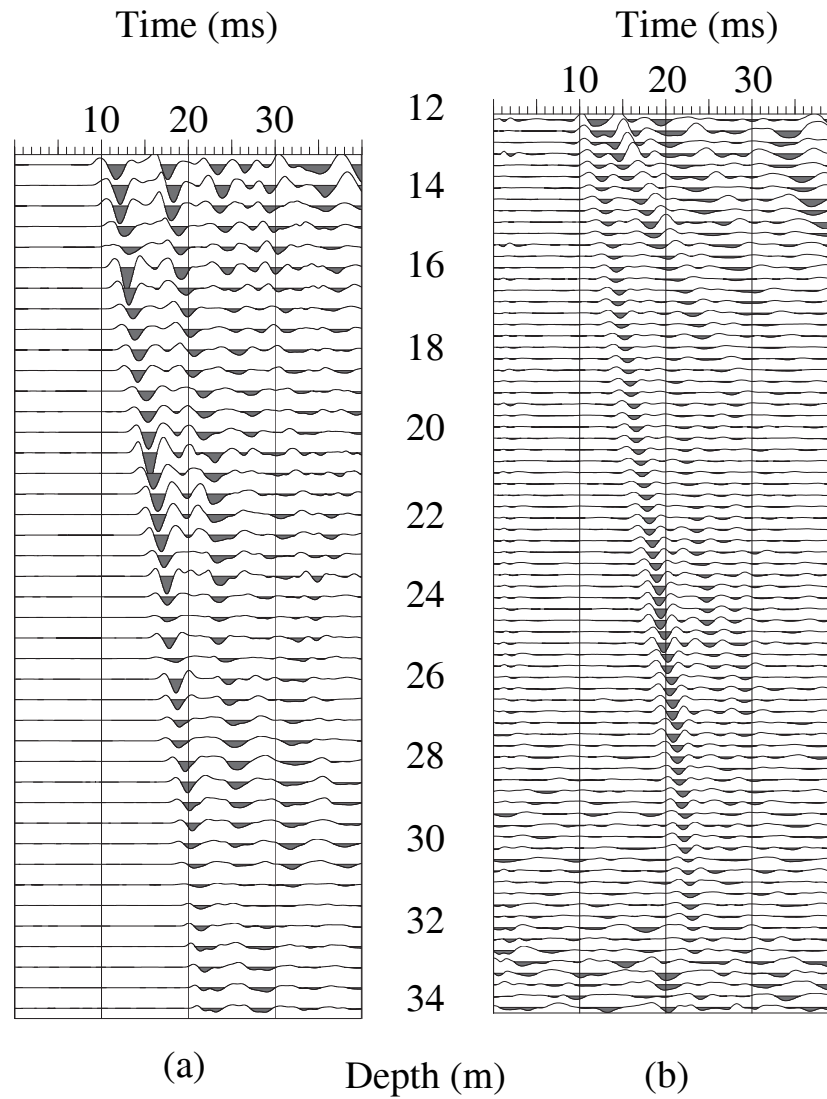
Figure 3.2: Seismic (a) and seismoelectric (b) arrivals as a function of depth in borehole UNB1-03. The traces in each compilation are plotted at their true relative amplitudes.

frequency limit may be expanded as follows (*Butler* (1996)):

$$E \approx \frac{-j\omega\epsilon_f\zeta(Q+R)}{\sigma\tau^2\eta\upsilon_c\upsilon}\dot{u}.$$

(3.1)

Here, $E$ is the electrical field, $\dot{u}$ is the particle velocity, $\omega$ is the angular frequency, $\epsilon_f$ is the fluid permittivity, $\zeta$ is the zeta potential, $Q$ and $R$ are poroelastic constants defined in *Biot and Willis* (1957), $\sigma$ is the conductivity, $\tau$ is the tortuosity, $\eta$ is the fluid viscosity, $\upsilon_c$ and $\upsilon$ are phase velocities.

Our in-situ measurements in UNB1-03 provide values for all the variables except for the zeta potential $\zeta$ and the tortuosity $\tau$. According to *Ishido and Mizutani* (1981) and *Morgan et al.* (1989), the $\zeta$ potential one can expect from most water-saturated geological sediments will range between -10 mV and -100 mV. In order to have an accurate value for $\zeta$ it should be measured in the lab from the sediment samples recovered at UNB1-03. We assume for this exercise that the $\zeta$ potential falls in the middle of the range at -50 mV. The porosity estimates in the sand and gravel aquifer can be converted into tortuosity if we assume that the medium is composed of spherical grains. For such a case, the tortuosity can be estimated by using the equation proposed by *Berryman* (1980), $\tau = (1 + 1/\beta)/2$, where $\beta$ is the porosity.

Given the values of the variables measured for UNB1-03 found in Table 3.1 and the assumptions for $\zeta$ and $\tau$ for the aquifer sand and gravel, the expected seismoelectric signal calculated with equation 3.1 is 10.7 $\mu$V/m. This is within a factor of three of the measured amplitude of 3.8 $\mu$V/m obtained in that layer (Figure 3.3). Thus, given the uncertainty in the values of $\tau$ and $\zeta$, the quasi-static theory of *Neev and Yeatts* (1989) seems to provide a reasonable explanation for the origins of the co-seismic seismoelectric signals observed in this case.

Table 3.1: Value of the variables used to compute the expected seismoelectric response in the sands of the aquifer

| Material property | Symbol | Value | Units |
|---|---|---|---|
| Electrical conductivity | $\sigma$ | 10 | mS/m |
| Zeta potential | $\zeta$ | - 50 | mV |
| Electrical permittivity | $\epsilon_f$ | 80 $\epsilon_0$ | F/m |
| Fluid viscosity | $\eta$ | 1 | mPa s |
| Porosity | $\beta$ | 35 | % |
| Tortuosity | $\tau$ | 1.92 | – |
| Poroelastic constant | $Q$ | $1.31 \times 10^9$ | N/m$^2$ |
| Poroelastic constant | $R$ | $7.10 \times 10^8$ | N/m$^2$ |
| P-wave velocity | $\upsilon$ | 1650 | m/s |
| Characteristic velocity | $\upsilon_c$ | 1719 | m/s |
| Particle velocity | $\dot{u}$ | $7.5 \times 10^{-6}$ | m/s |
| Angular frequency | $\omega$ | $2\pi \times (335)$ | rad/s |
| Bulk modulus (solid)[a] | $K_s$ | $37.9 \times 10^9$ | N/m$^2$ |
| Bulk modulus (fluid)[a] | $K_f$ | $2.25 \times 10^9$ | N/m$^2$ |
| Bulk modulus (dry frame)[a] | $K_{fr}$ | $2.20 \times 10^8$ | N/m$^2$ |

[a] Values required to compute $Q$ and $R$ from *Biot and Willis* (1957).
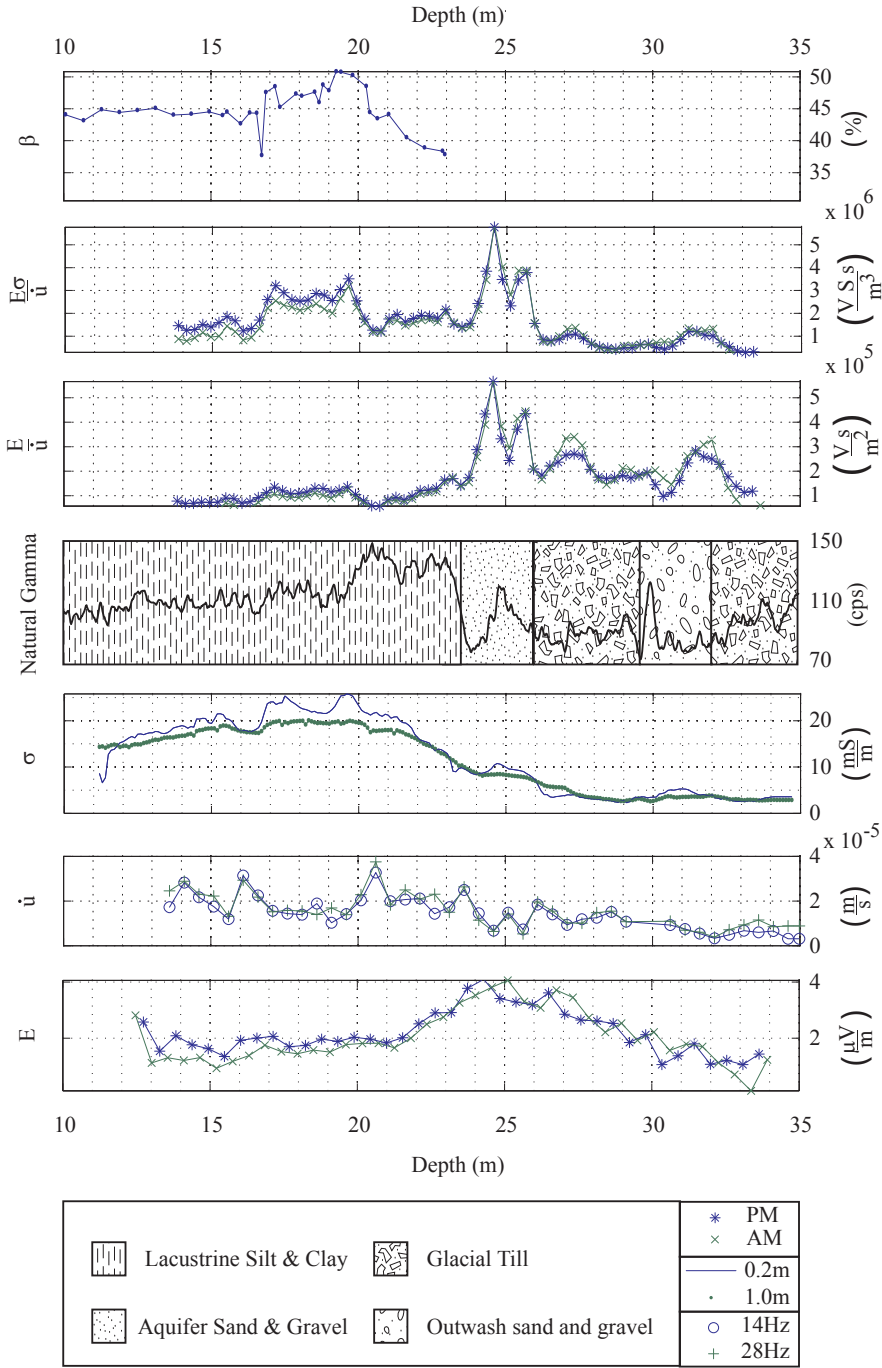
Figure 3.3: Comparison of the seismolectric log $E$ and conductivity $\sigma$, natural gamma and porosity log $\beta$. Also shown is the impact of normalizing the seismoelectric log by the particle velocity, $\dot{u}$, and by particle velocity and conductivity $(\sigma/\dot{u})$ log.

## 3.7   Discussion

In order to better see the effects of sediment type on the strength of the co-seismic seismoelectric signal, the amplitudes of the first pulse were measured and are compared to logs of seismic amplitude, conductivity, natural gamma ray emissions and porosity in Figure 3.3. We can see that the seismoelectric signal increases when we reach the aquifer sand and gravel at about 23 m.

Equation 3.1 dictates that the seismoelectric field is proportional to the particle velocity and inversely proportional to the electrical conductivity of the surrounding material. These characteristics mask the other properties contained in the seismo-electric measurements that could be of interest to determine permeability. If we normalize the measured seismoelectric field by the particle velocity we can see an increase of the normalized seismoelectric signal $E/\dot{u}$ in the aquifer sand and gravel in comparison to the less permeable clay/silt and glacial till. There is, more generally, evidence of an inverse relationship between $E/\dot{u}$ and natural gamma ray emissions that are normally indicative of clay content. If we normalize by both particle velocity and electrical conductivity, we can see that the effects of a localized increase or decrease in conductivity are removed. We also see that there is a region of higher signal strength in the clay/silt unit that was previously masked by higher conductivities and is correlated with elevated porosities ($\beta$ as high as 50%) based on water content measurements that were available for samples recovered from the clay/silt layer.

These normalized seismoelectric logs demonstrate that the strong seismoelectric response observed in the aquifer sands cannot be attributed to variations in particle velocity or electrical conductivity alone. Laboratory measurements on the sediment samples retrieved from UNB1-03 may allow us to measure the $\zeta$ potential and determine its role in the seismoelectric highs observed but porosity and pore space

tortuosity (which are in turn related to fluid flow permeability) and elastic constants must play an important role in the seismoelectric amplitudes observed.

Although the co-seismic seismoelectric signals have been the subject of interest in this work, it is worth noting that a second type of seismoelectric effect, emanating from interfaces in porous media, has also been reported, and predicted by theory. Such interfacial seismoelectric effects generated, for example, at the top or bottom of the aquifer sand, must have amplitudes less than the noise level of 0.2 $\mu$V/m in our processed data.

## 3.8   Conclusions

Seismoelectric effects were successfully acquired in a borehole which penetrates glaciofluvial sediments. It was shown that the co-seismic seismoelectric signal varies with sediment type. These results are of interest in light of ongoing efforts to determine how seismoelectric effects may be applied to assess pore fluid type, porosity and fluid flow permeability in aquifers or reservoirs. Our experiment shows that co-seismic seismoelectric effects, normally considered to be noise in surface seismoelectric experiments, have potential to be used as a porosity/permeability logging tool in the borehole environment.

This experiment has also shown that vertical seismoelectric profiling is a promising method to help validate theories for the generation of electrical signals through electrokinetic coupling. Calculated values for the predicted seismoelectric signals are within a factor of three of the measured values which constitute a reasonable agreement given the uncertainties in the values assumed for tortuosity and zeta potential.

## 3.9    Acknowledgements

# References

Berryman, J. G. (1980), Long wavelength propagation in composite elastic media, I. spherical inclusions, *Journal of the Acoustical Society of America*, *68*(6), 1809–1819, doi:10.1121/1.385171.

Biot, M. A., and D. G. Willis (1957), The elastic coefficients of the theory of consolidation, *Journal of Applied Mechanics*, *24*(4), 594–601.

Butler, K. E. (1996), Seismoelectric effects of electrokinetic origin, Ph.D. thesis, University of British Columbia, Vancouver, BC.

Butler, K. E., and R. D. Russell (2003), Cancellation of multiple harmonic noise series in geophysical records, *Geophysics*, *68*(3), 1083–1090, doi:10.1190/1.1581080.

Garambois, S., and M. Dietrich (2001), Seismoelectric wave conversions in porous media: Field measurements and transfer function analysis, *Geophysics*, *66*(5), 1417–1430, doi:10.1190/1.1487087.

Hunt, C. W., and M. H. Worthington (2000), Borehole electrokinetic responses in fracture dominated hydraulically conductive zones., *Geophysical Research Letters*, *27*(9), 1315–1318.

Ishido, T., and H. Mizutani (1981), Experimental and theoretical basis for electrokinetic phenomena in rock-water systems and its application to geophysics., *Journal of Geophysical Research*, *86*(B3), 1763–1775, doi:10.1029/JB086iB03p01763.

Mikhailov, O. V., J. Queen, and M. N. Toksöz (2000), Using borehole electroseismic measurements to detect and characterize fractured (permeable) zones, *Geophysics*, *65*(4), 1098–1112, doi:10.1190/1.1444803.

Morgan, F. D., E. R. Williams, and T. R. Madden (1989), Streaming potential properties of westerly granite with applications., *Journal of Geophysical Research*, *94*(B9), 12,449–12,461.

Nadeau, J. C. (2005), Geophysical imaging of a river valley aquifer, Master's thesis, University of New Brunswick, Fredericton, NB.

Neev, J., and F. R. Yeatts (1989), Electrokinetic effects in fluid-saturated poroelastic media, *Physical Review B*, *40*(13), 9135–9141, doi:10.1103/PhysRevB.40.9135.

Pride, S., and M. W. Haartsen (1996), Electroseismic wave properties, *Journal of the Acoustical Society of America*, *100*(3), 1301–1315, doi:10.1121/1.416018.

# Chapter 4

# Seismoelectric imaging of the vadose zone of a sand aquifer

## 4.1    Abstract

We have acquired a 300 m seismoelectric section over an unconfined aquifer to demonstrate the effectiveness of interfacial signals at imaging interfaces in shallow sedimentary environments. The seismoelectric data were acquired using a 40 kg accelerated weight drop source and a 24-channel seismoelectric recording system composed of grounded dipoles, preamplifiers and seismographs. Interfacial signals were remarkably clear in the shot records, arriving simultaneously at offsets up to 40 m from the seismic source. The most prominent signal was generated at the water table at a depth of approximately 14 m and had peak amplitudes on the order of 1 $\mu$V/m. A weaker response was generated at a shallower interface that is interpreted to be a water retentive layer. The validity of these two laterally continuous features, and of

other discontinuous events indicative of vadose zone heterogeneity, is corroborated by the presence of reflections exhibiting similar characteristics in a ground penetrating radar profile acquired along the same line.

## 4.2 Introduction

Mechanical wave propagation through porous media can generate electromagnetic signals, known as seismoelectric effects, by electrokinetic coupling mechanisms that involve the motion of charge in the electrical double layer at the solid-liquid interface (*Pride*, 1994). Such signals, and reciprocal phenomena (*Thompson et al.*, 2007), are of interest for the information they may be able to provide on pore fluid type and porous medium properties such as porosity and permeability (e.g. *Thompson and Gist*, 1993; *Garambois and Dietrich*, 2002).

Compressional waves in poroelestic media cause pore fluid to move relative to the solid matrix thereby moving the excess electrical charge in the outer, mobile portion of the electrical double layer. These streaming currents result in charge separations and hence electrical fields arising between zones of compression and rarefaction. In a homogenous medium, this phenomenon gives rise to a co-seismic electric field that is confined within the compressional wave (*Neev and Yeatts*, 1989; *Dupuis and Butler*, 2006). When a compressional wave encounters heterogeneity such as an interface that changes the streaming currents and distorts the resulting charge distribution, it generates an unbounded electric field, which we call an interfacial seismoelectric effect (*Haartsen and Pride*, 1997). These effects are expected to propagate (diffuse) through the earth as electromagnetic signals and therefore appear nearly simultaneously at widely separated receivers with an arrival time essentially equal to the

one-way seismic traveltime from shotpoint to interface.

Conceptual models (e.g. *Butler et al.*, 1996) and rigorous theoretical modeling (e.g. *Haartsen and Pride*, 1997; *Garambois and Dietrich*, 2002) indicate that the interfacial effect should be a multipole electrical source that develops over a Fresnel zone having a diameter that increases with depth and seismic wavelength. Higher order terms will diminish more rapidly with distance leaving the dipole term to dominate. Thus, an interfacial seismoelectric signal emanating from a horizontal boundary is expected to exhibit symmetry and amplitude characteristics similar to that of a vertical electrical dipole centered on the interface directly below the shot.

While the existence of interfacial seismoelectric effects in porous media has recently been confirmed by several investigators (e.g. *Butler et al.*, 1996; *Mikhailov et al.*, 1997; *Russell et al.*, 1997; *Garambois and Dietrich*, 2001; *Haines et al.*, 2007; *Strahser et al.*, 2007) only a handful of studies have shown that the method can be used to map interfaces. *Martner and Sparks* (1959) mapped lateral variations in seismic traveltimes through the weathered layer by exploiting the co-seismic effect associated with a seismic P-wave critically refracted at the base of that layer. *Thompson and Gist* (1993) were the first to attempt seismoelectric profiling making use of interfacial electrokinetic seismoelectric effects, and inferred that they were able to image high permeability water sands and low permeability shales at depths of up to 300 m. *Butler et al.* (1996) used interfacial seismoelectric effects to map variations in the depth to a layer of heavily compacted, impermeable glacial till underlying 1 – 3 m of organic-rich fill.

In this paper, we present measurements of remarkably clear interfacial effects obtained over an unconfined sand aquifer. The results prove that seismoelectric methods can be used to trace subsurface interfaces in a manner analogous to multi-channel

seismic reflection surveying.

## 4.3   Site description

The survey site was situated within the Gnangara Mound region on the northern fringes of Perth, Western Australia – a region hosting important groundwater resources including a sandy 'superficial' aquifer typically 50 m thick. The data were collected along Cypress Rd., 1.7 km west of groundwater production well P-90. Regional hydrogeological studies (*Davidson*, 1995) and the geological log from borehole P-90 indicate that the superficial aquifer at this site is composed of a series of fine to coarse-grained quartz sands underlain by a siltstone layer at 58 m depth. Shallow discontinuous water retentive layers exert control over aquifer recharge and help to maintain near-surface moisture needed to support local ecosystems (M. Martin, personal communication, 2007). The geological log from P-90 identifies such a layer between 6 and 8 m depth and refers to it as "coffee rock" – a friable, limonite-cemented sand (*Davidson*, 1995) that is also evident as a zone of slightly elevated counts on the borehole's gamma ray log.

We chose to survey a 300 m segment of the road where an earlier GPR survey had indicated the presence of a water retentive layer together with an increase in vadose zone heterogeneity and a shallowing of the water table in the approach to a topographic low. The objective was to determine whether seismoelectric conversions measured previously in boreholes at two nearby sites *Dupuis et al.* (2007) could be measured on the surface and used to map lateral variations in shallow subsurface interfaces.

## 4.4 Method

Our recording spread (Figure 4.1) consisted of 26 electrodes at 4 m intervals connected to form 24 dipoles arranged end-to-end except for a 4 m shot gap at the centre. Three 12-channel, 24-bit seismographs (Geometrics Geodes) with associated seismic cables were used to record the data after it was buffered by custom-built differential preamplifiers. Four shotpoints spaced 1 m apart were placed in the shot gap (offset about 2 m from the line for convenience) and three to five impacts from a 40 kg accelerated weight drop source were recorded at each point. The array advanced towards the west for 300 m as illustrated in Figure 4.1 with shot records collected at every metre.

The site chosen for this traverse was within 200 m of a power line. Electrical noise at 50 Hz and its harmonics, measured $0.1 - 0.4$ mV/m peak-to-peak. A harmonic subtraction algorithm applied during data processing (*Butler and Russell*, 2003) and band-pass filtering (60-375 Hz, minimum phase) proved effective in reducing this noise to a manageable level. Furthermore, the shot redundancy at each shotpoint allowed us to discard any records that exhibited excessive residual harmonic noise prior to stacking.

During preliminary tests, we found that high contact impedances between our 40 cm stainless steel rod electrodes and the dry surficial sands made our data more susceptible to contamination by demodulated AM radio broadcasts (*Kepic and Butler*, 2002). To alleviate this problem we augered shallow holes ( 50 cm deep) and either hammered one of our stainless steel rods into the bottom or inserted a sheet of aluminium foil before backfilling with sand and pouring on a mixture of water and soil-wetting agent.
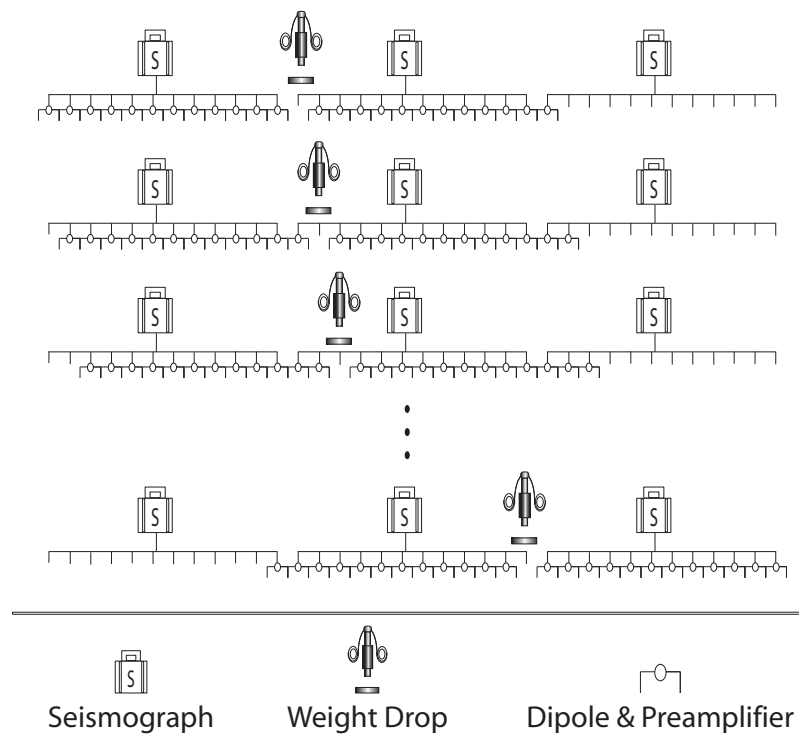
Figure 4.1: Illustration of the seismoelectric array geometry and shooting progression.

## 4.5 Results and discussion

To interpret the various arrivals in the shot records, we combined data from the four shotpoints in each shot gap following an approach suggested by *Kepic and Rosid* (2004) to form composite shot gathers, or "super gathers" with very dense spatial sampling (96 traces at 1 m intervals). This approach guards against spatial aliasing and therefore facilitates identification of various seismoelectric arrivals as well as wavefield separation techniques such as f-k filtering (although such filtering was not necessary to reveal the shallow seismoelectric events measured at this site).

Figure 4.2 (a) and (b) show seismic and seismoelectric super gathers centred at the 128 m mark on the survey line. In order to remove any risk of cross-talk, the seismoelectric data were acquired first before placing geophones at the dipole midpoints and repeating the shots. The two gathers exhibit many similarities. There are direct arrivals, ground roll and one or two shallow seismic reflections, which appear as hyperbolas. In the seismoelectric record, these events represent co-seismic signals. The two gathers differ at early time however where a remarkably clear seismoelectric signal, (1), can be seen arriving simultaneously at offsets up to 40 m from the shot. The signal is inverted in polarity on opposite sides of the shot and arrives 35 ms after impact, well before the arrival of co-seismic signals over most of the receiver spread. Both of these characteristics are consistent with the model of a vertical electric dipole-like source and we conclude that the signal is most likely an interfacial seismoelectric effect of electrokinetic origin.
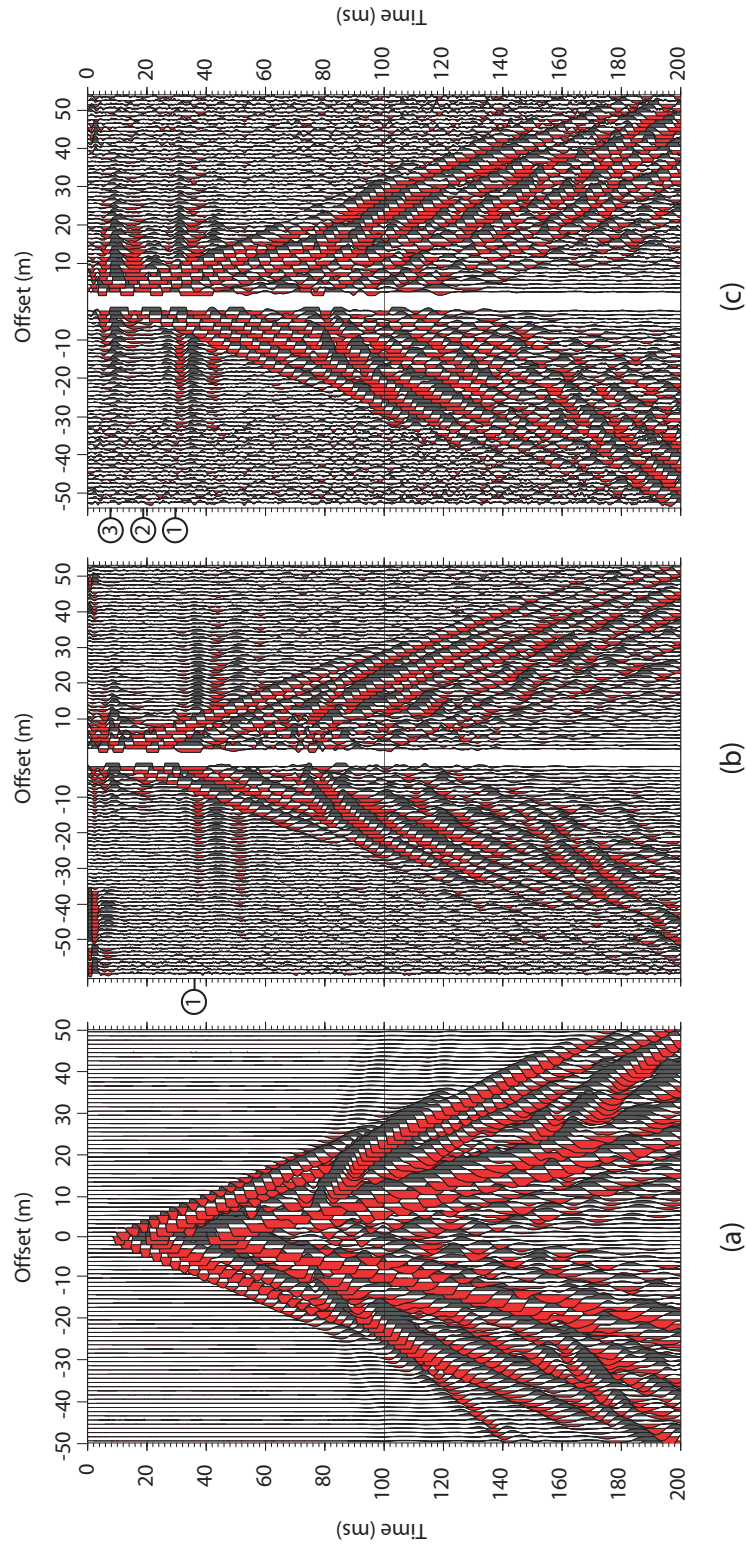
Figure 4.2: (a) Seismic and (b) seismoelectric supergathers centered at the 128 m mark along the line. (c). A second seismoelectric supergather, from the 36 m mark, reveals additional shallower interfacial effects. The signal-to-noise ratio in (b) has been improved further by stacking five adjacent supergathers. Trace spacing is 1 m, and the root mean square amplitude of each trace has been normalized to be the same value.

The arrival time of this prominent interfacial effect is one-half the arrival time of the reflection hyperbola appearing at 70 ms in the seismic data. This indicates that the same interface is responsible for the seismoelectric conversion and the seismic reflection. Based on the local geology and borehole experiments at nearby sites, we anticipate that this interface is the water table which is the strongest near-surface acoustic impedance contrast and commonly found at depths ranging from 10 to 20 m. The seismic data in Figure 4.2(a) provide two ways for us to estimate it's depth at this site. Refraction modelling suggests a two layer model consisting of 10.5 m of unsaturated sediments with a velocity of 320 m/s underlain by saturated sediments with a velocity of $\approx$ 1780 m/s. Alternatively, the two-way time to the onset of the reflection hyperbola, 70 ms, and the observed normal moveout velocity of 400 m/s suggest a depth of 14 m. We suspect that our refraction interpretation underestimates the depth because it is unable to resolve an increase in velocity through the vadose zone that would be expected due to increased sediment compaction and water saturation with depth.

This depth estimate allows us to compare the amplitude versus offset characteristics of the measured interfacial signal (1) to the amplitude variations that would be expected using the approximate model of a vertical dipole source located 14 m below the shotpoint. Figure 4.3 indicates that the dipole model is reasonable as a first order approximation although the measured amplitudes decay slightly more gradually than predicted. The difference may be attributed to the shallow depth of the interface (14 m) which is not much larger than the radius of the first Fresnel zone (approximately 8 m) over which the source is distributed (*Garambois and Dietrich*, 2002). The amplitudes best follow the trend between 12 and 35 m where they can be reliably measured.
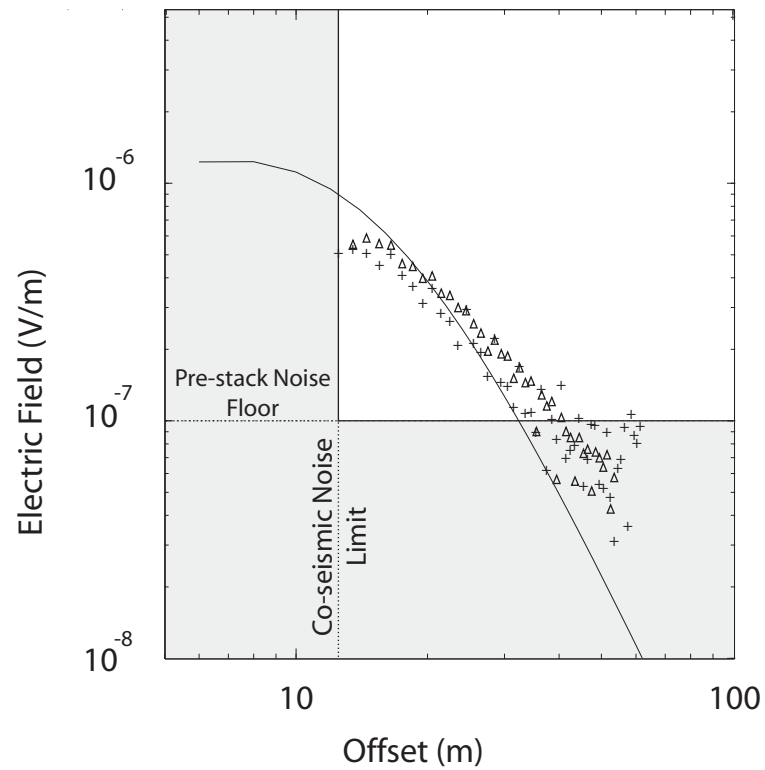
Figure 4.3: Predicted (solid line) and measured amplitude variation with offset for the interfacial seismoelectric signal (1) in Figure 4.2 (b) emanating from 14-m depth. Crosses and triangles represent measurements at positive and negative offsets, respectively. The dipole moment was adjusted to best fit the measured data.

Although the water table provides a strong interfacial signal, it is not the only interface detected. Figure 4.2 (c) illustrates two additional events, (2) and (3), which are seen in other super gathers along the profile. In spite of its weak amplitude, event (2) has the phase reversal expected for an electrokinetic interfacial signal; it appears more clearly in the stacked section presented later. The lack of polarity reversal on the shallowest event, (3), suggests that it is not electrokinetic in origin and not a "direct field" signal of the type reported by *Haines et al.* (2007). We are uncertain of its origin but speculate that it could be a result of strong downgoing seismic waves modulating the resistivity of a shallow layer through which telluric currents are flowing, thereby modulating the voltage drop from those currents across the dipole receivers. This 'resistivity modulation' mechanism has been recognized for some time (*Thompson*, 1936; *Long and Rivers*, 1975; *Russell et al.*, 1997) but has not been extensively studied.

### 4.5.1 Creation and interpretation of a seismoelectric section

Our survey was designed to yield a stacked seismoelectric section that would be analogous to a common depth point stack in multi-channel seismic reflection surveying. The approach was similar to that used by *Thompson and Gist* (1993) for their larger scale experiment but did not require wavefield separation filtering since the near-surface velocity structure at this site naturally provided good separation between the interfacial and co-seismic signals over a wide range of offsets.

The first step in the processing flow was to assemble vertical stacks of the shot records at each shotpoint and reverse the polarity of the traces at negative offsets. A tapered mute was used to remove the portion of each shot record dominated by co-seismic noise and mean scaling was then applied to the data before traces with

offsets between 14 and 40 m were stacked to form a single trace which was plotted at the shot location. Since seismoelectric conversions from near-horizontal interfaces are expected to be anti-symmetric about the shotpoint, the polarity reversal and stacking process enhances any interfacial effects relative to noise from distant sources which would be of the same polarity on either side of the shot. It would also tend to cancel event (3) in Figure 4.2 (c). This process was repeated for each of the 300 shots spaced 1 m apart. Each stacked trace was then averaged with six neighbouring traces (three from each side) to enhance coherency and yield the stacked seismoelectric section shown in Figure 4.4.
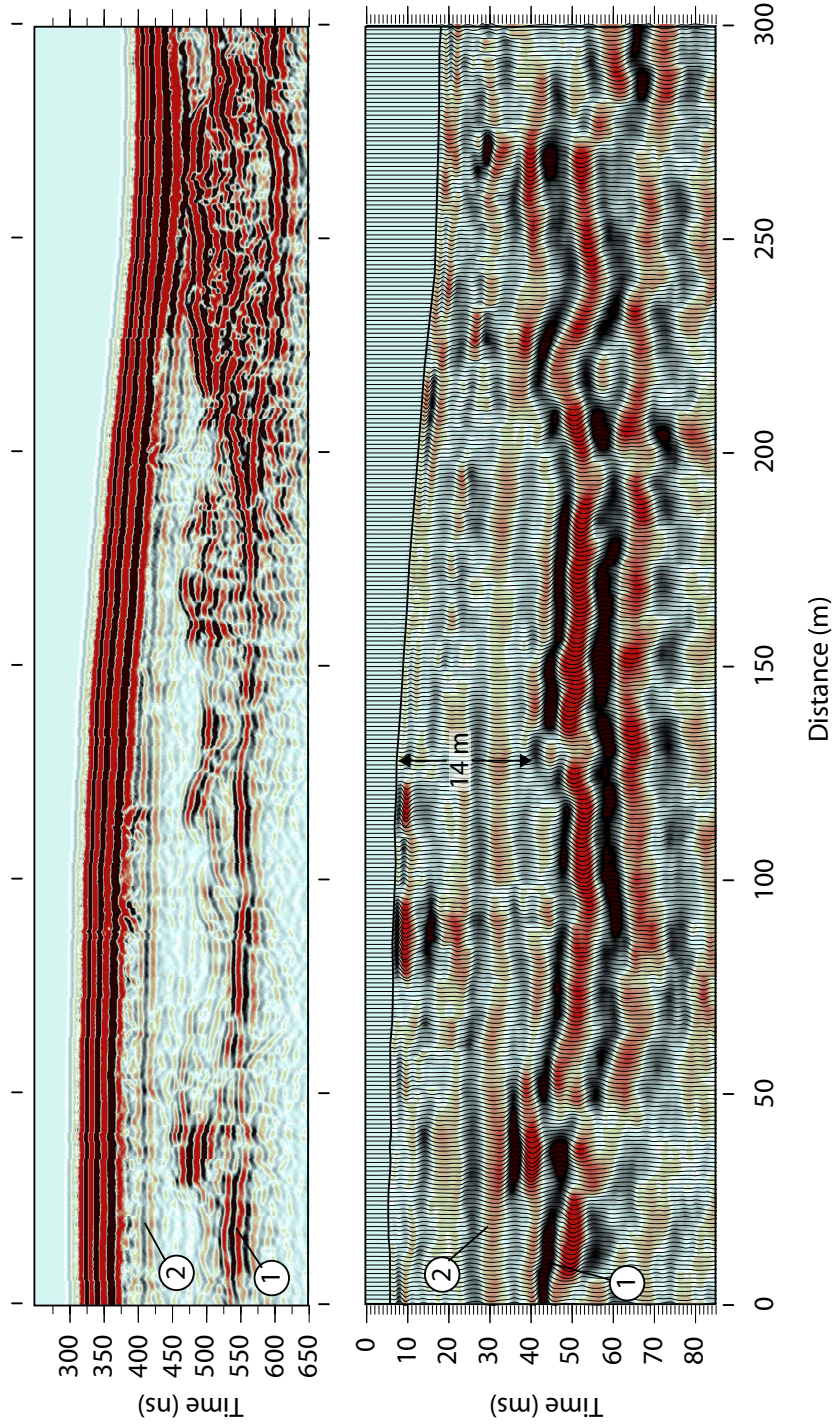
Figure 4.4: GPR (top) and seismoelectric (bottom) profiles acquired along a 300-m traverse. Variable time delays (elevation statics) have been applied to the traces in each profile to account for topography relative to arbitrary datums.

Figure 4.4 also shows a 50 MHz GPR profile collected at the same site although at a different time and on the other side of the road, approximately 5 m away. The resolution of the GPR data is better at this site because dry sandy conditions limited the seismic pulse bandwidth. However there are many similarities between the two profiles, including the indications of sedimentary heterogeneity that appear in the form of discontinuous events at 35 m, 128 m and 280 m along the line.

The strong coherent signal (1) related to the water table appears clearly in both profiles. The depth estimate of 14 m given above is consistent with the signal's arrival time on the GPR profile if we assume a radar wave velocity of 0.14 m/ns – a reasonable value for partially saturated sands. We note however that the GPR data were collected several months prior to the seismoelectric survey. A second interfacial signal (2), identified as a weak event in the super gather of Figure 4.2 (c), can also be traced across most of the seismoelectric section. We speculate that it originates at the same interface as a shallow GPR reflection exhibiting similar morphology and represents a water retentive layer. Depth estimates from the seismoelectric and GPR profiles place this interface at a depth between 6 and 7 meters – consistent with the depth of 6 m reported for the "coffee rock" layer in borehole P-90. The difference in the separation of events (1) and (2) on the seismoelectric and GPR time sections can be attributed to the tendency for seismic velocity to increase with depth due to sediment compaction and increased water saturation; in contrast radar wave velocity decreases with increasing moisture content.

Finally, we note that there are some differences between the seismoelectric and GPR profiles, particularly beneath the topographic low at the west end of the line where the GPR data exhibit more complexity. This suggests that the two methods provide complementary information given differences in their sensitivities to various

physical parameters. More work is required to ascertain which physical property variations are most important in the seismoelectric case.

## 4.6 Conclusions

The results of this experiment demonstrate that it is possible to use seismo-electric profiling to map subsurface interfaces within partially and fully saturated sediments. In particular, it allowed us to image the water table, as well as a shallower interface interpreted as a water retentive layer which was not resolved by seismic reflection or refraction. The observed variations in interfacial signal amplitude with offset provide a first order fit to the simple, approximate model of a vertical electrical dipole-like source, thereby supporting the interpretation that the signal is of electroki-netic origin. The physical property changes most important for the generation of the observed interfacial signals are not known conclusively. However, we suspect that the strong response from the water table is likely related to significant changes in acoustic impedance and electrical conductivity accompanying the relatively abrupt increase in water saturation that would be expected in coarse grained sediments such as sands. The signal generated at the water retentive layer is expected to be related to similar physical parameters but may also include variations in porosity or permeability.

Relatively dry, sandy near-surface conditions such as those found on the Gnan-gara Mound are challenging for seismic surveying because they typically exhibit high seismic absorption coefficients with a resultant decrease in high frequency content and resolution. In the case of this seismoelectric field trial however, the disadvan-tages were offset somewhat by the fact that (i) co-seismic signals associated with direct P-waves were slow to spread across the receiver array, and (ii) the water table

was sufficiently deep to allow for clear separation between different interfacial signals within the vadose zone.

Our results demonstrate that it is possible to measure interfacial seismoelectric effects from depths exceeding 10 m and show that the method may become a valuable tool, sensitive to the presence of pore water and complementary to GPR, for the characterization of aquifers. It is also foreseeable, that the method could be useful at much greater depths as it continues to evolve and more concerted efforts are made to separate interfacial effects from co-seismic interference.

## 4.7  Acknowledgements

## References

Butler, K. E., and R. D. Russell (2003), Cancellation of multiple harmonic noise series in geophysical records, *Geophysics*, *68*(3), 1083–1090, doi:10.1190/1.1581080.

Butler, K. E., R. D. Russell, A. W. Kepic, and M. Maxwell (1996), Measurement of the seismoelectric response from a shallow boundary, *Geophysics*, *61*(6), 1769–1778, doi:10.1190/1.1444093.

Davidson, W. A. (1995), Hydrogeology and groundwater resources of the Perth region Western Australia, *Bulletin 142*, Geological Survey of Western Australia.

Dupuis, J. C., and K. E. Butler (2006), Vertical seismoelectric profiling in a borehole penetrating glaciofluvial sediments, *Geophysical Research Letters*, *33*(16), doi:10.1029/2006GL026385.

Dupuis, J. C., K. E. Butler, A. W. Kepic, and B. D. Harris (2007), The seismoelectric response of a sandy aquifer: borehole experiments, in *69 th Conference & Exhibition, London,UK*, European Association of Geoscientists & Engineers.

Garambois, S., and M. Dietrich (2001), Seismoelectric wave conversions in porous media: Field measurements and transfer function analysis, *Geophysics*, *66*(5), 1417–1430, doi:10.1190/1.1487087.

Garambois, S., and M. Dietrich (2002), Full waveform numerical simulations of seismoelectromagnetic wave conversions in fluid-saturated stratified porous media, *Journal of Geophysical Research*, *107*(B7), doi:10.1029/2001JB000316.

Haartsen, M. W., and S. Pride (1997), Electroseismic waves from point sources in layered media, *Journal of Geophysical Research*, *102*(B11), 24,745–24,769.

Haines, S. S., S. L. Klemperer, and B. Biondi (2007), Seismoelectric imaging of shallow targets, *Geophysics*, *72*(2), G9–G20, doi:10.1190/1.2428267.

Kepic, A., and K. Butler (2002), The art of measuring very low amplitude seismoelectric signals, in *64th Meeting*, p. 193, European Association of Geoscientists & Engineers.

Kepic, A., and M. Rosid (2004), Enhancing the seismoelectric method via a virtual shot gather, in *74th Annual International Meeting*, pp. 1337–1340, Society of Exploration Geophysicists, doi:10.1190/1.1851111.

Long, L. T., and W. K. Rivers (1975), Field measurements of the electroseismic response, *Geophysics*, *40*(2), 233–245, doi:10.1190/1.1440521.

Martner, S. T., and N. R. Sparks (1959), The electroseismic effect, *Geophysics*, *24*(2), 297–308, doi:10.1190/1.1438585.

Mikhailov, O. V., W. M. Haartsen, and M. N. Toksöz (1997), Electroseismic investigation of the shallow subsurface: Field measurements and numerical modeling, *Geophysics*, *62*(1), 97–105, doi:10.1190/1.1444150.

Neev, J., and F. R. Yeatts (1989), Electrokinetic effects in fluid-saturated poroelastic media, *Physical Review B*, *40*(13), 9135–9141, doi:10.1103/PhysRevB.40.9135.

Pride, S. (1994), Governing equations for the coupled electromagnetics and acoustics of porous media, *Physical Review B*, *50*(21), 15,678–15,696, doi:10.1103/PhysRevB.50.15678.

Russell, R. D., K. E. Butler, A. W. Kepic, and M. Maxwell (1997), Seismoelectric exploration, *The Leading Edge*, *16*(11), 1611–1615, doi:10.1190/1.1437536.

Strahser, M. H. P., W. Rabbel, and F. Schildknecht (2007), Polarisation and slowness of seismoelectric signals, a case study, *Near Surface Geophysics*, *5*, 97–114.

Thompson, A. H., and G. A. Gist (1993), Geophysical applications of electrokinetic conversion, *The Leading Edge*, *12*(12), 1169–1173, doi:10.1190/1.1436931.

Thompson, A. H., et al. (2007), Field tests of electroseismic hydrocarbon detection, *Geophysics*, *72*(1), N1–N9, doi:10.1190/1.2399458.

Thompson, R. R. (1936), The seismic-electric effect, *Geophysics*, *1*(3), 327–335, doi:10.1190/1.1437119.

# Chapter 5

# Anatomy of a seismoelectric conversion: Measurements and modelling in boreholes penetrating a sandy aquifer

## 5.1 Abstract

Conversions of compressional seismic waves to electric fields have been measured in two boreholes drilled within an unconfined sandy aquifer on the Gnangara Mound near Perth, Australia. The seismoelectric conversion at both field sites occurred in vicinity of the water table at 13 m depth and yielded maximum amplitudes of 1 $\mu$V/m using a sledgehammer source on surface. Partially cemented layers, inferred from geological and geophysical logs, straddle the water table, and may also play a role in generating the conversion and influencing its amplitude distribution.

The dense vertical sampling used in these borehole experiments reveals spatial and temporal polarity reversals of the interfacial signal, which provide new evidence in support of the conceptual model for seismoelectric conversions at interfaces. We demonstrate that the growth rate of the source zone and its maximum vertical extent below the water table are encoded in the polarity of the interfacial signal. The results of these experiments confirm that vertical seismoelectric profiling can be used to gain further insight into seismoelectric conversions at interfaces and to assess which interfaces may be amenable to detection by surface seismoelectric surveys.

## 5.2   Introduction

Electrokinetic coupling between seismic waves and electrical fields has attracted significant attention over the last 15 years because of its expected sensitivity to pore fluid properties and fluid flow permeability. There is particular interest in using the phenomenon to image subsurface interfaces, combining the resolution of seismic methods with material property sensitivities more akin to those of electrical methods. While theoretical models and numerical simulations for such seismoelectric effects now exist, there remains a need for convincing field measurements that can be used to evaluate the models and identify the types of interfaces most amenable to detection.

We have recently measured remarkably clear interfacial seismoelectric effects generated within a sandy aquifer on the Gnangara Mound near Perth, Australia. *Dupuis et al.* (2007) presented data from a 300 m long traverse that imaged two distinct interfaces interpreted as a water retentive layer and the base of the vadose zone at depths up to 15 m. In this paper we concentrate on the origin of interfacial

signals in the Gnangara Mound area by presenting the results of measurements made in boreholes. Comparisons of geological and geophysical logs show that a strong seismoelectric effect is associated with a partially cemented zone that lies at the base of the vadose zone. Measurements of signal polarity and amplitude as a function of depth provide compelling new evidence in support of the current conceptual model for the generation of seismoelectric effects at interfaces.

Electrokinetic coupling arises from the flow or oscillation of ions in the electric double layer that forms between the pore fluid and the solid grains in rocks or soils. Two different types of electrokinetic seismoelectric signals can be generated by compressional seismic waves. The first is termed co-seismic, because it is local to the seismic wave and is observed in homogeneous media, as a result of charge separation between zones of compression and dilatation associated with the seismic wave (*Neev and Yeatts*, 1989; *Pride and Haartsen*, 1996). The second is termed an interfacial signal because it is generated at an interface where the symmetry of the charge distribution within the seismic wave is altered. The resulting electric field radiates away from the interface at the speed of an electromagnetic wave and exhibits amplitude variations similar to that of an electric dipole positioned at the heterogeneity (*Thompson and Gist*, 1993; *Butler et al.*, 1996; *Haartsen and Pride*, 1997; *Garambois and Dietrich*, 2002).

Other poroelastic wave modes such as shear waves (*Bordes et al.*, 2006), and Stoneley waves in boreholes (*Mikhailov et al.*, 2000; *Hunt and Worthington*, 2000; *Singer et al.*, 2005) can generate seismoelectric signals, but the compressional wave (P-wave) has generally received the most attention in field experiments (*Martner and Sparks*, 1959; *Thompson and Gist*, 1993; *Butler et al.*, 1996; *Mikhailov et al.*, 1997; *Russell et al.*, 1997; *Beamish*, 1999; *Butler et al.*, 1999; *Garambois and Dietrich*,

2001; *Dupuis and Butler*, 2006; *Kulessa et al.*, 2006; *Dupuis et al.*, 2007; *Strahser et al.*, 2007). It is favored because models predict that it has the best potential to generate interfacial signals of sufficient strength to be observed on surface and used to map heterogeneities (*Haartsen and Pride*, 1997; *Garambois and Dietrich*, 2002). However, the measurement of these weak interfacial signals under field conditions is challenging – particularly on surface, where both ambient environmental noise and co-seismic arrivals tend to cause the most interference.

The geometry of a vertical seismoelectric profiling (VSEP) survey, as described in *Dupuis and Butler* (2006), provides several benefits over surface-based field measurements in terms of signal-to-noise ratio. Since the measurements are made in-situ they are made closer to the seismoelectric source, and the receivers, immersed in the borehole fluid, have low contact impedance and hence lower overall electrical noise. A further advantage of this geometry is the ability to separate the interfacial seismoelectric signal from the co-seismic signal associated with the direct arrival. This separation is achieved by placing the receivers below an interface so that interfacial signals reach the receivers before the co-seismic arrivals.

*Martner and Sparks* (1959), *Butler et al.* (1996), and *Russell et al.* (1997) used boreholes for the signal separation they can provide. Shots were fired at varying depths below the interface and the interfacial signal was measured at surface before the arrival of the seismic wave. *Martner and Sparks* (1959) also performed a second experiment in which explosives were detonated in deep shot holes, while the seismoelectric signal was measured by a single electrode referenced to the surface. This experiment revealed an interfacial signal, which was generated when the P-wave reached the base of the weathered layer. To date, this is the only record in the literature of an interfacial signal having been measured in a borehole.

The ability of VSEP surveys to provide in-situ measurements of the seismo-electric effect from well-characterized, naturally occurring interfaces, with seismic sources that have frequency content identical to the seismic sources used in surveys, is also a significant advantage in understanding the phenomenon. Many properties including seismic velocity, elastic constants, electrical conductivity and porosity (but notably excluding $\zeta$ potential) can be measured or inferred from borehole logs. This is an important advantage since the amplitudes, frequency content and character of the seismoelectric fields can be studied directly and compared with numerical results given the known properties of the media.

This paper reports on seismoelectric experiments conducted in two boreholes penetrating a sandy unconfined aquifer. Interfacial co-seismic effects are generated in both holes upon arrival of the seismic P-wave at the water table, which lies in very close proximity to the top of a partially cemented zone. We investigate the origins of these seismoelectric conversions and how their detectability varies with the electrical conductivity structure in the two boreholes. We also examine the polarity and amplitude characteristics of the more prominent interfacial signal and show how they are consistent with the predictions of a vertical bipole-like model for the seismoelectric source.

## 5.2.1 Site description

The VSEP experiments were performed on the Gnangara Mound, which is an important water recharge and storage area for Perth, Western Australia (*Salama et al.*, 2005). Two PVC-cased boreholes, P220 and GG1(O), were chosen because of their long slotted intervals (allowing galvanic contact between the electrodes and the formation) and their relatively simple geology. The map in Figure 5.1 locates

these two boreholes as well as the location of the seismoelectric imaging experiment of *Dupuis et al.* (2007), labeled P-90 on the map.

The surficial sediments at P220 and GG1(O) have very different characteristics that affect the land use at these field sites (*Salama et al.*, 2005). P220 is located within a pine plantation in a region where the surficial geology consists of Tamala Limestone – a calcareous wind blown deposit, also known as eolianite, composed of varying proportions of quartz sands, fine to medium grained shell fragments and clayey lenses (*Davidson*, 1995). The quartz sands in this formation are predominantly medium grained and moderately sorted and commonly stained with limonite. The upper surface of the Tamala limestone at this site is leached and consists of unconsolidated sands. The water table depth in this borehole remained at 12.65 m during the period when all measurements were made.

GG1(O) is located within native bush-land where the surficial geology is composed of Bassendean sands. *Davidson* (1995) indicates that the quartz sands found in this region are moderately sorted and commonly have an upward fining progression in grain size. He also reports that a layer of friable, limonite-cemented sand, colloquially called "coffee rock", occurs throughout most of the area near the water table. The water table depth in this borehole remained at 13.00 m during the period when all the measurements were made.

The surficial geology near borehole P-90, where the seismoelectric traverse was acquired (*Dupuis et al.*, 2007), is similar to that at GG1(O) although the ground cover included native bush on one side of the survey line and a pine plantation on the other.
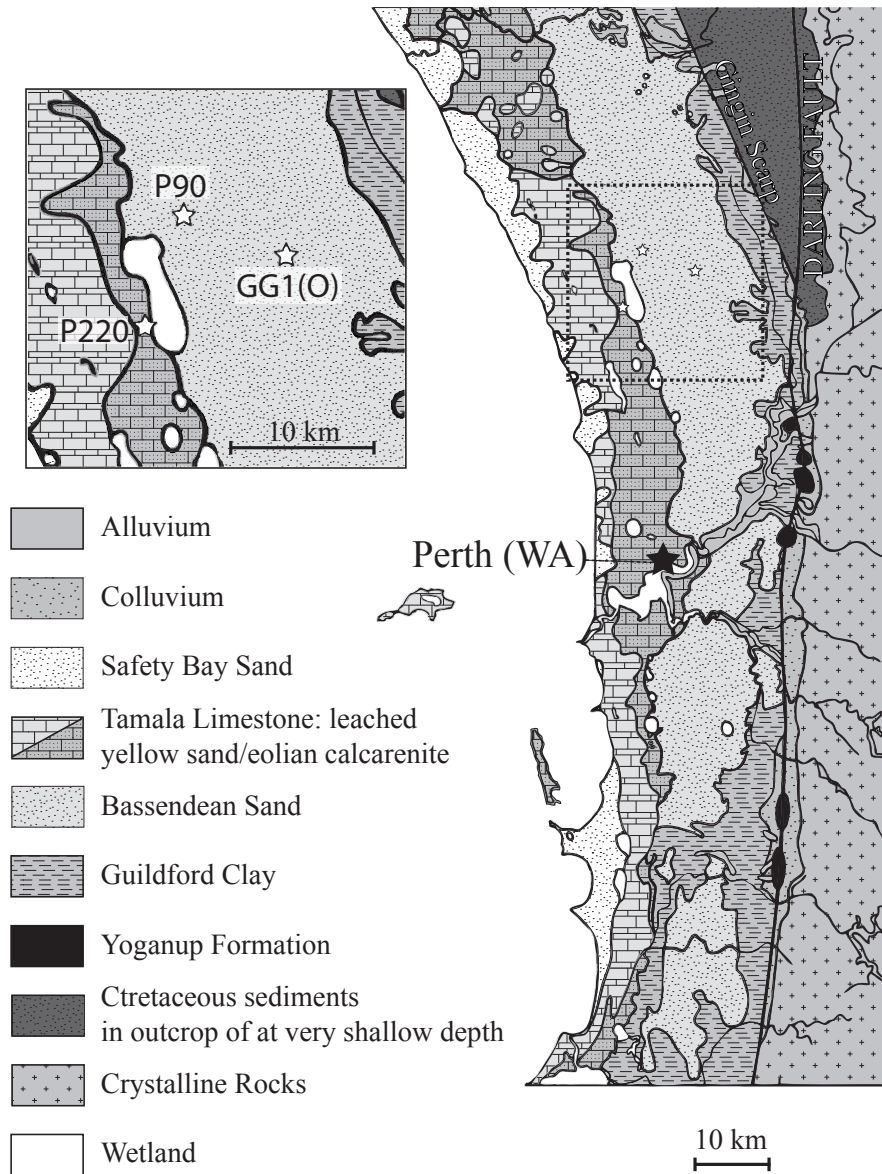
Figure 5.1: Location of boreholes used in this study, P220 and GG1(O), and the location of the seismoelectric imaging experiment of *Dupuis et al.* (2007) labelled P-90. This map is an adaptation from the surficial geology map of *Davidson* (1995)

## 5.3 Field experiments

### 5.3.1 Vertical seismic and seismoelectric profiles

The VSEPs were acquired by lowering a multi-electrode array down a slotted, PVC-cased borehole and using a sledgehammer seismic source on surface, offset 3.5 m from the borehole collar. The electrodes were made of tinned copper wire wrapped around segments of PVC pipe that were 10 cm long and 2.5 cm in diameter. Seven electrodes, spaced two meters apart, were connected to a 36-m multi-paired cable and the connections were waterproofed with a urethane compound. The measurements reported in this paper were made by pairing the electrodes so as to give six dipoles each 2 m in length as shown in Figure 5.2.

The signals from the dipoles were buffered at surface using custom-built differential pre-amplifiers which provided a gain of 10, and were digitized using a 24-bit seismograph (Geometrics Geode) with a sample rate of 62.5 $\mu$s. The electrode array was raised in 25 cm increments and 20 sledgehammer blows were recorded at every depth, thereby providing a maximum fold of 120 shots at each depth (taking into consideration the redundancy provided by 6 dipoles). All shots were acquired and processed individually for harmonic noise removal (*Butler and Russell*, 2003) so that unusually noisy records could be identified and discarded prior to stacking. Typical powerline noise levels were relatively low at 0.1 to 5 $\mu$V/m. On average, the number of traces rejected at each depth was less than 2%.

Vertical seismic profiles (VSPs) were also acquired at each site. A hydrophone was lowered to the bottom of the boreholes and raised in 25 cm increments until it reached the water table. As in the VSEP survey, the shotpoint was located on surface 3.5 m from the borehole casing. Due to the high sensitivity of the hydrophone, a
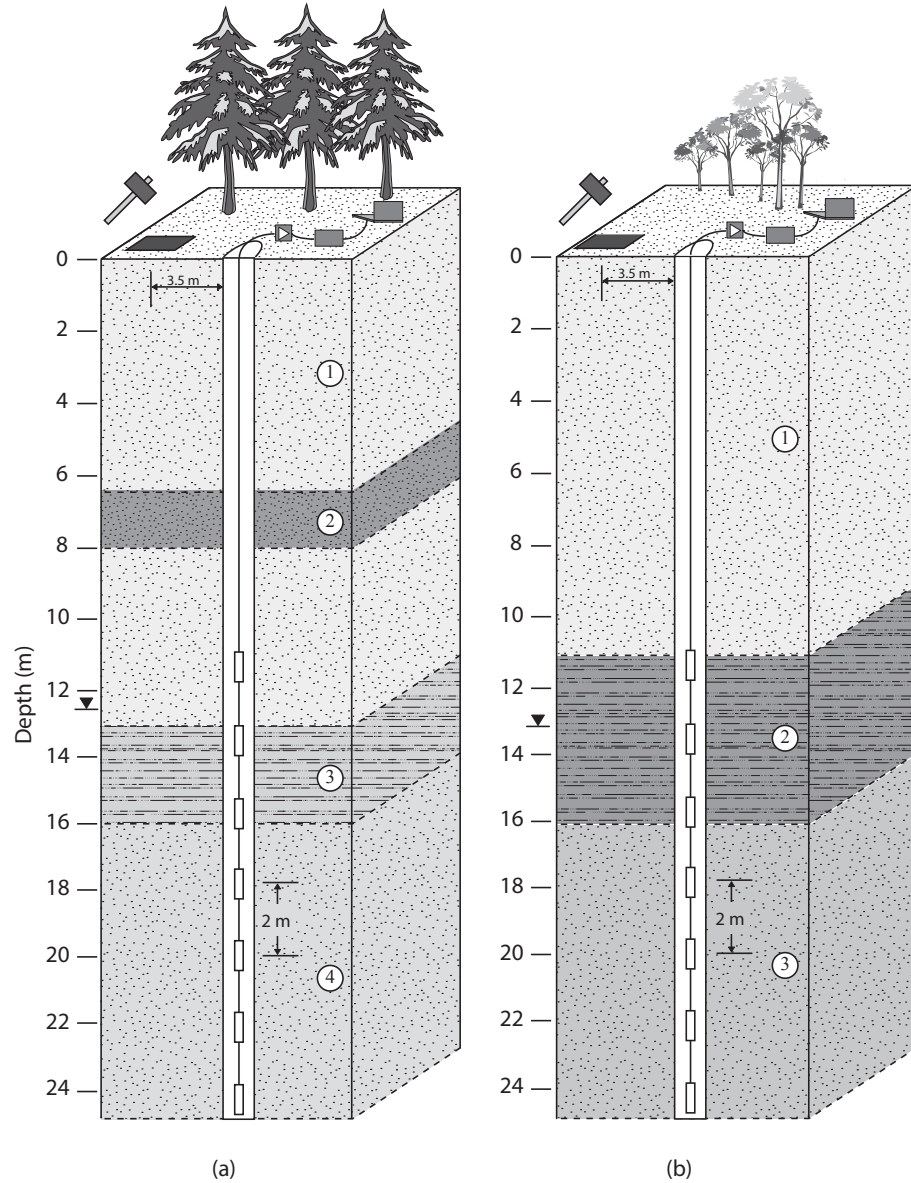
Figure 5.2: Experimental setup for vertical seismoelectric profiling at borehole P220 (a) and GG1(O) (b). Inferred interfaces from the geophysical logs are indicated by dashed lines. The inferred sediments at P220 (a) are composed of (1) unsaturated sands, (2) water-retentive sediments richer in clay, (3) partially cemented sands, and (4) saturated sands. The inferred sediments at GG1(O) on the other hand are composed of (1) unsaturated sands, (2) limonite cemented sands, and (3) saturated sands.

lighter hammer was used as a source and only two shots were required to obtain sufficient signal-to-noise ratio. A second VSP was acquired at P220, with a wall locking borehole geophone and a sledgehammer source, in order to obtain a velocity profile for the vadose zone above the water table.

## 5.4  Results and discussion

The VSP and VSEP data for borehole P220 are displayed in Figures 5.3 (a) and (b). The VSP exhibits direct P-wave arrivals (A) followed by lower velocity and lower frequency tube waves. The pressure associated with the direct P-wave arrivals at P220 varies from a maximum of 50 $\mu$bars, when the hydrophone is placed at the top of the watertable, down to 20 $\mu$bars at the bottom of the profile. The VSEP is more complex as several wave modes, absent from the VSP, interfere with one another. The most interesting signal for the purpose of this work is the event labeled (B) that is generated at approximately 26.25 ms and shows both polarity and amplitude variations with depth. The arrival of this signal appears simultaneously at the receivers irrespective of their depth and precedes the arrival of any seismic waves at depth. These characteristics are expected of seismoelectric interfacial signals measured below the interface where they are generated. The maximum peak amplitude of the interfacial signal is 1 $\mu$V/m.

In addition to the direct arrivals and the interfacial signal there is an interesting lower frequency signal of much larger amplitude that appears at approximately 35 ms and 14.75 m depth. It exhibits minimal moveout with depth although interference with other wave modes makes it difficult to ascertain whether it can be considered to arrive simultaneously over its whole depth range. It also changes polarity between

19 and 21 meters depth. This signal may be attributed to conversions of tube waves but its origin is not easily determined from the information available.

The VSP and VSEP data acquired at GG1(O) are displayed in Figures 5.4 (a) and (b). The direct P-wave arrivals are labeled (A) and the pressure pulse associated with the direct arrival varies from 30 to 5 $\mu$bars, with the highest pressures being recorded when the hydrophone is placed at the water table. As was done for P220, the times of the direct arrivals are transposed onto the VSEP. The direct (co-seismic) arrivals in this borehole are much easier to observe and it is evident that their amplitude varies with depth, which is similar to the results from *Dupuis and Butler* (2006). The maximum peak amplitudes of the co-seismic signal occurs between 19 and 21 m depth with a maximum amplitude of 6 $\mu$V/m . The interfacial signal, labeled (B) on Figure 5.4 (b), shows similar characteristics as the one measured at P220 (i.e. simultaneous arrival at receivers irrespective of their depth and polarity variations with depth) but has important distinguishing characteristics. While the interfacial signal at P220 is observed at numerous receiver positions that span more than 14 m depth, the interfacial signal observed in GG1(O) decays much more rapidly with depth and is evident over a much more limited range ($\approx$ 2.5 m), despite having a comparable maximum amplitude of 0.9 $\mu$V/m.

## 5.4.1 Origin of the interfacial signal

In order to identify the interfaces that generate the seismoelectric conversions, we examine the velocity model derived from the VSP surveys, induction-conductivity and gamma-ray logs acquired in 2006 surveys, and the simple geological logs taken when the boreholes were drilled, more than 30 years ago.

The elevated electrical conductivity and gamma ray counts observed between
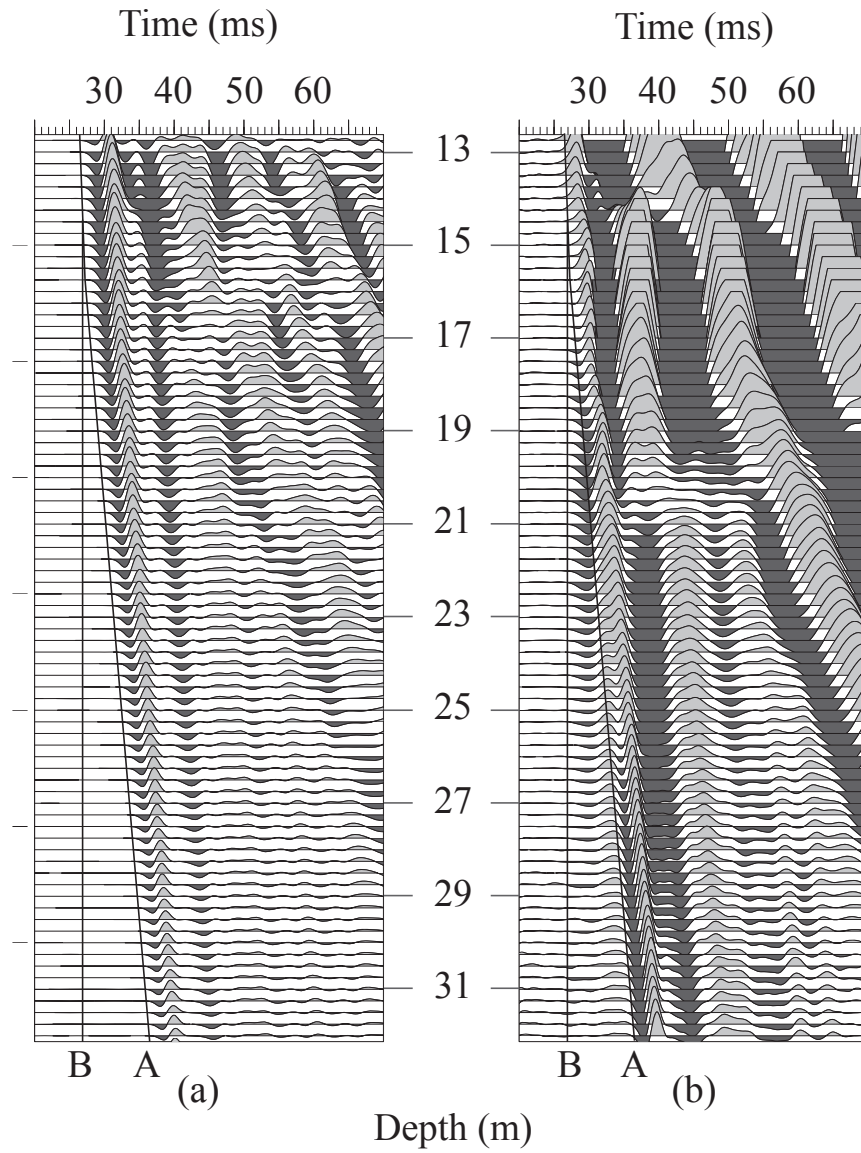
Figure 5.3: Vertical seismic (a) and seismoelectric (b) profiles for borehole P220. A Butterworth bandpass filter (60-500 Hz) has been applied to both datasets and traces are plotted at true relative amplitudes. The clipping exhibited on higher amplitude traces is caused by a display setting and not clipping of the signal at acquisition time.
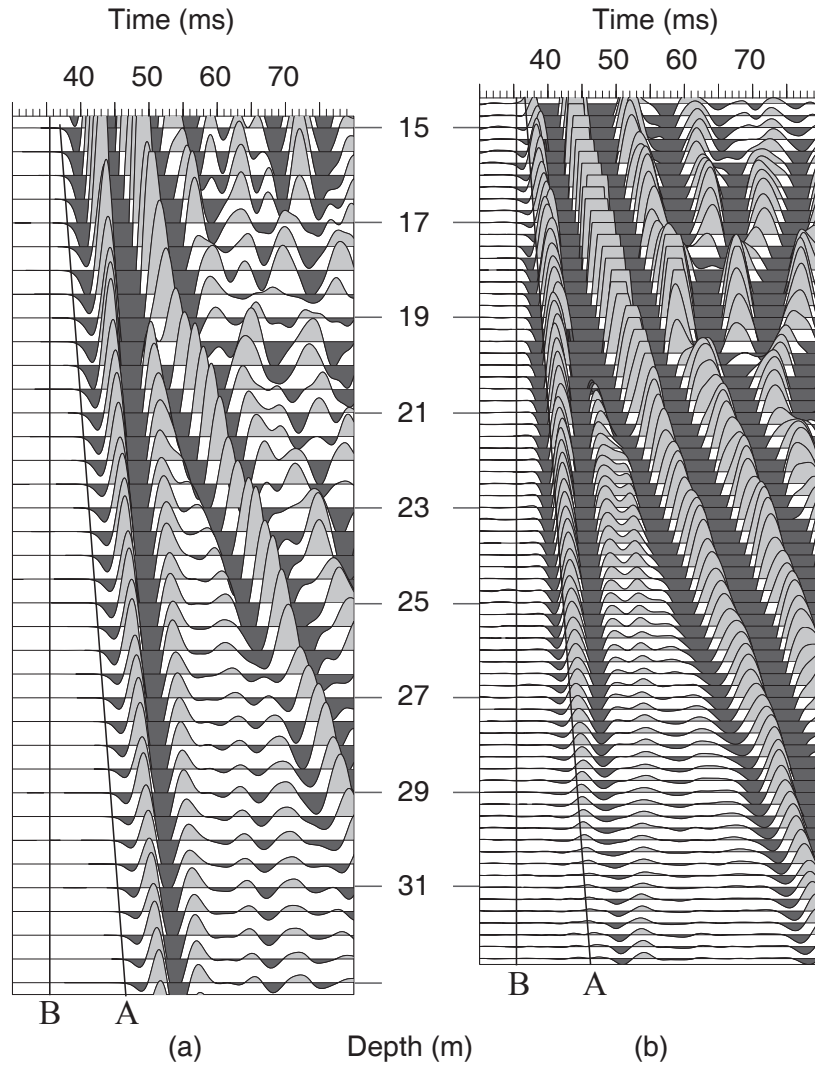
Figure 5.4: Vertical seismic (a) and seismoelectric (b) profiles acquired for borehole GG1(O). A Butterworth bandpass filter (120-300 Hz) has been applied to both datasets and traces are plotted at true relative amplitudes. The clipping exhibited on higher amplitude traces is caused by a display setting and not clipping of the signal at acquisition time.

6 and 8 m depth in borehole P220 (Figure 5.5 (a) and (b)) are suggestive of a layer with elevated clay content. Moving down the hole, an abrupt increase in conductivity from about 6 to 60 mS/m is observed on crossing the water table which was measured in the hole at a depth of 12.65 m. A closer inspection of the gamma log reveals a small drop in gamma ray emissions for a region starting just above the water table ($\approx$ 12.2 m) and extending down to 16 m depth. The P-wave velocity model (Figure 5.5 (c)), derived from the first arrivals of the VSP acquired with a hydrophone and a wall locking borehole geophone, indicates an elevated P-wave velocity of 3000 m/s between 13 and 16 m depth. This is well above the more usual range of 1500 – 2000 m/s expected from water-saturated sands and gravels, suggesting that the region may be partially cemented.

The onset of the interfacial signal at 26.25 ms (Figure 5.3 (b)) corresponds to the arrival of the P-wave at the water table. It is to be expected, therefore, that the interfacial signal observed at P220 is related to two important variations in porous media properties: (i) a sharp increase in conductivity due to a conductive pore fluid, and (ii) a strong acoustic impedance contrast from the water table and the coincident partially cemented layer.

Figure 5.6 presents the conductivity and gamma ray logs and the P-wave velocity profile for borehole GG1(O). The conductivity and gamma-ray logs remain relatively constant from surface to a depth of 11 m. The API and conductivity values throughout this interval are lower than those measured at P220 which indicates that the sands at this site contain very little clay. The increase in the gamma log response at approximately 11 m depth corresponds with a layer of brown sand and black sandstone reported in the geological log, that probably corresponds to the limonite-cemented sands (coffee rock)reported by *Davidson* (1995). The velocity log, derived
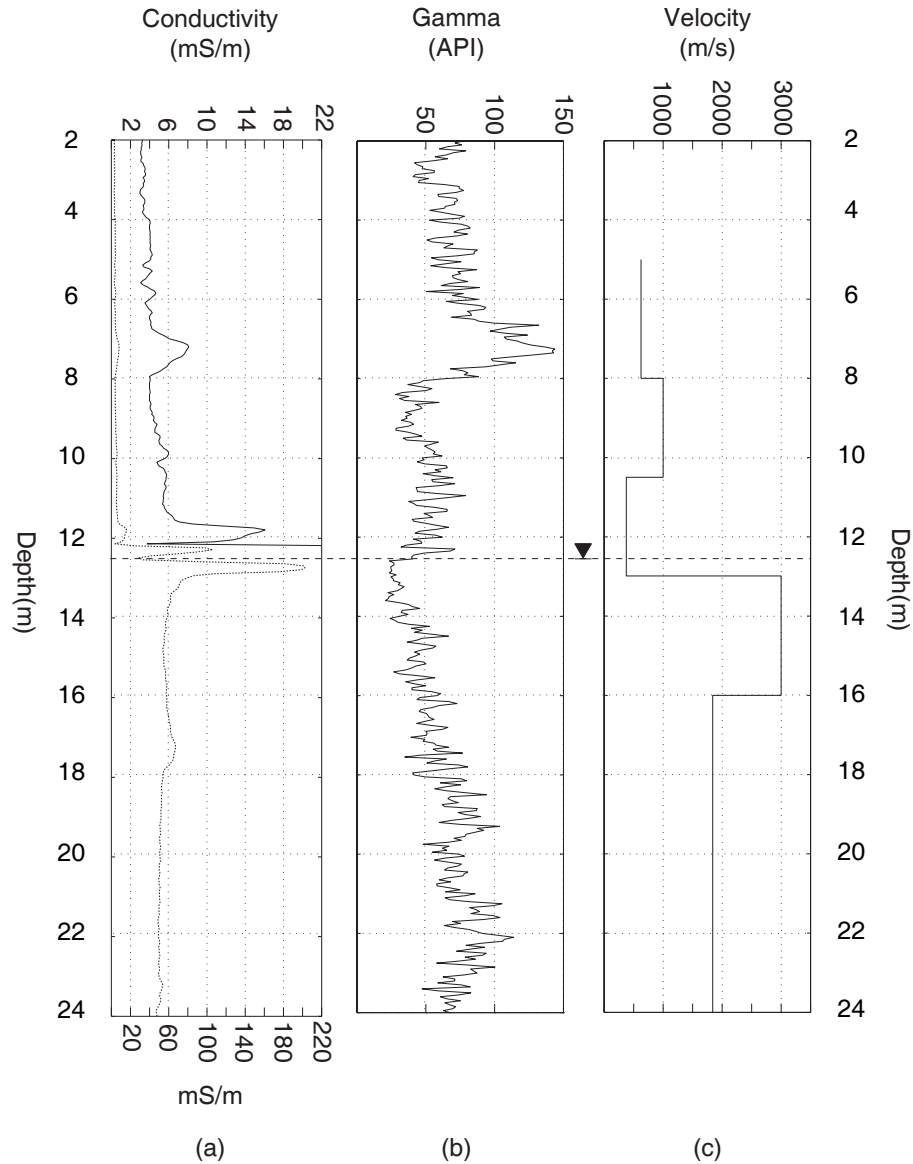
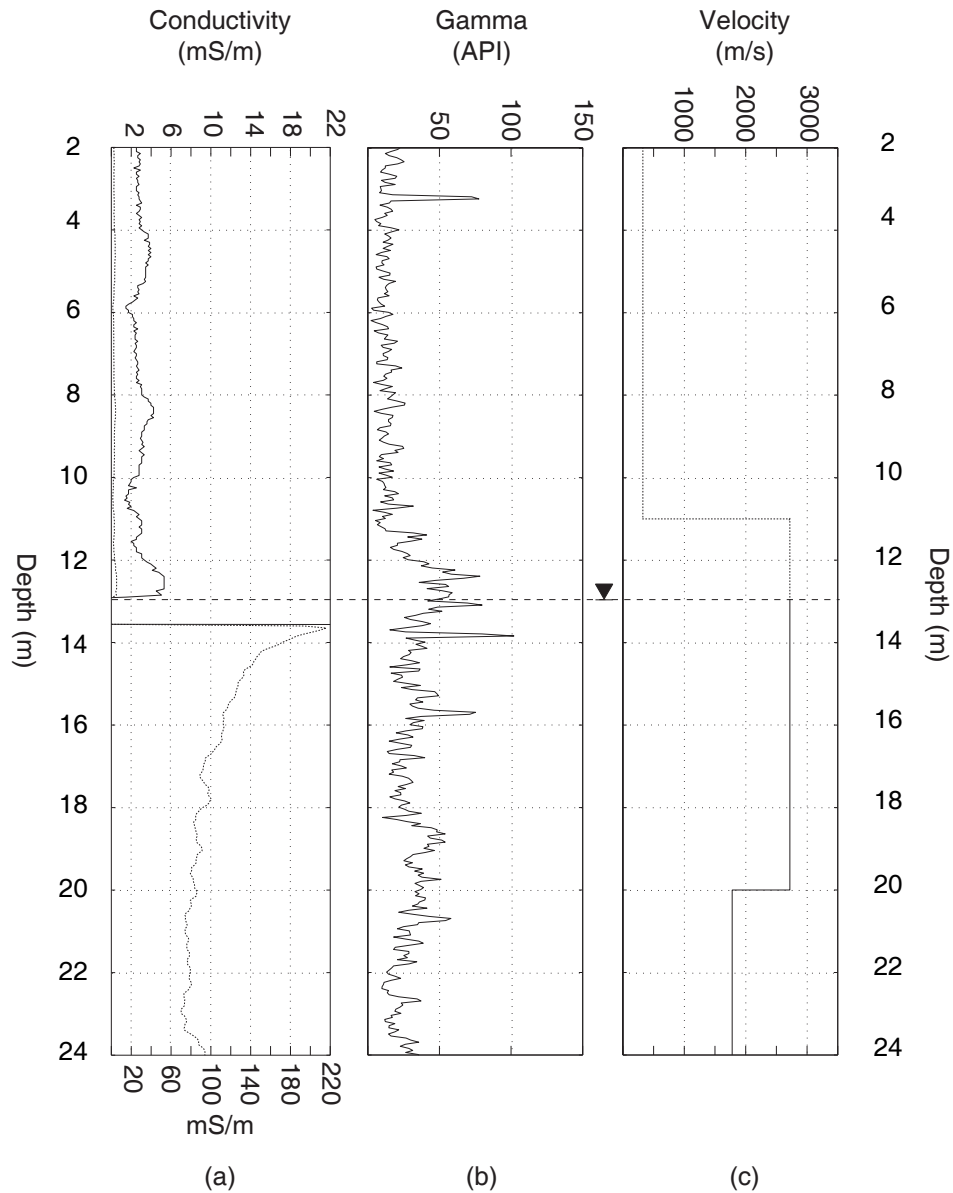Figure 5.5: Conductivity (a) and gamma-ray (b) logs acquired in borehole P220. The conductivities above and below the watertable differ by an order of magnitude and thus two scales are required to maintain the character of the log. The conductivities above the watertable are read from the top scale, while the conductivities in the saturated sediments are read from the lower scale. The velocity profile (c) is derived from the direct P-wave arrivals from a VSP acquired using a borehole geophone and hydrophone.

from the P-wave direct arrivals measured at this site with a hydrophone, shows a velocity of 2800 m/s for a region that spans from the water table to 20 m depth. Since only hydrophone data is available, the VSP at GG1(O) cannot provide information on the full extent of this partially cemented layer above the water table. We expect, however, that the top of the cemeted layer corresponds with the increased response in the gamma log at 11 m and the brown sand and black sandstone reported at that depth.

The compressional wave reaches the top of the water table at 36 ms, $\approx$ 1 ms after the onset of the interfacial signal in Figure 5.6 (b). If the velocity of the partially cemented layer remains constant above the water table, the 1 ms difference would place the origin of the interfacial signal at the top of the partially cemented layer at $\approx$ 11 m.

## 5.4.2 Polarity of the interfacial signal

The polarity reversal of the interfacial signal measured in borehole P220 is important because it encodes important information about the spatial and temporal evolution of the seismoelectric source. To demonstrate, we begin this section with a simple conceptual model.

The diagram in Figure 5.7 represents a simplified conceptual model of the electric charge distribution and resulting electric fields comprising the seismoelectric conversion generated by a P-wave reflecting at a perfect reflector (*Butler et al.*, 1996). The assumption of a perfect reflector is a reasonable first order approximation in this case because of the large acoustic impedance contrast that exists between the unsaturated sediments and the saturated partially cemented layer. Other abrupt changes in the mechanical and/or electrical characteristics of a porous medium –

Figure 5.6: Conductivity (a) and gamma-ray (b) logs acquired in borehole GG1(O). The conductivities above and below the watertable differ by an order of magnitude and thus two scales are required to maintain the character of the log. The conductivities above the watertable are read from the top scale, while the conductivities in the saturated sediments are read from the lower scale. The velocity profile (c) is derived from the direct P-wave arrivals from a VSP acquired using a hydrophone.

such as electrical conductivity, zeta potential, porosity and permeability are also expected to alter the charge distribution and give rise to interfacial signals (*Haartsen and Pride*, 1997; *Garambois and Dietrich*, 2002). The diagram in Figure 5.7 (a) schematically depicts the instant in time when the first seismic Fresnel zone for this reflector has formed; thus, the lateral extent of this lens-shaped zone is the Fresnel radius, while the vertical extent is the dominant wavelength of the seismic P-wave in the top material. This instant in time is important, because according to *Thompson and Gist* (1993) and *Garambois and Dietrich* (2002), the interfacial signal is expected to reach its maximum once the first Fresnel zone has taken shape.

The dipoles used as receivers in the borehole are small in comparison to the height of the source zone which contributes to the signal. So it is possible to measure the potential differences at points inside and outside this zone. Receivers placed above and below the source zone will record positive potential difference since the field lines are directed downward (the lower electrode is used as the reference or negative electrode in each of our dipole pairs). On the other hand, dipoles located within the source region will sense upward electric fields and will record negative potential difference as illustrated in Figure 5.7 (b). From this model, the transition from negative to positive should occur once the mid point of the receiver dipole goes to a depth $\lambda/2$ beyond the generating interface (where $\lambda$ is the dominant wavelength of the seismic P-wave in the top material).

Apart from the above-mentioned change in polarity with receiver depths, some receivers will also experience a change in signal polarity with time. To understand this concept, let us consider a receiver positioned below the interface as in Figure 5.7 (c). At time $t_1$ the receiver will measure a small positive potential difference because it is outside the zone where the interfacial signal is being generated. As the positive front

Electric potential difference



(a)          (b)

(c)          (d)
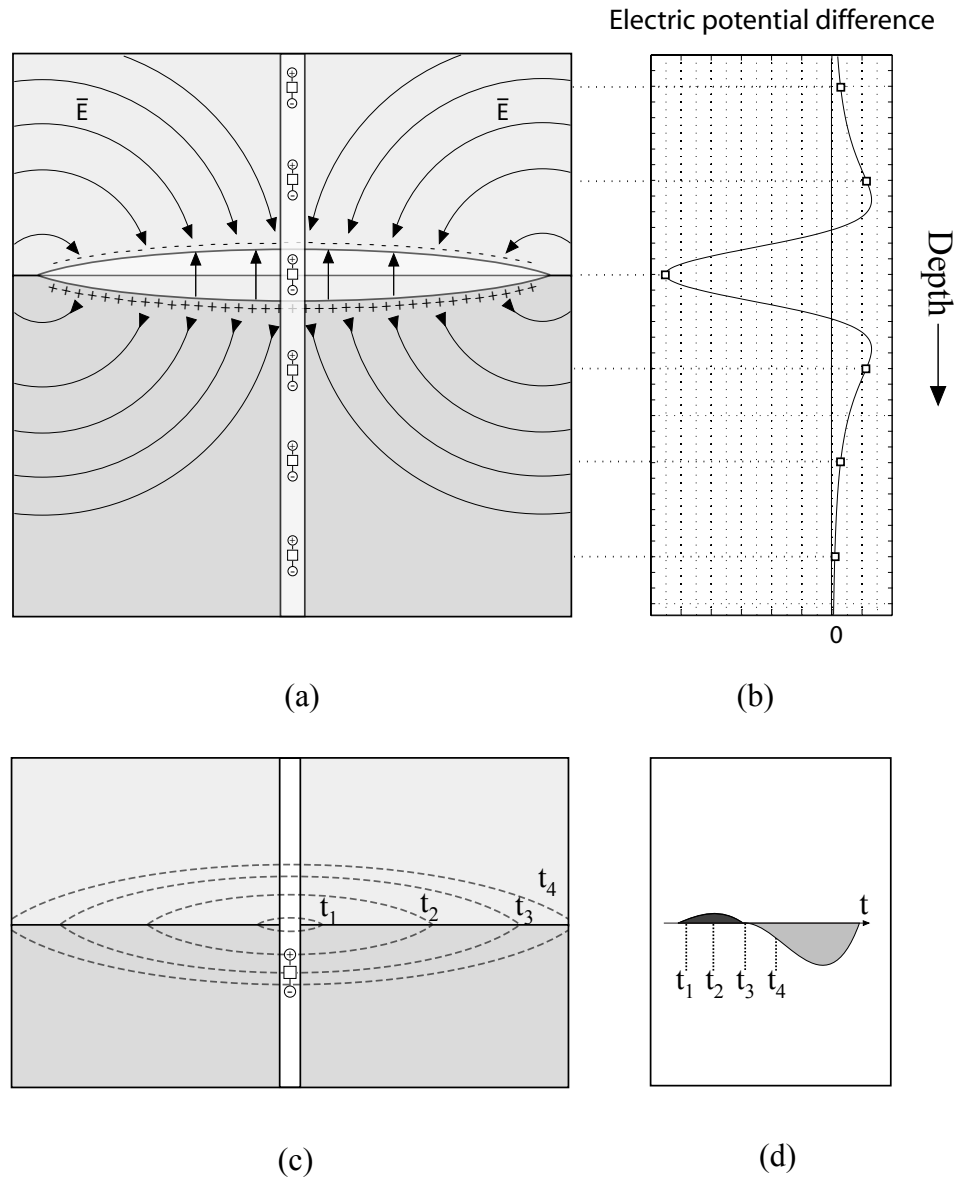
Figure 5.7: Schematic representations of spatial (a,b) and temporal (c,d) polarity variations expected for an interfacial seismoelectric conversion when the length of the receiving dipole is small compared to the maximum height of the source zone.

moves toward the positive electrode of the receiver, the potential difference measured at the receiver will increase. After reaching a maximum at time $t_2$, the potential difference will start to decrease until the electric fields inside and outside the active zone cancel each other ($t_3$). As the source continues to expand, leaving the receiver dipole completely inside, the receiver will measure negative potential differences ($t_4$). This evolution of signal polarity with time can be seen in the VSEP for borehole P220 for traces at depth between 16.5 and 18.125 m as shown in Figure 5.8. The polarity inversion over this transition interval causes the measured interfacial signal to have a higher frequency content than the signal measured outside the transition zone.

### 5.4.2.1 Decyphering the polarity information

The information encoded in the polarity transitions observed over both time and depth at P220 can be used to determine the rate at which the source zone takes shape and the maximum vertical extent it reaches. We begin this analysis by identifying the known quantities obtained from the VSEP and the VSP.

The first observation that can be made is that the onset of the interfacial signal (labeled $t_1$ on Figure 5.8) coincides closely with the 26.25 ms arrival time of the P-wave at the water table (12.65 m). According to the velocity profile of Figure 5.5 (c), however, the acoustic impedance contrast at this interface is not only due to water saturation, because a partially cemented layer begins $\approx$ 35 cm below the water table and extends 3 m down to 16 m. It is difficult to establish beyond any doubt if the water table or the cemeted layer is responsible for the interfacial signal, since arrival times would differ by only 0.1 ms. We therefore assume that the interfacial signal is caused by a combination of the large acoustic impedance of the cemented layer and the large increase in conductivity at the water table. We also assume, for purpose of
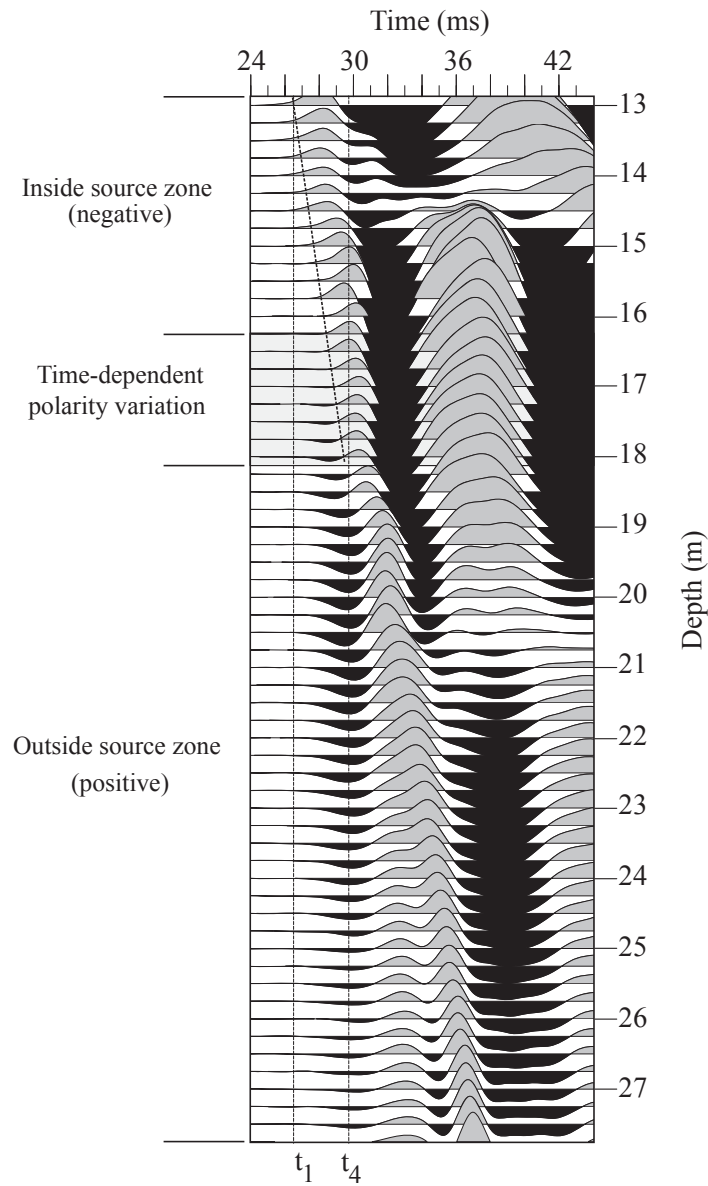
Figure 5.8: Enlarged portion of the P220 VSEP that shows the two types of polarity reversal measured in a borehole and the three regions that exist for an interfacial signal measured in-situ.

the modelling that follows, that the top of the cemented layer and the water table are coincident.

The second observation necessary for this analysis can be made by considering the time at which the interfacial signal reaches its maximum amplitude, which is labeled $t_4$ on Figure 5.8. At this instant in time (29.75 ms), the source zone has reached its maximum vertical extent. The exact point where this maximum is positioned can be determined by considering the polarity of the signal along line $t_4$. Following this line, we can observe the polarity of the signal flipping from negative to positive in the interval between 18 and 18.25 m which means that the edge of the source zone probably occurs in this interval.

The last necessary piece of information is obtained by considering the higher frequency signal in the transition zone where the polarity switches from positive to negative during development of the seismoelectric source. In this transition zone, the polarity of the signal depends on the progression of the source zone at a given instant in time. Fitting a line through the points where the transition occurs gives the velocity at which the source zone is expanding ($\approx 1500$ m/s) which is comparable to the P-wave velocity in the saturated sediments below the partially cemented layer (1780 m/s). If we use this line to project back to $t_1$, as is done in Figure 5.8 we get a confirmation that the signal originated from a depth of approximately 13 m.

### 5.4.3   Modelling the interfacial signal

#### 5.4.3.1   Simple bipole model

The source region for the interfacial signal of the conceptual model presented in section 5.4.2 can be described by using charged spherical caps (*Butler et al.*, 1996) which in turn can be modelled by a multipole expansion. Numerical results (*Garam-*

*bois and Dietrich*, 2002) have shown that the dipole term dominates the multipole expansion and it has therefore become common to compare the amplitude versus offset characteristics of numerical simulations and field measurements to those of a short electric dipole positioned at the interface.

In this case however, the far-field dipole model is inappropriate, because the measurements are made in the near field of the source. We therefore propose to decompose the dipole into a positive and negative point charge to form a bipole with a charge strength chosen to best fit measured data. The suitability of a bipole source to model an interfacial signal measured in a borehole is demonstrated below.

The bipole at the water table starts to take shape once the symmetry of the co-seismic field is broken at 26.25 ms. We know from the data that the charged front of the source zone, represented here by a positive charge, moves at a velocity of 1500 m/s in the downwards direction. The rate of expansion of the source zone above the water table cannot be constrained by the VSEP data, but we can assume that it is slower, in keeping with the slower P-wave velocity of unsaturated sediments. In this model, we assume that the negative charged front, represented here by a negative point charge, is moving towards surface with a velocity of 560 m/s which represents the average P-wave velocity in the unsaturated sediments obtained from the VSP.

The VSEP data provides us with the opportunity to study the signal at any instant in time. We choose two discrete times to compare measured amplitude distributions to those predicted by a bipole model. The first is at 28 ms, which is the halfway mark between the times of signal onset and maximum development, and the second is at 29.75 ms when the source zone has reached its maximum size. The amplitudes of the electric field measured as a function of depth are compared to the predictions of the bipole model for those two instants in time in Figure 5.9. We can

see that the bipole model provides a good fit to the data below the water table at both instants in time and that the shift of the peak amplitude to greater depth over time corresponds well to the shift associated with the expansion of the source zone. The fit of the model, however, is not as good in the region immediately below the water table interface. This is in part because of a lack of information on the rate of expansion of the source zone above the water table and because of the interference with the co-seismic arrival at these depths.

### 5.4.3.2  Importance of the conductivity structure

It is not possible to do the same type of signal analysis on the interfacial signal observed at GG1(O) because it is only evident on a very limited number of traces. We attribute this to the different conductivity structures evident in the induction logs (Figures 5.5 (a) and 5.6 (a) respectively) from boreholes P220 and GG1(O). In both boreholes the conductivity log exhibits a high amplitude oscillation where it crosses the water table. This is interpreted as an artifact of the induction tool's response to an abrupt and large change in conductivity. In borehole P220 (Figure 5.5 (a)) this artifact extends approximately 1 m below the water table, below which the conductivity log exhibits a stable reading of approximately 60 mS/m. The extent of the artifact in borehole GG1(O) should be the same as both holes were logged upwards with the same tool and logging speed. It is clear, therefore, by comparison of the logs in Figures 5.5 (a) and 5.6 (a) that formation conductivities in the upper part of the saturated zone are two to three times higher in borehole GG1(O), dropping gradually from a high of 180 mS/m at a depth of 1 m below the water table to a background value of 80 mS/m 6 m below the water table. These elevated conductivities are expected to limit the depth of penetration of the interfacial seismoelectric for two
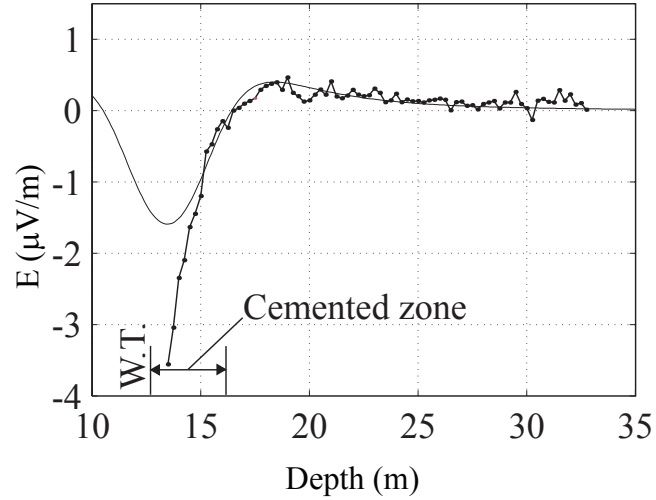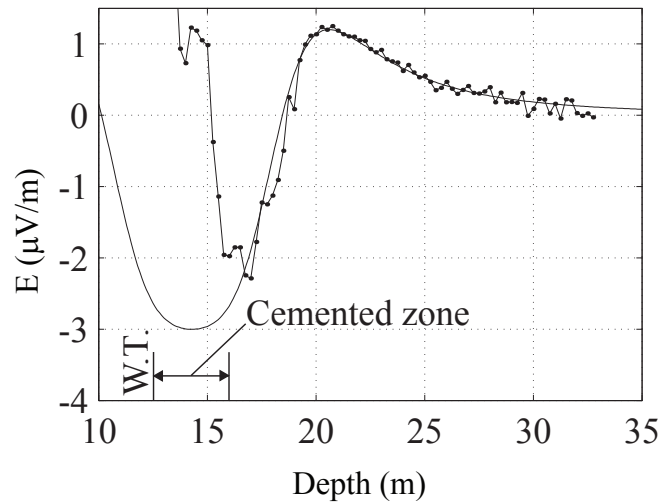
Figure 5.9: Potential differences normalized by dipole length (2 m) versus depth for interfacial signal measured (dots) and modeled (solid line) in the VSEP experiment at P220 at 28.0 ms (a) and 29.75 ms (b). The modeled bipole is positioned directly below the shot point (3.5 m from the borehole) and pole separation is determined by the instant in time and the expansion rate of the source zone. The water table level is indicated by W.T.

reasons – one being that electric field amplitudes will vary inversely with formation conductivity and the second being that the electric field pattern will remain more concentrated in the high conductivity zone within a few meters of the water table. It is also possible that the $\zeta$ potential was lower at GG1(O) because of an increase in electrolyte concentration, which lowers the $\zeta$ potential at the silica surface (*Revil et al.*, 1999).

From the logs (Figures 5.5 and 5.6), we suspect that the sources of cementation at the two test sites are different. This hypothesis is supported by the work of *Tapsell et al.* (2003) who demonstrate that the sediments found in the Bassendean and Spearwood sands differ in composition and in age (early and late Pleistocene respectively). The brown sand and black sandstone reported at GG1(O) is most likely the coffee rock described by *Davidson* (1995) which he expects to have formed in a shallow marine environment. The origin of the cementation at P220 is unknown and requires further investigation. The geological logs make no mention of anomalous conditions, suggesting that the material filling the pore space must have a color which resembles that of the sand. Relatively low gamma ray values suggest that the interval may have a lower clay content than the sands above and below.

### 5.4.4 Surface seismoelectric measurements

While the interfacial signal in borehole GG1(O) is weak below the interface, it can nonetheless be measured well above the interface as demonstrated by surface seismoelectric records acquired at that site. Figure 5.10 shows a comparison of seismic and seismoelectric shot gathers acquired approximately 15 m east of borehole GG1(O). The records are actually supergathers formed by combining the traces from eight shots spaced 50 cm apart at the centre of (a) and array of 36 vertical 28 Hz

geophones and (b) an array of 24 grounded dipole antennas, 4 m in length. The seismic source was the same 40 kg accelerated weight drop used for the seismoelectric traverse presented in *Dupuis et al.* (2007). Higher resistivities in the unsaturated sediments have made it possible to resolve the interfacial signal (C) over a greater range of offset ($\approx 20\ m$) on surface, in comparison to the VSEP dataset ($\approx 2$ m), despite the fact that the interfacial signal is significantly weaker on surface with a peak amplitude of $0.1 \mu V/$m. This signal strength is an order of magnitude smaller than measured by *Dupuis et al.* (2007) from a comparable depth at another site in the Bassendean Sand Formation approximately 10 km away.

The seismic dataset from GG1(O) is interesting because it shows that the direct P-wave arrivals at this site are very weak and are overwhelmed by an (acoustic) air wave (A). The air wave is absent from the seismoelectric dataset because the electrodes are not affected by this wave type. The refracted arrivals (B) seen on the seismic dataset are absent from the seismoelectric record, but the reflection at the top of the water table (D) is better resolved in the seismoelectric virtual shot gather, because the electrodes seem to be less affected by ground roll. The velocity of the refracted wave ($\approx 1600$ m/s) is comparable to that of the water saturated sands found below the cemented layer in the borehole, which indicates that the cemented zone was too thin to support a measurable refracted head wave.
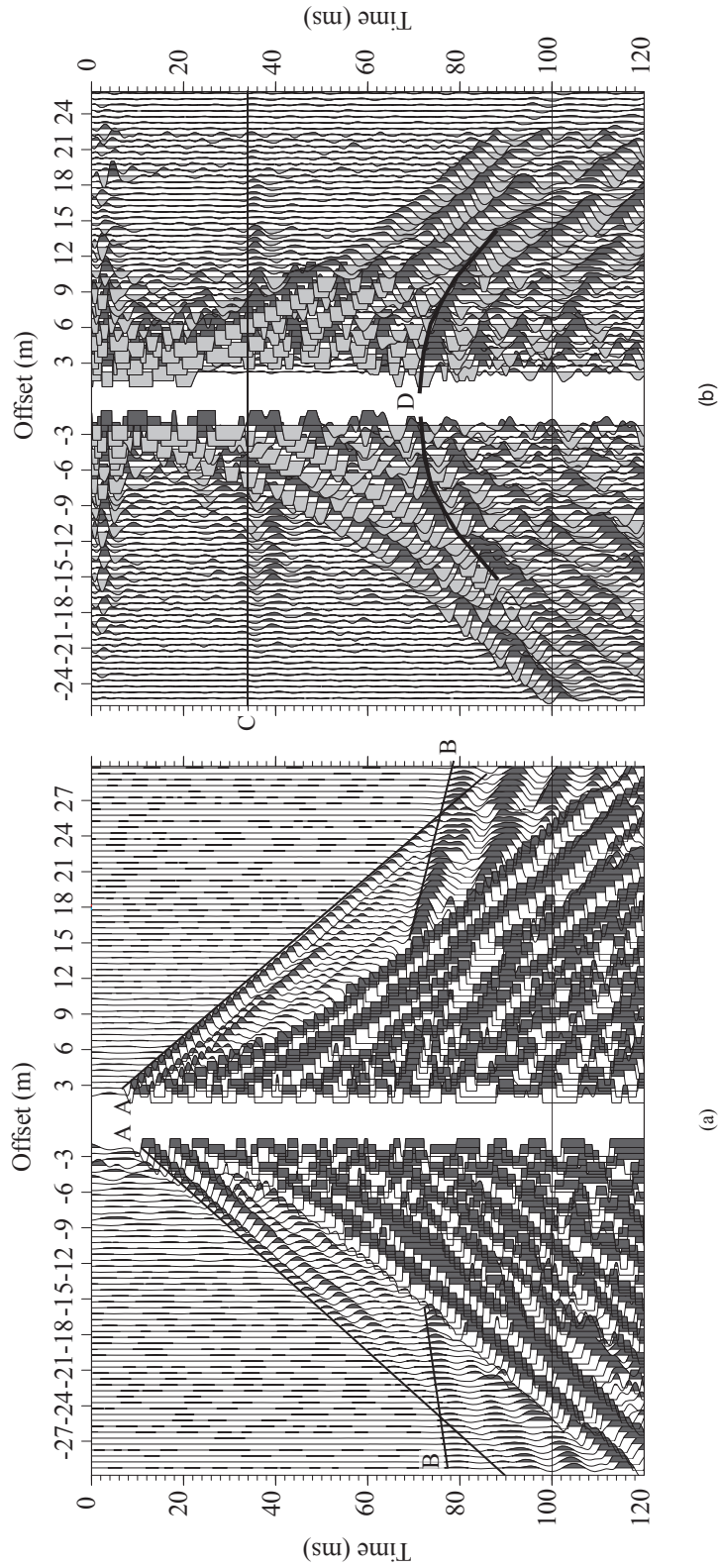
Figure 5.10: Surface seismic (a) and seismoelectric (b) supergathers acquired near borehole GG1(O). A is the direct wave, B is the refraction at the water table, C is the interfacial seismoelectric signal generated in vicinity of the watertable and D is a co-seismic seismoelectric arrival associated with the P-wave reflection from the water table.

## 5.5   Conclusions

Results from VSEP experiments have demonstrated that it is possible for seismoelectric conversions to be measured in a borehole environment, where the source-receiver geometry provides separation between interfacial and co-seismic signals. The interfacial signals at P220 and GG1(O) were generated in the vicinity of the water tables measured in the boreholes. Close examination of the velocity logs revealed partially cemented zones having upper surfaces roughly co-incident with the water table. Although we can deduce from the geological and geophysical logs that the sources of the cementation are different at these sites, we expect that these partially cemented layers may play a role in the generation of the interfacial signals by elevating the acoustic impedance of the sediment, in addition to the changes in water saturation and electrical conductivity associated with the water table itself. The nature of the interface observed at GG1(O) has potential significance for interpretation of the results from the seismoelectric traverse in *Dupuis et al.* (2007), since the traverse site and GG1(O) are both found in the same surficial sedimentary unit.

The fact that the interfacial signal is measureable over a much larger depth range in one borehole compared to the other is attributed to significant differences in the electrical conductivity structure at the two sites. Thus, although VSEP should be considered as a good screening tool to assess which interfaces may be amenable to detection by surface seismoelectric surveys, the conductivity structure of the sediments should also be considered when attempting to predict signal strengths on surface from those measured at depth.

Finally, the spatial and temporal characteristics of the interfacial signal measured at P220 have provided new information that support the conceptual model for seismoelectric conversion at interfaces. In particular, it was demonstrated that it is

possible to observe the expansion of the source zone and to determine its maximum depth attained below the interface by observing the polarity and amplitude of the interfacial signal.

## 5.6 Acknowledgments

## References

Beamish, D. (1999), Characteristics of near-surface electrokinetic coupling, *Geophysical Journal International*, *137*(1), 231–242.

Bordes, C., L. Jouniaux, M. Dietrich, J. P. Pozzi, and S. Garambois (2006), First laboratory measurements of seismo-magnetic conversions in fluid-filled Fontainebleau sand, *Geophysical Research Letters*, *33*(1), doi:10.1029/2005GL024582.

Butler, K. E., and R. D. Russell (2003), Cancellation of multiple harmonic noise series in geophysical records, *Geophysics*, *68*(3), 1083–1090, doi:10.1190/1.1581080.

Butler, K. E., R. D. Russell, A. W. Kepic, and M. Maxwell (1996), Measurement of the seismoelectric response from a shallow boundary, *Geophysics*, *61*(6), 1769–1778, doi:10.1190/1.1444093.

Butler, K. E., S. W. Fleming, and R. D. Russell (1999), Field test for linearity of seismoelectric conversions, *Canadian Journal of Exploration Geophysics*, *35*(1-2), 20–23.

Davidson, W. A. (1995), Hydrogeology and groundwater resources of the Perth region Western Australia, *Bulletin 142*, Geological Survey of Western Australia.

Dupuis, J. C., and K. E. Butler (2006), Vertical seismoelectric profiling in a borehole penetrating glaciofluvial sediments, *Geophysical Research Letters*, *33*(16), doi:10.1029/2006GL026385.

Dupuis, J. C., K. E. Butler, and A. W. Kepic (2007), Seismoelectric imaging of the vadose zone of a sand aquifer, *Geophysics*, *72*(6), A81–A85, doi:10.1190/1.2773780.

Garambois, S., and M. Dietrich (2001), Seismoelectric wave conversions in porous media: Field measurements and transfer function analysis, *Geophysics*, *66*(5), 1417–1430, doi:10.1190/1.1487087.

Garambois, S., and M. Dietrich (2002), Full waveform numerical simulations of seismoelectromagnetic wave conversions in fluid-saturated stratified porous media, *Journal of Geophysical Research*, *107*(B7), doi:10.1029/2001JB000316.

Haartsen, M. W., and S. Pride (1997), Electroseismic waves from point sources in layered media, *Journal of Geophysical Research*, *102*(B11), 24,745–24,769.

Hunt, C. W., and M. H. Worthington (2000), Borehole electrokinetic responses in fracture dominated hydraulically conductive zones., *Geophysical Research Letters*, *27*(9), 1315–1318.

Kulessa, B., T. Murray, and D. Rippin (2006), Active seismoelectric exploration of glaciers, *Geophysical Research Letters*, *33*(7), doi:10.1029/2006GL025758.

Martner, S. T., and N. R. Sparks (1959), The electroseismic effect, *Geophysics*, *24*(2), 297–308, doi:10.1190/1.1438585.

Mikhailov, O. V., W. M. Haartsen, and M. N. Toksöz (1997), Electroseismic investigation of the shallow subsurface: Field measurements and numerical modeling, *Geophysics*, *62*(1), 97–105, doi:10.1190/1.1444150.

Mikhailov, O. V., J. Queen, and M. N. Toksöz (2000), Using borehole electroseismic measurements to detect and characterize fractured (permeable) zones, *Geophysics*, *65*(4), 1098–1112, doi:10.1190/1.1444803.

Neev, J., and F. R. Yeatts (1989), Electrokinetic effects in fluid-saturated poroelastic media, *Physical Review B*, *40*(13), 9135–9141, doi:10.1103/PhysRevB.40.9135.

Pride, S., and M. W. Haartsen (1996), Electroseismic wave properties, *Journal of the Acoustical Society of America*, *100*(3), 1301–1315, doi:10.1121/1.416018.

Revil, A., P. A. Pezard, and P. W. J. Glover (1999), Streaming potential in porous media:1. theory of the zeta potential, *Journal of Geophysical Research*, *104*(B9), 20,021–20,031, doi:10.1029/1999JB900089.

Russell, R. D., K. E. Butler, A. W. Kepic, and M. Maxwell (1997), Seismoelectric exploration, *The Leading Edge*, *16*(11), 1611–1615, doi:10.1190/1.1437536.

Salama, R. B., R. Silberstein, and D. Pollock (2005), Soils characteristics of the Bassendean and Spearwood sands of the Gnangara mound (Western Australia) and their controls on recharge, water level patterns and solutes of the superficial aquifer, *Water, Air,and Soil Pollution: Focus*, *5*(1-2), 3–26, doi:10.1007/s11267-005-7396-8.

Singer, J., J. Saunders, L. Holloway, J. B. Stoll, C. Pain, W. Stuart-Bruges, and G. Mason (2005), Electrokinetic logging has the potential to measure permeability, in *46th Annual Logging Symposium*, pp. 1–16, Society of Petrophysicists and Well Log Analysts.

Strahser, M. H. P., W. Rabbel, and F. Schildknecht (2007), Polarisation and slowness of seismoelectric signals, a case study, *Near Surface Geophysics*, *5*, 97–114.

Tapsell, P., D. Newsome, and L. Bastian (2003), Origin of yellow sand from Tamala Limestone on the Swan Coastal Plain, Western Australia, *Australian Journal of Earth Sciences*, *50*, 331–342, doi:10.1046/j.1440-0952.2003.00989.x.

Thompson, A. H., and G. A. Gist (1993), Geophysical applications of electrokinetic conversion, *The Leading Edge*, *12*(12), 1169–1173, doi:10.1190/1.1436931.

# Chapter 6

# Conclusions and recommendations

Despite being the subject of scientific curiosity for over seventy years, the potential of seismoelectric effects of electrokinetic origin as a geophysical exploration tool has yet to be realized. Recent important advances in quantitative understanding of the phenomenon have made it possible to create full-waveform numerical models that can assist in determining the expected response of seismoelectric interfaces, but our ability to make field measurements has lagged behind. Examples of high quality field measurements that can be used to validate theoretical and numerical models are still scarce in the literature.

For this reason, the emphasis in this work was placed on field methods and experiments, paying special attention to characteristics of the measured signals and using them to verify simple conceptual and quantitative models. The merit in restricting the discussion to simple models is that they can provide more intuitive explanations of the mechanisms at play in the generation of seismoelectric signals. They also provide researchers who develop full-waveform numerical codes with expected signal characteristics, such as polarity and amplitude distribution, that can be used to verify their solution.

It is important for the reader to note that despite the apparent ease of obtaining the results presented in this thesis, substantial field and development efforts were required. More than a dozen multi-day field programs at ten separate sites over a period of four years were carried out to refine acquisition and experimental methods and achieve the results presented herein.

In the first field experiment presented, co-seismic signals were acquired in a borehole penetrating unconsolidated glaciofluvial sediments using a high resolution surface seismic source. Any interfacial signals generated at this site fell below the noise level of about 0.2 $\mu$V/m in the processed data and were too weak to be observed. We found, however, that the amplitude of the co-seismic signals depended on the sediment and was largest in the aquifer sand and gravel and smallest in lacustrine silt and clay. Furthermore, measured amplitudes within a sand interval were consistent with expected values calculated using a transfer function developed by *Butler* (1996) based on a quasi-static model derived by *Neev and Yeatts* (1989). This transfer function provides insights into ways that the co-seismic signal may be normalized to account for particle velocity (or acceleration) and electrical conductivity so as to emphasize variations in other physical properties (such as porosity and the electrokinetic $\zeta$ potential). If porosity logs were available in future experiments, the seismoelectric log could be normalized by it and dependence on the $\zeta$ potential would emerge.

In the second set of experiments, seismoelectric conversions were used to image subsurface interfaces within partially and fully saturated sediments. The remarkable interfacial signals measured during this surface experiment are, arguably, the most convincing ever published. They appear over a large range of offsets (up to 40 m from the shot) and are free of interference from co-seismic signals because of slow surficial velocities. In addition, the water table was at a sufficient depth to allow

clear separation between different interfacial signals within the vadose zone. This natural signal separation meant that no velocity filters or deconvolution were required and thus processing artifacts were avoided. Two important hydrogeological targets, interpreted as a shallow water-retentive layer and the water table, were identified on the seismoelectric section and corroborated by ground penetrating radar (GPR) profiling along the same line. Seismic reflection and refraction methods did not resolve the water-retentive layer. The results from this experiment demonstrated that it is possible to measure interfacial seismoelectric effects from depths exceeding 10 m and that seismoelectric imaging, which is sensitive to the presence of pore water, could be complementary to GPR for the characterization of aquifers.

In the last set of experiments, the focus returned to vertical seismoelectric profiles and it was shown that interfacial signals can be measured in boreholes. It was found that the onset of the interfacial signal on the VSEP corresponded to the arrival of the P-wave at the water table. Closer inspection of geological and geophysical logs revealed the presence of partially cemented layers that either straddled, or coincided with, the water table. These partially cemented layers caused the acoustic impedance contrast around the water table to be higher than normal and thus may have contributed to the conversion at the interface at these sites and is a potential factor in the strength of the signals measured in the seismoelectric traverse experiment near borehole P-90. The conductivity structure of these partially cemented layers was shown to have an impact on the amplitude of the seismoelectric signal measured in-situ. At the site where the conductivity was highest in the saturated partially cemented layer, the interfacial signal appeared over a smaller depth range, despite being of comparable amplitude (1 $\mu$V/m vs 0.9 $\mu$V/m) close to the source zone. The analysis of spatial and temporal polarity reversals observed for the interfacial signal has provided new

information in support of the conceptual model for seismoelectric conversions. In particular, it was shown that the rate of expansion of the source zone and its maximum vertical extent below the water table can be determined from these polarity reversals. These encouraging results illustrate that VSEPs surveys help to further our understanding of the signal conversion that takes place at real hydrogeological interfaces. They may also be used to assess which interfaces are amenable to detection by surface seismoelectric surveys, given an appropriate conductivity structure around the source zone and between the source zone and surface.

In summary, the work presented in this thesis has shown that it is possible to acquire high quality seismoelectric records in the field and to use these measurements to verify models for co-seismic and interfacial signals. In particular, the amplitude of the co-seismic signal measured in a borehole was shown to compare well to the expected value computed using a transfer function derived by *Butler* (1996), based on the quasistatic quantitative model derived by *Neev and Yeatts* (1989). Field data from borehole and surface experiments were also used to test the hypothesis that a vertical dipole/bipole model provides a good first order fit for the amplitude distribution of the electric field generated by seismoelectric conversion at an interface.

Field experiments also provided valuable information about the type of conditions and environments most hospitable for seismoelectric exploration. Regions of the world where ground wires are used as a return path for unbalanced currents provide much quieter electromagnetic environments than regions where these currents are simply returned through the earth. Making measurements in quieter electromagnetic locations allow us to use more of the dynamic range of the acquisition system for measurements of seismoelectric signals, instead of sacrificing part of it to record strong signals that will be removed during post-processing. Lower powerline harmonic noise

also make it possible to observe other sources of noise, such as radio frequency interference, on seismoelectric records. The ability to see these other sources of interference in the field provide an opportunity to take corrective action to reduce, or eliminate, these additional noise sources that are difficult to remove during post-processing.

Field examples from the Gnangara Mound have shown that low velocity surficial sediments can help delay the direct arrival at surface receivers such that the interfacial signal can be observed without the need for velocity filtering. Interfaces where acoustic and electrical properties vary together seem to be the particularly amenable to detection. These include the water retentive layer imaged with the seismoelectric traverse and the water table that was coincident with a partially cemented layer in the VSEP experiments. It was also shown that the conductivity structure of the sediments surrounding a source zone has an impact on the amplitude of the signal being measured in-situ. For best results, the VSEP experiments should be performed in boreholes where the conductivity is low.

## 6.1 Recommendations

The results of field experiments presented in Chapters 3, 4 and 5 provide important information that can be used to ascertain the validity of theoretical models and numerical simulations. Of particular interest are the amplitude and phase characteristics of seismoelectric signals observed during field experiments and the ability of current models to replicate those results. In a first instance there are at least four particular tests that could be conducted which are described briefly below.

1. An extensive set of borehole logs are available to constrain physical property variations in borehole UNB1-03 that penetrates glaciofluvial sediments at Fred-

ericton. Using this information and measured seismic amplitudes for control, can existing modeling codes replicate the measured variations in co-seismic signal strength, and the lack of any observable interfacial signal at that site?

2. Figure 4.3 shows that the interfacial seismoelectric signal associated with the water table (and possible cementation) near borehole P90 on the Gnangara Mound decays slightly more gradually with offset than would be expected for a simple small vertical dipole located at the interface. The discrepancy was tentatively attributed to the size of the source zone and its close proximity to the receivers on surface. This observation, however, is at odds with results of a published numerical simulation (*Garambois and Dietrich*, 2002) which shows a faster amplitude falloff in comparison to the short dipole estimate. This apparent disagreement between simulation and measurement should be investigated to determine the source of the problem.

3. The vertical seismoelectric profile (VSEP) in Figure 5.3 is the first data set to show near-source characteristics of an interfacial seismoelectric signal such as the rate of expansion of the source zone and its vertical extent. Can modeling codes replicate the seismoelectric amplitude variations, as well as temporal and spatial polarity variations observed in this experiment, and verify the conceptual model presented in that chapter?

4. The very limited extent of the interfacial signal observed in borehole GG1(O), by comparison with that observed in borehole P220, was tentatively attributed to electrical screening associated with the high electrical conductivity of the zone immediately below the water table at that site. Numerical simulations should be used to investigate the validity of that suggestion and, more generally, to

investigate how high conductivity layers bend or focus seismoelectric fields with particular emphasis on the implications for interfacial signal detectability in surface and borehole surveys.

In the longer term, it would be worthwhile to extend the seismoelectric theory and numerical models to encompass their generation in unsaturated sediments. Theoretical models derived up to this point only take into consideration fully saturated sediments, while surface experiments often report interfacial signals at the transition between the vadose zone and the water table. Seismoelectric imaging could become an important tool for detecting important hydrogeological targets found in the vadose zone, as shown by the detection of a water retentive layer at one of the field sites on the Gnangara Mound, but theoretical models and numerical simulations have not yet been developed for this purpose. In order to assist the development of these models and simulations, VSEP experiments could be devised to measure the seismoelectric signal in a partially saturated medium. In order for the electrodes to make galvanic contact with the formation in absence of a fluid filled borehole they could be attached to the outside of the casing for the portion above the water table and an electrode eel similar to the ones constructed for this work could be used below the water table. The deployment of electrodes above and below the water table would make it possible to observe in-situ the signal conversion at an interface and provide further evidence of the validity of the conceptual model proposed in Chapter 5. Physical and electrical characteristics of the sediments measured in-situ and in the laboratory from recovered samples could be used in combination with measured seismoelectric signals to verify the results of numerical simulations and theoretical models.

The most obvious obstacle remaining in the pursuit of high quality seismoelectric measurements is the lack of suitable seismoelectric preamplfiers that can either

be purchased or easily constructed. Appropriate signal buffering remains one of the major stumbling block, albeit not always recognized by people attempting to make seismoelectric measurements. As demonstrated in Chapter 2, the use of step-up transformers should be discouraged and signal should be appropriately buffered if their amplitudes are to be used to verify quantitative models.

In conclusion, I expect that the use of interfacial signals to map interfaces, as demonstrated in Chapter 4 of this thesis, will probably remain the driving force behind future commercial developments. Prospective researchers however, should not overlook the important role that vertical seismoelectric profiling can play for evaluating theory, models and applications of seismoelectric phenomena in saturated and unsaturated media.

# References

Butler, K. E. (1996), Seismoelectric effects of electrokinetic origin, Ph.D. thesis, University of British Columbia, Vancouver, BC.

Garambois, S., and M. Dietrich (2002), Full waveform numerical simulations of seismoelectromagnetic wave conversions in fluid-saturated stratified porous media, *Journal of Geophysical Research*, *107*(B7), doi:10.1029/2001JB000316.

Neev, J., and F. R. Yeatts (1989), Electrokinetic effects in fluid-saturated poroelastic media, *Physical Review B*, *40*(13), 9135–9141, doi:10.1103/PhysRevB.40.9135.

# Appendix A

# Field Photographs

Figure A.1: Accelerated weight drop used for the seismoelectric traverse near borehole P-90.

Figure A.2: Seismoelectric instrumentation consisting of preamplifiers (silver boxes), Geode seismograph (yellow box) and recording computer (in background) deployed along Cypress Rd. near borehole P-90 (Western Australia). The inset image shows a typical foil electrode used during that survey.
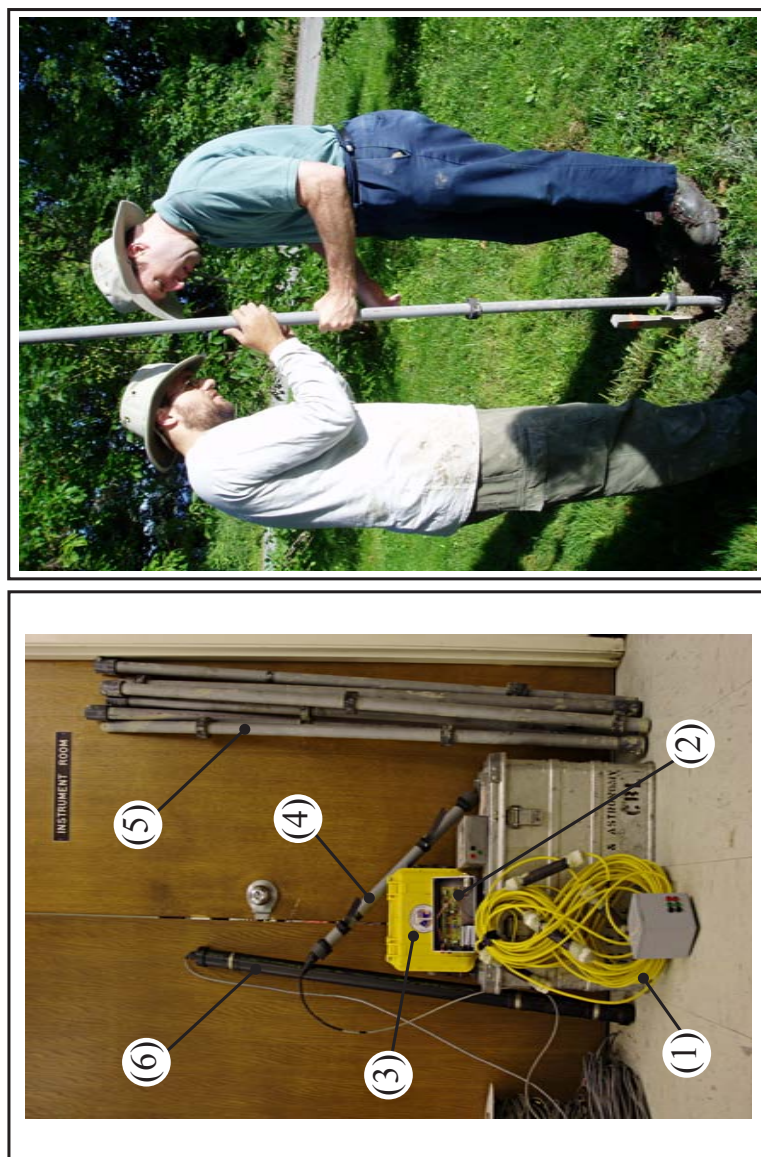
(a)

(b)

Figure A.3: (a) Instrumentation used for the surveys at borehole UNB1-03. In this photograph it is possible to see (1) the first generation electrode eel, (2) a seismoelectric preamplifier, (3) a Geode seismograph, (4) a borehole geophone, (5) PVC striking rod, (6) a short and long normal resistivity tool. (b) Assembled PVC striking rod being lowered in position in the shallow borehole adjacent to UNB1-03.
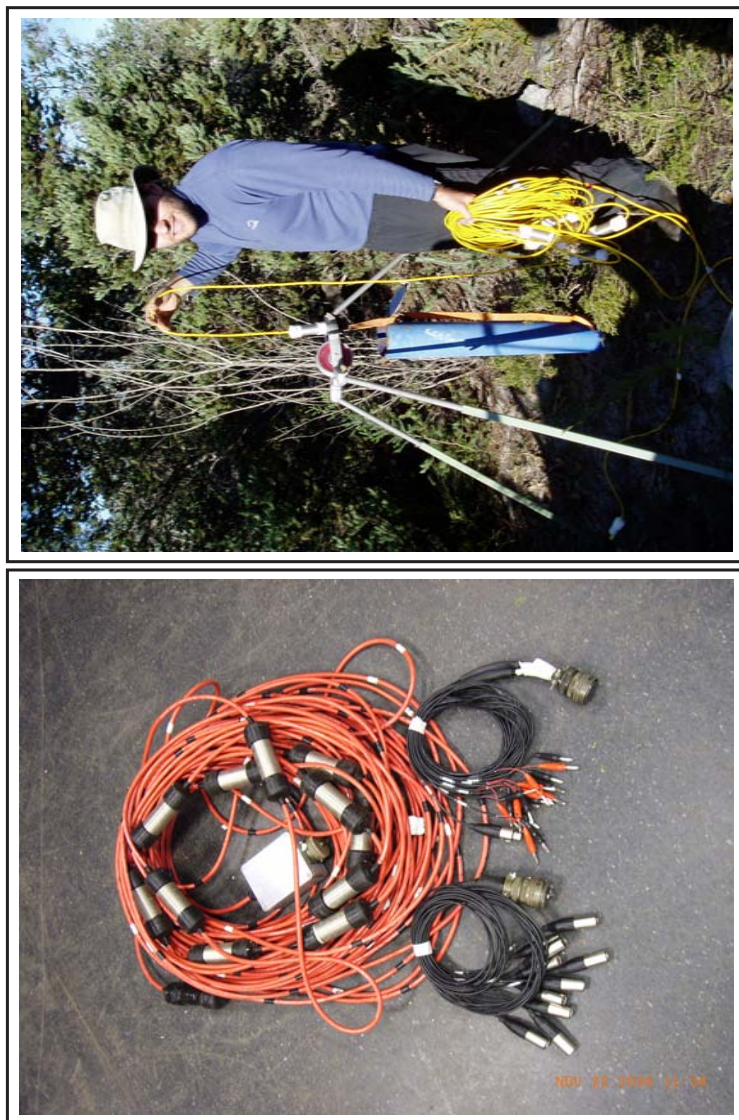
Figure A.4: (a) Third generation electrode eel comprised of ten dipoles and one hydrophone. (b) Second generation electrode eel being deployed at GG1 (Western Australia).

# Author Index

# Vita

**Candidate's full name:** Jerome Christian Dupuis
**University attended:** University of New Brunswick, B.Sc.E., 1995-2001
University of New Brunswick, M.Sc.E., 2001-2004
University of New Brunswick, Ph.D., 2004-2008

**Refereed Journal Papers, Published:**

J. Christian Dupuis and Karl E. Butler, 2006, "Vertical seismoelectric profiling in a borehole penetrating glaciofluvial sediments," *Geophysical Research Letters*, 33, L16301, doi:10.1029/2006GL026385.

J. Christian Dupuis, Karl E. Butler, and Anton W. Kepic, 2007, "Seismoelectric imaging of the vadose zone of a sand aquifer," *Geophysics*, 72, A81-A85, doi:10.1190/1.2773780.

**Refereed Journal Papers, Submitted for publication:**

J. Christian Dupuis, Karl E. Butler, Anton W. Kepic and Brett D. Harris, "Anatomy of a seismoelectric conversion: Measurements and modelling in boreholes penetrating a sandy aquifer," *Journal of Geophysical Research*, July 2008.

**Patents, Issued**

Jerome Christian Dupuis, Bruce Gordon Colpitts and Brent Robert Petersen, "Induction Magnetometer" U. S. Patent No. 7 375 529, assignee University of New Brunswick, Canada, issued May 20, 2008.

**Expanded Abstracts:**

J. Christian Dupuis and Karl E. Butler, "Borehole seismoelectric measurements using a broadband surface seismic source and downhole electric field antennas," *19th an-*

*nual Symposium on the Application of Geophysics to Engineering and Environmental Problems*, Seattle, Washington, April 2006.

J. Christian Dupuis, Karl E. Butler, Anton W. Kepic and Brett D. Harris, "The seismoelectric response of a sandy aquifer: borehole experiments," *69th Conference & Exhibition of the European Association of Geoscientists & Engineers*, London, England, June 2007.

J. Christian Dupuis, Karl E. Butler and Anton W. Kepic, "The seismoelectric response of a sandy aquifer: surface profiling experiment," *69th Conference & Exhibition of the European Association of Geoscientists & Engineers*, London, England, June 2007.

Karl E. Butler, J. Christian Dupuis and Anton W. Kepic, "Signal-to-Noise Improvements in Seismoelectric Data Acquisition," *Exploration 2007*, Toronto, Canada, September 2007.

**Presentations:**

J. Christian Dupuis, Karl E. Butler and Anton W. Kepic , "Pinnacles and pitfalls in seismoelectric measurement," *CMOS-CGU-AMS Congress 2007*, St. Johns, Newfoundland and Labrador, Canada, May 2007.

Karl E. Butler, J. Christian Dupuis, Anton W. Kepic and Brett D. Harris, "Borehole Measurements of Interfacial and Co-seismic Seismoelectric Effects," *American Geophysical Union Fall Meeting 2006*, San Francisco, California, USA, December 2006.

J. Christian Dupuis, Susan E. Pullan, Karl E. Butler and D. V. Venugopal, "Investigating the extent and structure of the cretaceous basin at Vinegar Hill, NB using seismic reflection and seismoelectric surveys," *AGS 2005 Colloquium*, St-John, New Brunswick, Canada, February 2005.

J. Christian Dupuis, Susan E. Pullan, Karl E. Butler and D. V. Venugopal, "Investigation of the Vinegar Hill Silica deposit with shallow seismic, seismoelectric and borehole logging surveys," *Exploration and Mining New Brunswick 2004*, Fredericton, New Brunswick, Canada, November 2004.

J. Christian Dupuis, Bruce G. Colpitts and Brent R. Petersen, "Optimization of a 3-axis Induction Magnetometer for Airborne Time Domain EM Geophysical Surveys," *AGS 2004 Colloquium*, Moncton, New Brunswick, Canada, January 2004.

**Theses:**

J. Christian Dupuis, "Optimization of a 3-axis Induction Magnetometer for Airborne Time Domain EM Geophysical Surveys," Master's thesis, Dept. of Electrical and Computer Engineering, University of New Brunswick, Fredericton, New Brunswick, Canada, Dec. 2003, supervisors Professor Brent R. Petersen and Professor Bruce G. Colpitts.

J. F. Daigle and C. Dupuis, "Design of an autonomous robot (Part II)", B.Sc.E. undergraduate thesis, Dept. of Electrical and Computer Engineering, University of New Brunswick, Fredericton, New Brunswick, Canada, 2001, supervisor Professor Mary Kaye.

**Posters:**

J. Christian Dupuis, Karl E. Butler and Anton W. Kepic, "Seismoelectric imaging of the vadose zone in a sandy aquifer," *European Association of Geoscientists and Engineers 69th Conference and Exhibition*, London, United Kingdom, 11-14 June 2007.

J. Christian Dupuis and Karl E. Butler, "The Effects of the Seismic Frequency on Seismoelectric Measurements in a Borehole Penetrating Glaciofluvial Sediments," *Australian Earth Sciences Convention 2006*, Melbourne, Australia, 2-7 July 2006.